Accession No. _____

13

SID 65-1730

AN ANALYTICAL STUDY OF SEPARATED FLOW ABOUT A CIRCULAR CYLINDER

25 January 1966

NAS8-20140

Prepared by
B.H. Ujihara
B. H. Ujihara
Principal Investigator

Approved by
R.F. Stevenson
R. F. Stevenson
Chief, Loads and Criteria

F. C. Hung
F. C. Hung
Director, Dynamic Sciences

NORTH AMERICAN AVIATION, INC.
SPACE and INFORMATION SYSTEMS DIVISION

Accession No._____

SID 65-1730

AN ANALYTICAL STUDY OF SEPARATED FLOW ABOUT A CIRCULAR CYLINDER

25 January 1966

NAS8-20140

Prepared by

B. H. Ujihara
Principal Investigator

Approved by

R. F. Stevenson
Chief, Loads and Criteria

F. C. Hung
Director, Dynamic Sciences

NORTH AMERICAN AVIATION, INC.
SPACE and INFORMATION SYSTEMS DIVISION

FOREWORD

This report presents the technical findings of contract NAS8-20140, "An Analytical Study of Periodic Vortex Shedding from a Circular Cylinder." The study was conducted by the Space and Information Systems Division of North American Aviation, Inc., for the Marshall Space Flight Center, National Aeronautics and Space Administration, Huntsville, Alabama. Dr. F.C. Hung, Director of the Dynamic Sciences Department, was Project Manager. B.H. Ujihara was the Principal Investigator, responsible for the success of the total effort. Mr. Ujihara was assisted by the following staff: T. Sugimura, who was responsible for the theoretical development; J.E. Davis, who developed the computer programs, assisted by D. Almanza; G.M. Steuart, G.A. Curney, and H.P. Valentijn, who operated the computer programs and analyzed computed results; and M.K. Chapman, who edited the final report. Dr. A. Roshko participated in the study as a part-time consultant. At MSFC, the Project Monitor was Mr. Heinrich Struck; alternate Project Monitor was Dr. Max F. Platzer.

In addition to this report, a short movie was prepared to demonstrate the dynamic nature of the results obtained from this study.

Page

Radial Position of Feeding Point 54
Effect of Incremental Integration Time Period 56
Flow Model II 56

COMPUTER PROGRAMS 59

SOLUTIONS WITH MODEL I PROGRAM 65
Unsymmetrical Separated Flow Around a Circular Cylinder . . 65
Cylinder Pressure Distributions 65
Force Computations 66
Wake Characteristics 70
Wake Velocities for Vortex Shedding 76
Symmetrical Separated Flow About a Circular Cylinder . . . 79
Symmetrical Separated Flow About a Flat Plate 84

SOLUTIONS WITH MODEL II PROGRAM 87
Unsymmetrical Flow About a Circular Cylinder 87
Unsymmetrical Flow Streamlines 94
Symmetrical Separated Flow About a Circular Cylinder . . . 96
Symmetrical Flow Streamlines 101

RESULTS OF INVESTIGATION 113
Vortex Instability 113
Symmetrical Flow 114
Periodic Vortex Shedding 116

REFERENCES 121

BIBLIOGRAPHY 123

CONTENTS

	Page
SUMMARY	1
INTRODUCTION	3
CONCLUSIONS	5
RECOMMENDED AREAS OF FURTHER STUDY	7
Reduction of Pressure Discontinuities	7
Practical Two-Dimensional Problems	7
Aeroelastic Response of a Two-Dimensional Cylinder	7
Lift on Bodies of Revolution	8
Further Development of Basic Technique	8
VORTEX SHEDDING PROBLEM	9
THEORETICAL DEVELOPMENT	11
Circular Cylinder	11
Flow Field for a System of Vortices Outside a Circular Cylinder in Uniform Flow	11
Pressure Coefficient	14
Forces	17
Elliptical Cylinder	26
Flow Field for a System of Vortices Outside an Elliptical Cylinder in Uniform Flow	26
Forces	30
FUNDAMENTAL INVESTIGATIONS	35
Shear Layer Instability	35
Vorticity Transport Rate	35
Vortex Strength	37
Formation of a Growing Shear Layer in Flow Past a Half-Plane	38
Effects of Changing Integration Mode	45
Cylinder Forces due to Vortex Growth Rate	46
FLOW MODELS	51
Flow Model I	51
Effect of Vortex Feeding Period	54
Peripheral Position of Feeding Point	54

ILLUSTRATIONS

Figure		Page
1	Formation of Shear Layer in Flow Past Half-Plane (Case 1)	40
2	Formation of Shear Layer in Flow Past Half-Plane (Case 2)	40
3	Formation of Shear Layer in Flow Past Half-Plane (Case 3)	41
4	Formation of Shear Layer in Flow Past Half-Plane (Case 4)	41
5	Formation of Shear Layer in Flow Past Half-Plane (Case 7)	42
6	Computed Plots of Vortex Development (Model I) (A) $U_o \Delta t/a = 0.07$; (B) $U_o \Delta t/a = 0.174$	44
7	Lift and Drag Time Histories	44
8	Vorticity Transport Rate	53
9	Comparison of Effects of Vortex Feeding Period on Flow Development	55
10	Computer Program Flow Chart	60
11	Cylinder Pressure Distributions at Times of Max and Min C_L	66
12	Pressure Coefficients for 11 Points on Wake-Exposed Portion of Cylinder	67
13	Time-Averaged Distributions of Cylinder Pressure Coefficient	68
14	Effects of Vortex Feeding Period on Lift and Drag	69
15	Characteristic Vortex Configuration (Model I)	70
16	Instantaneous Wake Velocity Profiles	72
17	Instantaneous Wake Pressure Profiles	74
18	Average Wake Pressure on Center Line	76
19	Computed Mean Wake Velocity Compared with Experimental Data	77
20	Wake RMS Velocity Fluctuations	78
21	Center-Line Wake Velocity vs Distance Downstream	79
22	Effects of Variation in Vorticity Transport Rate	81
23	Wake Development for an Impulsively Started Cylinder	83
24	Typical Cylinder Pressure Distribution for Symmetrical Flow	83

Figure		Page
25	Model I Solution for Flat Plate	85
26	Initial Cell Locations	87
27	Unsymmetrical Flow About a Circular Cylinder (Model II)	89
28	Vortex Configuration for Unsymmetrical Flow	90
29	Lift and Drag Time Histories (Model II Unsymmetrical Flow)	90
30	Variation in C_L and C_D at Time of Second Peak in C_L (Ref. Figure 29)	91
31	Vortex Patterns and Cylinder Pressures for ϵ = 0.5 and 0.6	92
32	Vortex Patterns and Cylinder Pressures for ϵ = 0.7	93
33	Unsymmetrical Flow Streamlines	95
34	Symmetrical Flow About a Circular Cylinder (Model II)	97
35	Vortex Configuration at t = 62.65 a/U_o	98
36	Variation in Feed Point and Transport Rate for Different ϵ	98
37	Symmetrical Flow Solutions for ϵ = 0.6	99
38	Flow Pattern and Related Drag Time History Without Initial Vortices	100
39	Symmetrical Flow Streamlines	102

TABLES

Table		Page
I	Growth of Shear Layer	39
II	Computer Program Input Definition	62
III	Wake Pressure Bias From Zero	75
IV	Stream Functions	103

SUMMARY

Results of this study have purportedly shown that two-dimensional incompressible separated flow past circular cylinders, and bluff bodies in general, can be determined analytically on the basis of potential theory. The key to successful application of this approach lies in implicit determination of vorticity transport rate and feeding point locations in the solution.

For the case of an impulsively started cylinder, the drag buildup is characteristically similar to that of Schwabe (1943), peaking at the same maximum value, but at a slightly later time. While the pressure distributions, particularly over the wake-exposed portion of the cylinder, do not agree with Schwabe's data, the reason is evidently due to the fact that vorticity cancellation effects in the wake were not considered. No great difficulty is anticipated in devising a technique for incorporating this effect in the mathematical model, although the elementary approach attempted in this study to account for vorticity cancellation was not satisfactory for symmetrical flow analysis.

The flow past a flat plate normal to the flow was analyzed only for symmetrical flow, using fixed vorticity transport rate and feeding point location. Basic similarity of the flow development to the analogous solution for the circular cylinder led to the conclusion that symmetrical flow past a flat plate is also governed by flow stability criteria similar to the cylinder, and requires implicit solution of vorticity transport rates and feeding point location.

For the case of unsymmetrical flow, periodic vortex shedding was demonstrated at a Strouhal number of 0.2, in agreement with experimental data for subcritical Reynolds numbers. Lift and drag coefficients were satisfactorily brought into agreement with experimental data by introducing the vorticity reduction parameter, ϵ, as a factor applied to the vorticity transported from the primary feeding points. The improved method of accounting for vorticity reduction mentioned above for symmetrical flow could also be incorporated in solution of the unsymmetrical problem.

INTRODUCTION

Periodic vortex shedding, in the flow of fluids past bluff bodies, refers to the orderly development of counter vortices in the wake. Its intriguing and sometimes destructive manifestations in nature have attracted many eminent researchers. The "von Kármán vortex street" is undoubtedly the most universally recognized phraseology describing this phenomenon. It relates to von Kármán's analytical solution a half century ago in which he showed that a stable arrangement of a row of counter vortices occurs for a width-to-spacing ratio of 0.281. But because the inception of separated flow occurs within the viscosity-important regions of the boundary layer, complete analytical solutions to the vortex shedding problem have remained unattainable.

In recent years, the vortex shedding problem has become important to the structural design of launch vehicles. These vehicles are of long, slender construction, required to stand vertically on the ground for extended periods during launch preparation. The vehicles in this attitude, when subjected to ground winds, invariably exhibit vortex shedding flow. Critical structural loads induced by ground winds act on these vehicles under certain conditions of resonance between vehicle bending and vortex shedding frequencies. Instances of limit cycle instability involving interaction between vehicle motion and shedding forces have also been noted (Reference1).

In June, 1965, S&ID began a six-month study to develop an analytical technique for determining the self-excited motion of an aeroelastic two-dimensional structure, as a necessary first step toward the ultimate objective of solving the three-dimensional problem of ground wind effects on aerospace vehicles. The approach to development of such a method was based on application of the potential flow theory to the study of separated wake flow. The exploratory nature of the study, coupled with its brevity, made it necessary to demonstrate the feasibility of this approach as quickly as possible. Correlation studies of pressure and velocity profiles on the cylinder and in the wake were therefore made using interim solutions having known discrepancies. The approximate agreement of these solutions with existing experimental data established confidence in the method, and successive refinements were made. Later in the study, significantly improved solutions were obtained, but time did not permit intensive analysis of these solutions.

This report presents a discussion of the basic problem of two-dimensional flow about circular cylinders and traces the development of the

theoretical method. A detailed account is given of the fundamental investigations, including development of shear layer in flow past a halfplane, symmetrical flow past a 10:1 ellipse normal to the stream, and symmetrical and unsymmetrical flow past a circular cylinder. Conclusions were reached based on correlating results of the theoretical solutions with experimental data, and specific recommendations are made for further study.

CONCLUSIONS

Incompressible separated flow past a two-dimensional, circular cylinder has been investigated on the basis of potential flow theory. It has been shown that the primary non-steady force characteristics can be adequately predicted in agreement with experimental data for subcritical Reynolds numbers, both for symmetrical flow and periodic vortex shedding.

It is believed that a numerically accurate solution with the approach utilized herein should correspond to the infinite Reynolds number case. However, the roughness of numerical integration techniques used to solve the problem have introduced a certain "insensitivity" to inherent instabilities. This insensitivity has produced an effect very similar to that of viscosity in real flow. The phenomenon is believed to be the same as that discussed by Takami (Reference 13). In this context, the flow solution for higher Reynolds numbers simply requires progressive improvement in the method of numerical integration. A quantitative definition of the practical maximum Reynolds number attainable by current computer capability remains to be established.

Computed pressure distributions on the cylinder contain local discontinuities as a result of limitations in the assumed mathematical model. Practical improvements can be made and conceptual details for implementing these improvements are presented.

The conclusion is made that the separated near wake flow past a circular cylinder is indeed essentially nonviscous. In the same sense that the Kutta condition makes possible the hydrodynamic analysis of airfoils by potential flow techniques, additional "conditions" are indicated to permit the analysis of separated wake flows with potential theory. Such analyses are made possible today by utilizing digital computers such as the IBM 7094 with its simultaneous tape, digital print and graphical output.

Compared with the relatively complete formulation of fluid flow by the Navier-Stokes equations, the potential flow theory appears simple and elementary. Yet it is this very simplicity that makes it a practical engineering tool. The versatility which such an approach provides cannot help but be important in leading to better understanding of separated flow mechanics.

It is hoped that these study results will stir further interest in better defining the role of Reynolds number in separated near wake flows.

RECOMMENDED AREAS OF FURTHER STUDY

REDUCTION OF PRESSURE DISCONTINUITIES

The total pressure distributions obtained in this study contain pressure discontinuities at the points of vortex sheet attachment to the cylinder. Consideration of means to alleviate this undesirable feature leads to a review of the somewhat arbitrary selection of the minimum pressure point as the vortex feeding point. To be more precise about this matter, it is noted that the transport of vorticity past any given point on the cylinder is $V_T^2/2$, where V_T is the local tangential velocity. Then the rate at which this transport is increasing or decreasing is $\frac{\partial}{2r\partial\theta}\left(V_T^2/2\right)$. The total vorticity in the boundary layer at this point is

$$\frac{1}{2}\int_{\text{stagnation point}}^{\text{flow detachment point}} \frac{\partial V_T^2}{\partial\theta}\, d\theta$$

If it can be assumed that vorticity in the boundary layer, once created, is not destroyed, then the feeding shear layer will grow from a surface area rather than a single point. This area is determined by those points at which $\frac{\partial\left(V_T^2/2\right)}{\partial\theta}$ is positive, with the strength distribution proportionate to its magnitude. Resorting again to the use of vortex sheets, several sheets could now be used with strengths proportional to the vorticity growth rate each sheet represents. In this manner, the single large pressure discontinuity could be reduced to several smaller ones in an improved idealization of the actual problem.

PRACTICAL TWO-DIMENSIONAL PROBLEMS

Aeroelastic Response of a Two-Dimensional Cylinder

General agreement of study results with experimental data has basically validated the analytical approach followed in this study. With the state of development achieved herein, it is believed that practical

two-dimensional problems may be treated. Of these, the aeroelastic response of a two-dimensional cylinder in separated flow is first considered. Evidence of self-excited motion of launch vehicles has been obtained in wind tunnel tests by Buell, Reference 21 and Reed, Reference 1. Thus a better understanding of the nature of this phenomenon is of importance to launch vehicle structural design.

Study of this problem would be subject to subcritical Reynolds number limitation as described in this report, and a rigid circular cylinder on elastic support with structural or viscous damping would be assumed. Within this framework, the nature of self-excited motion could be explored, and stability boundaries determined.

Lift on Bodies of Revolution

The subject of lift on bodies of revolution using the NACA analogy with flow about a two-dimensional cylinder may be investigated under the same subcritical Reynolds number limitation. Cylinder-cone frustum combinations as well as smooth ogival shapes could be investigated. Depending upon further limitations that may be encountered in such a study, the restriction to bodies of revolution may be extended to include those of elliptical cross section.

FURTHER DEVELOPMENT OF BASIC TECHNIQUE

Most important, in discussing areas of further study, it should be emphasized that the study approach developed herein demonstrates applicability of a basic technique for analysis of two-dimensional, incompressible, separated flow past bluff bodies. The technique is by no means completely developed. Investigations into the simulation of supercritical and transcritical Reynolds number flow conditions should be made to more fully determine the applicability of this technique. The technique of accounting for vorticity cancellation requires improvement. Relieving the pressure discontinuity by multiplex vortex feeding sheets may improve the flow solution. The flat plate problem should be investigated more thoroughly, since it is the one physical flow that does appear to be independent of Reynolds number.

It is stated, optimistically perhaps, that once the limitations of this approach are well understood, the application to separated, incompressible, two-dimensional flow problems in principle, would be straightforward.

VORTEX SHEDDING PROBLEM

Until recently, available experimental data on flow about the two-dimensional circular cylinders was limited to maximum Reynolds numbers on the order of one or two million (Reference 2). These data consistently show that periodic vortex shedding occurs at Reynolds numbers in the approximate range between 100 and 100,000. At higher Reynolds numbers the periodicity degenerates into a random shedding. Significantly, the mean drag coefficient also undergoes a large drop together with loss in periodicity as Reynolds number is increased through this critical range. Although a classical explanation was developed for the large decrease in drag coefficient, a concomitant explanation for the loss in periodicity of vortex shedding could not be developed. In the face of these data it appears to have been generally concluded that the loss in periodicity was permanent beyond the critical Reynolds number (Reference 3). The reason for this loss was best explained simply as a Reynolds number effect. It remained an enigma until Roshko, in 1960 (Reference 2), performed tests on a circular cylinder at Reynolds numbers up to ten million. In these tests, periodic vortex shedding appeared once more at Reynolds number of 3.5 million and persisted to all higher test values. Roshko identified this range above 3.5×10^6 to infinity as the transcritical range.

This experimental finding was of far-reaching significance, for with it Roshko was able to postulate a far more complete explanation of periodic vortex shedding than had heretofore been possible. It meant that periodic vortex shedding is characteristic of cylinder cross-flow at all Reynolds numbers above 100 except for a relatively narrow region between approximately 100,000 and 3.5 million. The supercritical Reynolds number range of random vortex shedding is confined to this relatively narrow region. A tentative explanation for the basic cause of randomness of vortex shedding in this supercritical region is given in Reference 2. The randomness results from the fact that the point of shear layer transition from laminar to turbulent flow moves forward from the wake region toward the separation point as supercritical Reynolds number is approached. In the supercritical range, a laminar separation may be followed by reattachment if boundary layer transition to turbulence can occur closely enough. The result is a separation bubble whose position is highly sensitive to small perturbations in local pressure. The findings of Spitzer (Reference 4) and Tani (Reference 5) substantiate this point of view. Perhaps the most profound conclusion to be drawn from these observations is that the periodic nature of vortex shedding is basically not dependent upon Reynolds number, except for secondary

characteristics. For example, the subcritical Strouhal number for a circular cylinder is about 0.2 whereas at transcritical Reynolds number its value is 0.27 (Reference 2).

Further indication that periodic vortex shedding may not be Reynolds-number dependent is obtained from Reference 6. In this work, Abernathy and Kronauer show that two parallel vortex sheets a distance h apart roll up into a vortex street following an initial disturbance. Their analysis utilized numerical solutions of potential flow equations for discrete vortex approximations of the vortex sheets.

Finally, these basic considerations combine to reinforce Prandtl's original observation (Reference 7) that "...the flow about a solid body can be divided into two regions: a very thin layer in the neighborhood of the body (boundary layer) where friction plays an essential part, and the remaining region outside this layer, where friction may be neglected."

Interpreted with a certain degree of optimism, an exciting possibility has thus been afforded the application of potential flow theory to the analysis of separated wake flow. The key to its successful application must be in the proper simulation of vorticity transport from the boundary layer. The study of separated wake flows based directly upon the Navier-Stokes equation is certainly the most exact approach. However the use of potential theory has certain distinctive features making its application attractive.

First, the numerical techniques used to effect solutions of the Navier-Stokes equations are limited by computer capacity and computational speed to investigation of fairly low Reynolds number flows.

Second, if successful, the use of potential theory in solving periodic vortex shedding should establish the nature of its independence from Reynolds number.

Third, the potential theory, being basically simple in application, should prove correspondingly versatile in providing insight to the mechanics of vortex formation and shedding.

THEORETICAL DEVELOPMENT

The velocity field about a source-sink circular cylinder in a field of free vortices, some of which are growing, is developed with potential theory. Non-steady pressures in the field and forces on the cylinder are then derived. These are extended to the case of an elliptical cylinder by the use of conformal transformations.

CIRCULAR CYLINDER

Flow Field for a System of Vortices Outside a Circular Cylinder in Uniform Flow

For incompressible, inviscid, irrotational, two-dimensional flow, the flow field may be described by a potential function of the complex variable ($z = x + iy$). The complex potential, $w(z)$, of a system of vortices outside a circular cylinder of radius "a" in a uniform stream may be written as the sum of two potentials

where $$w(z) = w_1(z) + w_2(z)$$

$w_1(z)$ ~ uniform flow past a circular cylinder ($r = a$) at angle of attack

$w_2(z)$ ~ system of vortices outside a circular cylinder ($r = w$)

The velocity components are found from the relation

$$(u - iv) = -\frac{dw(z)}{dz} \tag{1}$$

From Reference (8), $w_1(z)$ and $w_2(z)$ are found to be

$$w_1(z) = -U_o \left[ze^{-i\alpha} + \frac{a^2}{z} e^{i\alpha} \right] \tag{2}$$

and for n vortices

$$w_2(z) = -i \sum_{j=1}^{n} K_j \log (z-z_j) + i \sum_{j=1}^{n} K_j \log \left(z - \frac{a^2}{z_j} \right)$$

$$-i \sum_{j=1}^{n} K_j \log z + i \sum_{j=1}^{n} K_j \log \bar{z}_j \qquad (3)$$

where $K_j \sim$ strength of the j^{th} vortex filament—positive rotation taken clockwise.

For a vortex outside the cylinder at $z = z_j$ the position of the image vortex inside the cylinder $\frac{a^2}{z_j}$, will be denoted;

$$z_j^i = \frac{a^2}{z_j} = \frac{a^2 (x_j + iy_j)}{x_j^2 + y_j^2} \qquad (3a)$$

therefore

$$x_j^i = \frac{a^2 x_j}{x_j^2 + y_j^2} \quad y_j^i = \frac{a^2 y_j}{x_j^2 + y_j^2}$$

The velocity of the m^{th} vortex filament outside the circular cylinder is given by

$$(u-iv)_m = - \left\{ \frac{d}{dz} \left[w_2(z) - iK_m \log (z-z_m) \right] + \frac{dw_1(z)}{dz} \right\}$$

$$= i \sum_{\substack{j=1 \\ j \neq m}}^{n} \frac{K_j}{z_m - z_j} - i \sum_{j=1}^{n} \frac{K_j}{z_m - z_j^i} + i \sum_{j=1}^{n} \frac{K_j}{z_m}$$

$$+ U_o \cos \alpha \left(1 - \frac{a^2}{z_m^2} \right) - iU_o \sin \alpha \left(1 + \frac{a^2}{z_m^2} \right) \qquad (4)$$

The third summation term above, while correctly obtained by the circle theorem, is henceforth excluded by virtue of the condition that total circulation in the fluid region remains zero. Separating Eq. (4) into real and imaginary parts gives the velocity components in non-dimensional form

$$\left(\frac{u}{U_o}\right)_m = \sum_{\substack{j=1 \\ j\neq m}}^{n} \left(\frac{K_j}{U_o a}\right)\left[\frac{y_m - y_j}{(x_m - x_j)^2 + (y_m - y_j)^2}\right]$$

$$- \sum_{j=1}^{n} \left(\frac{K_j}{U_o a}\right)\left[\frac{y_m (x_j^2 + y_j^2) - y_j}{1 - 2(x_j x_m + y_j y_m) + (x_m^2 + y_m^2)(x_j^2 + y_j^2)}\right]$$

$$+ \left[1 - \frac{x_m^2 - y_m^2}{(x_m^2 + y_m^2)^2}\right]\cos\alpha - \frac{2x_m y_m}{(x_m^2 + y_m^2)^2}\sin\alpha \qquad (5)$$

and

$$\left(\frac{v}{U_o}\right)_m = - \sum_{\substack{j=1 \\ j\neq m}}^{n} \left(\frac{K_j}{U_o a}\right)\frac{x_m - x_j}{(x_m - x_j)^2 + (y_m - y_j)^2}$$

$$+ \sum_{j=1}^{n} \left(\frac{K_j}{U_o a}\right)\left[\frac{x_m (x_j^2 + y_j^2) - x_j}{1 - 2(x_j x_m + y_j y_m) + (x_m^2 + y_m^2)(x_j^2 + y_j^2)}\right]$$

$$- \left[\frac{2x_m y_m}{(x_m^2 + y_m^2)^2}\right]\cos\alpha + \left[1 + \frac{x_m^2 - y_m^2}{(x_m^2 + y_m^2)^2}\right]\sin\alpha \qquad (6)$$

where the lengths have been nondimensionalized by the radius (r=a).

Pressure Coefficient

The pressure equation for incompressible, inviscid, irrotational flow under conservative forces is

$$\frac{P}{\rho} + \frac{1}{2}q^2 + \Omega - \frac{\partial \phi}{\partial t} = C(t) \tag{7}$$

If there are no body forces ($\Omega = 0$) and the flow is steady at $x = \infty$, Equation (7) becomes

$$\frac{P}{\rho} + \frac{1}{2}q^2 - \frac{\partial \phi}{\partial t} = C_o \tag{8}$$

where

$$C_o = \left[\frac{P}{\rho} + \frac{1}{2}q^2\right]_{x=\infty}$$

The pressure coefficient is

$$C_p = \frac{p-p_\infty}{\rho q^2/2} = \left[1 - \left(\frac{q}{q_\infty}\right)^2\right] + \frac{2}{q_\infty^2}\frac{\partial \phi}{\partial t} \tag{9}$$

For the situation described for a system of vortices outside a circular cylinder in uniform flow, the velocity potential, ϕ, may be found from the complex potential w(z).

$$w(z) = w_1(z) + w_2(z) = \phi(z) + i\psi(z) \tag{9a}$$

where

$$\phi(z) = \phi_1(z) + \phi_2(z) = \text{velocity potential}$$

$$\psi(z) = \psi_1(z) + \psi_2(z) = \text{stream function}$$

Since

$$w_1(z) = -U_o\left[ze^{-i\alpha} + \frac{a^2}{z}e^{i\alpha}\right] \tag{10}$$

therefore, on the cylinder $(z = ae^{i\theta})$,

$$w_1 = -2U_o \cos(\theta - \alpha) = \phi_1 \tag{11}$$

when $\alpha = 0$

$$\phi_1(x, y) = -2U_o \cos\theta = -2U_o x$$

The complex potential due to the vortex system may be written

$$w_2(z) = -i\sum_{j=1}^{n} K_j \left[\log|z - z_j| + i\theta_{(z-z_j)}\right]$$

$$+ i\sum_{j=1}^{n} K_j \left[\log|z - z_j^i| + i\theta_{\left(z-z_j^i\right)}\right]$$

$$+ i\sum_{j=1}^{n} K_j \left[\log|\bar{z}_j| + i\theta_{\left(\bar{z}_j\right)}\right] \tag{12}$$

where

$$\log|z - z_j| = \log\left[(x - x_j)^2 + (y - y_j)^2\right]^{1/2}$$

$$\theta_{(z-z_j)} = \tan^{-1}\left(\frac{y - y_j}{x - x_j}\right)$$

thus

$$\theta_2(z) = \sum_{j=1}^{n} K_j \left[\tan^{-1}\left(\frac{y - y_j}{x - x_j}\right) - \tan^{-1}\left(\frac{y - y_j^i}{x - x_j^i}\right) - \tan^{-1}\left(-\frac{y_j}{x_j}\right) \right] \qquad (13)$$

The velocity potential, ϕ, on the cylinder $(r = a)$ becomes

$$\phi(x, y) = \phi_1(x, y) + \phi_2(x, y)$$

$$= -2U_o \cos(\theta - \alpha)$$

$$+ \sum_{j=1}^{n} K_j \left[\tan^{-1}\left(\frac{y - y_j}{x - x_j}\right) - \tan^{-1}\left(\frac{y - y_j^i}{x - x_j^i}\right) - \tan^{-1}\left(-\frac{y_j}{x_j}\right) \right] \qquad (14)$$

Differentiating with respect to time at a particular point on the cylinder (x, y are fixed) with K_j a function of time gives,

$$\left.\frac{\partial \phi}{\partial t}\right|_{x,y} = U_o^2 \sum_{j=1}^{n} \left(\frac{K_j}{U_o a}\right) \left[\frac{(y - y_i)u_j - (x - x_j)v_j}{(x - x_j)^2 + (y - y_j)^2} + \frac{\left(x - x_j^i\right)v_j^i - \left(y - y_j^i\right)u_j^i}{\left(x - x_j^i\right)^2 + \left(y - y_j^i\right)^2} + \frac{x_j v_j - y_j^i u_j}{x_j^2 + y_j^2} \right]$$

$$+ U_o^2 \sum_{j=1}^{n} \frac{\partial\left(\frac{K_j}{U_o a}\right)}{\partial t} \left[\tan^{-1}\left(\frac{y - y_j}{x - x_j}\right) - \tan^{-1}\left(\frac{y - y_j^i}{x - x_j^i}\right) - \tan^{-1}\left(\frac{-y_j}{x_j}\right) \right] \qquad (15)$$

where the velocities have been put in nondimensional form by division by (U_o) and the lengths have been nondimensionalized by dividing by $(r=a)$, and

$$u_j^i \equiv \frac{dx_j^i}{dt} = \frac{1}{\left(x_j^2 + y_i^2\right)^2}\left[\left(y_j^2 - x_j^2\right)u_j - 2x_j\, y_j\, v_j\right]$$

$$v_j^i \equiv \frac{dy_j^i}{dt} = \frac{1}{\left(x_j^2 + y_j^2\right)^2}\left[\left(x_j^2 - y_j^2\right)v_j - 2x_j\, y_j\, u_j\right] \qquad (16)$$

The pressure coefficient $C_p(x, y)$ at a particular point (x_k, y_k) on the cylinder becomes, $(q_\infty = U_o)$

$$C_p(x_k, y_k) = \left[1 - \left(u_k^2 + v_k^2\right)\right]$$

$$+2\sum_{j=i}^{n}\left(\frac{K_j}{U_o a}\right)\left[\frac{(y_k - y_j)u_j - (x_k - x_j)v_j}{(x_k - x_j)^2 + (y_k - y_j)^2} + \frac{\left(x_k - x_j^i\right)v_j^i - \left(y_k - y_j^i\right)u_j^i}{\left(x_k - x_j^i\right)^2 + \left(y_k - y_j^i\right)^2} + \frac{x_j v_j - y_j u_j}{x_j^2 + y_j^2}\right]$$

$$+2\sum_{j=1}^{w}\frac{\partial\left(\frac{K_j}{U_o a}\right)}{\partial t}\left[\tan^{-1}\left(\frac{y_k - y_j}{x_i - x_j}\right) - \tan^{-1}\left(\frac{y_k - y_j^i}{x_k - x_j^i}\right) - \tan^{-1}\left(\frac{-y_j}{x_j}\right)\right] \qquad (17)$$

Forces

The forces may be computed by integration of Equation (17) about the circular cylinder, but it is found that the following analysis greatly simplifies the problem.

For the case of a fixed cylinder in steady, irrotational flow the force components (D, L), neglecting external forces, are given by the Blasius theorem.

$$D - iL = \frac{1}{2} i\rho \oint \left(\frac{dw}{dz}\right)^2 dz \tag{18}$$

where

D = force component in positive x-direction

L = force component in positive y-direction

w(z) = complex potential

ρ = density

When the motion is not steady the term $\rho\, \partial\phi/\partial t$, where ϕ = velocity potential, is contained in the pressure equation, and Equation (18) must be modified by the addition of the term

$$-i\rho \oint \frac{\partial \phi}{\partial t} d\bar{z} = -i\rho \frac{\partial}{\partial t} \oint \bar{w}\, d\bar{z} \tag{19}$$

which then gives

$$D - iL = \frac{1}{2} i\rho \oint \left(\frac{dw}{dz}\right)^2 dz - i\rho \frac{\partial}{\partial t} \oint \bar{w}\, d\bar{z} \tag{20}$$

Equation (20) may be evaluated in two parts

$$D = D_1 + D_2$$

$$L = L_1 + L_2$$

where

$$D_1 - iL_1 = \frac{\rho}{2} \oint \left(\frac{dw}{dz}\right)^2 dz \tag{21}$$

and

$$D_2 + iL_2 = i\rho \frac{\partial}{\partial t} \oint w \, dz \tag{22}$$

Equation (21) may be found from an extension of Lagally's theorem to a system of vortex filaments outside a circular cylinder, thus

$$D_1 = -2\pi\rho \sum_{j=1}^{n} K_j (U_o \sin\alpha - v_j) \tag{23}$$

$$L_1 = 2\pi\rho \sum_{j=1}^{n} K_j (U_o \cos\alpha - u_j) \tag{24}$$

The second integral (Equation 22) may be evaluated by first differentiating under the integral. The complex potential $w(z)$ is

$$w(z) = -U_o \left[z\, e^{-i\alpha} + \frac{a^2}{z} e^{i\alpha} \right] - i \sum_{j=1}^{n} K_j \left[\log (z - z_j) \right.$$

$$\left. - \log \left(z - z_j^i \right) - \log \bar{z}_j \right] \tag{25}$$

In general, U_o and K_j may be functions of time, e.g.,

$U_o = U_o(t)$ for a cylinder started impulsively or for a cylinder in accelerated motion.

Differentiating Equation (25) with respect to time for z-fixed gives,

$$\left.\frac{\partial w}{\partial t}\right|_z = -\left[ze^{-i\alpha} + \frac{a^2}{z}e^{i\alpha}\right]\frac{\partial U_o}{\partial t}$$

$$+ i\sum_{j=1}^{n}\frac{\partial K_j}{\partial t}\left[\log(z - z_j) - \log(z - z_j^i) + \log\left(\frac{z}{\bar{z}_j}\right)\right]$$

$$-1\sum_{j=i}^{n} K_j\left[-\frac{1}{z - z_j}\frac{\partial z_j}{\partial t} + \frac{1}{z - z_j^i}\frac{\partial z_j^i}{\partial t} - \frac{1}{\bar{z}_j}\frac{\partial \bar{z}_j}{\partial t}\right] \qquad (26)$$

where

$$\frac{\partial z_j}{\partial t} = u_j + iv_j$$

$$\frac{\partial z_j^i}{\partial t} = u_j^i + iv_j^i$$

and

u_j , v_j ~ velocity components of j^{th} vortex

u_j^i , v_j^i ~ velocity components of the image of the j^{th} vortex

The integral becomes

$$i\rho\oint\frac{\partial w}{\partial t}\,dz = i\rho\oint -\left(ze^{-i\alpha} + \frac{a^2}{z}e^{i\alpha}\right)\frac{\partial U_o}{\partial t}\,dz$$

(Continued on next page)

$$+ i\rho \oint \left[- i \sum_{j=1}^{n} \frac{\partial K_i}{\partial t} \left\{ \begin{array}{l} \log (z - z_j) - \log (z - z_j^i) + \\ \log (z) - \log (\bar{z}_j) \end{array} \right\} \right] dz$$

$$+ i\rho \oint \left[- i \sum_{j=1}^{n} K_j \left\{ \frac{-1}{z - z_j} \frac{\partial z_j}{\partial t} + \frac{1}{z - z_j^i} \frac{\partial z_j^i}{\partial t} - \frac{1}{\bar{z}_j} \frac{\partial \bar{z}_j}{\partial t} \right\} \right] dz$$

$$= I_1 + I_2 + I_3 \tag{27}$$

Utilizing the "residue theorem" from complex analysis, the integral about the unit circle $(z = e^{i\theta})$ becomes

$$I_1 = i\rho \oint - \left[ze^{i\alpha} + \frac{a^2}{z} e^{i\alpha} \right] \frac{\partial U_o}{\partial t} dz$$

$$I_1 = 2\pi\rho a^2 \frac{\partial U_o}{\partial t} e^{i\alpha} \tag{28a}$$

and

$$I_3 = \rho \sum_{j=1}^{w} K_j \oint \left[\frac{-1}{z - z_j} \frac{dz_j}{dt} + \frac{1}{z - z_j^i} \frac{dz_j^i}{dt} - \frac{1}{\bar{z}_j} \frac{d\bar{z}_j}{dt} \right] dz$$

$$I_3 = i\, 2\pi\rho \sum_{j=1}^{w} K_j \frac{dz_j^i}{dt}$$

$$I_3 = 2\pi\rho \sum_{j=1}^{w} K_j \left(iu_j^i - v_j^i \right) \tag{28b}$$

The second integral, I_2, must be treated in a different manner. One part of the integral vanishes:

$$i\rho \oint \left[-i \sum_{j=1}^{w} \frac{\partial K_j}{\partial t} \left\{ \log (z - z_j) - \log \bar{z}_j \right\} \right] dz = 0 \qquad (28c)$$

since the integrand is analytic at every point within and on the unit circle.

The remaining contribution cannot be evaluated by residues since the log function does not have an isolated singularity; thus, we have to integrate directly. Outside the unit circle the function, $\log \left[(z - z_j^i)/z \right]$, has the following expansion

$$- \log \left(1 - \frac{z_j^i}{z} \right) = \frac{z_j^i}{z} + \frac{1}{2} \left(\frac{z_j^i}{z} \right)^2 + \frac{1}{3} \left(\frac{z_j^i}{z} \right)^3 + \cdots \qquad (28d)$$

Integrating this series term by term about a circle $(r = R > 1)$ results in

$$- \oint \log \left(1 - \frac{z_j^i}{z} \right) dz = 2\pi i z_j^i$$

$$|z| = R$$

Since the function is analytic in the annulus $(1 \leq |z| \leq R)$

$$- \oint \log \left(1 - \frac{z_j^i}{z} \right) dz = 2\pi i z_j^i$$

$$|z| = a$$

therefore

$$I_2 = i\rho \oint \left[-i \sum_{j=1}^{w} \frac{\partial K_j}{\partial t} \left\{ \begin{array}{l} \log (z - z_j) - \log \bar{z}_j \\ \\ -\log \dfrac{z - z_j^i}{z} \end{array} \right\} \right] dz$$

$$I_2 = \rho \sum_{j=1}^{w} \frac{\partial K_j}{\partial t} \oint - \log\left(\frac{z - z_j^i}{z}\right) dz$$

$$I_2 = 2\pi\rho \sum_{j=1}^{w} i z_j^i \frac{\partial K_j}{\partial t} = 2\pi\rho \sum_{j=1}^{w} \left(i x_j^i - y_j^i\right) \frac{\partial K_j}{\partial t} \tag{28e}$$

Therefore

$$D_2 + iL_2 = I_1 + I_2 + I_3$$

$$= \left[2\pi\rho\, a^2 \frac{\partial U_o}{\partial t} e^{i\alpha} - 2\pi\rho \sum_{j=1}^{n} y_j^i \frac{\partial K_j}{\partial t} - 2\pi\rho \sum_{j=1}^{n} K_j v_j^i \right]$$

$$+ i \left[2\pi\rho \sum_{j=1}^{n} x_j^i \frac{\partial K_i}{\partial t} + 2\pi\rho \sum_{j=1}^{n} K_j u_j^i \right] \tag{29}$$

or

$$D_2 = 2\pi\rho \left[a^2 \frac{\partial U_o}{\partial t} \cos\alpha - \sum_{j=1}^{n} \left(y_j^i \frac{\partial K_j}{\partial t} + K_j u_j^i \right) \right]$$

$$L_2 = 2\pi\rho \left[a^2 \frac{\partial U_o}{\partial t} \sin\alpha + \sum_{j=1}^{n} \left(x_j^i \frac{\partial K_j}{\partial t} + K_j u_j^i \right) \right] \tag{30}$$

The total forces are

$$D = D_1 + D_2$$

$$= 2\pi\rho \left[\sum_{j=1}^{n} K_j \left(-U_o \sin\alpha + v_j - v_j^i - \sum_{j=1}^{n} y_j^i \frac{\partial K_j}{\partial t} + a^2 \frac{U_o}{t} \cos\alpha \right] \right. \quad (31)$$

and

$$L = L_1 + L_2$$

$$= 2\pi\rho \left[\sum_{j=1}^{n} K_j \left(U_o \cos\alpha - u_j + u_j^i \right) + \sum_{j=1}^{n} x_j^i \frac{\partial K_j}{\partial t} + a^2 \frac{\partial U_o}{\partial t} \sin\alpha \right] \quad (32)$$

The above evaluation of I_2, while considered to be mathematically correct, is subject to further scrutiny. The principal objection is that evaluation of I_2 in this manner violates physical aspects of the problem. This is made clearer by the following discussion of physical implications involved. The crucial point to be made is that a vortex cannot simply grow without some means to provide for its growth.

In the ideal fluid framework of this study, this growth rate is provided by a vortex sheet connecting the growing vortex to some boundary point. The product of the average of the velocities on either side of this sheet and the strength distribution represents the rate at which the vorticity is being fed to the growing vortex.

Thus

$$2\pi \frac{\partial K}{\partial t} = \left(\frac{U_1 + U_2}{2} \right) \left(U_1 - U_2 \right) = \frac{U_1^2 - U_2^2}{2} = \frac{1}{2} \alpha^2$$

where U_1 and U_2 are velocities on either side of the vortex sheet.

Now, if the integral expression of Equation (28c) around the unit circle is to be zero, the feeding sheet attached to the growing vortex at z_j cannot be connected to the circle, since this would cause a branch point and a non-zero integral value. Only one other possibility exists; the vortex sheet must

extend to infinity. Vortices in the interior of the circle are governed by the circle theorem, so the image vortex must be connected by a vortex sheet to the center.

If the strength distribution of the external vortex sheet is assumed to be finite at all points, the "image" sheet reaches an infinite strength distribution at the center.

But the integral expression of Equation (28C) is not defined along the branch cut. Mathematical development has not been carried out for incorporating distributed singularities along the branch cut corresponding to this vortex sheet. Even without this development it is clear that this system does not represent the physical situation of a growing vortex being fed from vorticity generated within the boundary layer. This result, with its shortcomings, are presented herein primarily because it has apparently been used elsewhere in the literature in determining forces on a cylinder in a field of moving and growing vortices (Reference 9).

A more plausible representation of the physical situation is one wherein the external vortex is attached to the cylinder surface. By the circle theorem, the image vortex is also attached to the cylinder surface by a vortex sheet of opposite sign.

Rather than employ the Blasius theorem to determine cylinder forces for this system, recourse is had to an approach similar to that employed by Bryson (Reference 10) and explained conceptually in Reference 11. Accordingly, the impulse of a pair of vortices of equal and opposing strength located a distance, Δz , apart, is

$$I_j = i\,2\pi\rho K_j\ \Delta z_j \tag{32.1}$$

Since each discrete vortex has its "image" within the circle, the impulse from all the vortices in the field may be described by superposition of such elementary impulses. If the external vortices are all free, the force acting on the cylinder then becomes the time derivative of this impulse.

$$D + iL = \frac{dI}{dt} \tag{32.2}$$

where

$$I = i\,2\pi\rho \sum_{j=1}^{n} K_j\,(z_j - z_j^i) \tag{32.3}$$

hence

$$D - iL = i2\pi\rho \left[\sum_{j=1}^{n} K_j \left(\dot{z}_j - \dot{z}_j^i \right) + \sum_{j=1}^{n} \frac{\partial K_j}{\partial t} \left(z_j - z_j^i \right) \right] \qquad (32.4)$$

It is seen that the first summation term in Equation (32.4) agrees with the corresponding term in Equations (31) and (32) derived by the Blasius theorem. But the second term, containing the vorticity growth rate, involves the complex distance between each external vortex and its respective image. Certain fundamental investigations were made in this study to learn the significance of components in the second term. These are discussed in a subsequent section of this report.

ELLIPTICAL CYLINDER

Flow Field for a System of Vortices Outside an Elliptical Cylinder in Uniform Flow

The previous analysis for the circular cylinder may be extended to the case of an elliptical cylinder by a conformal transformation. The circular cylinder is mapped into an elliptical cylinder by the well-known Joukowski transformation.

In the plane of the circular cylinder, say the z_1-plane, the circle of radius $r_o = (a+b)/2$ is mapped by the transformation

$$z = z_1 + \frac{C^2}{4z_1} \quad \text{where} \quad C^2 = a^2 - b^2 \qquad (33)$$

into an ellipse in the z-plane with major axis, 2a, and minor axis, 2b.

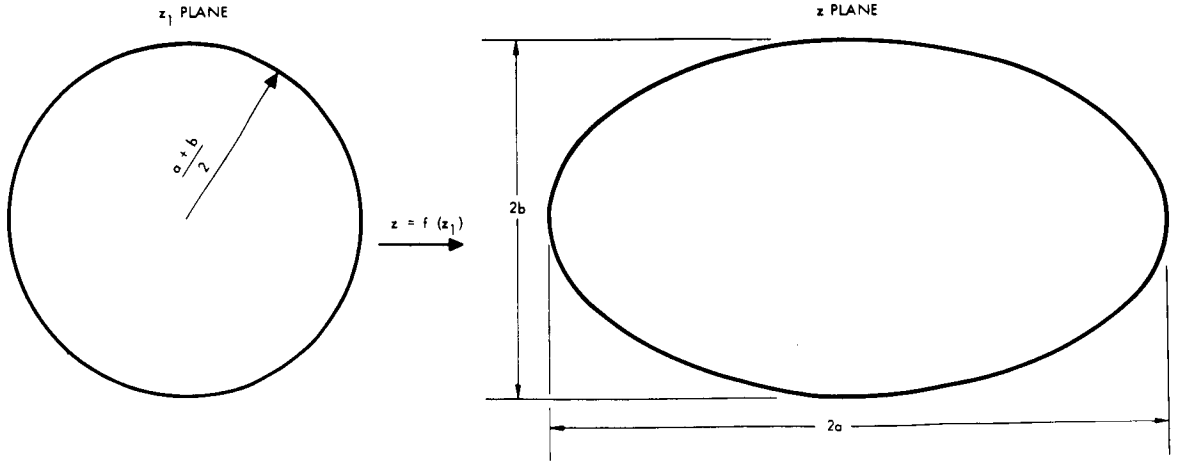

When $b \to 0$ we have the degenerate case of a flat plate of length 2a in the z-plane.

The velocity field in the z-plane is completely determined from the z_1-plane and the mapping transformation. For a general system of vortices in the z-plane (plane of ellipse), the velocity of the m^{th} vortex is

$$(u - iv)_m = \frac{dF(z)}{dz} \tag{34}$$

where

$$F(z) = -w(z_1) + iK_m \log (z - z_m) \tag{35}$$

and from Equations (2) and (3);

$$w(z_1) = -i \sum_{j=1}^{n} K_j \left[\log (z_1 - z_{1j}) - \log \left(z_1 - \frac{1}{\bar{z}_{ij}} \right) + \log z_1 - \log \bar{z}_{ij} \right]$$

$$- U_o \left[z_1 e^{-i\alpha} + \frac{1}{z_1} e^{i\alpha} \right] \tag{36}$$

where the circle in the z_1-plane is chosen to have unit radius.

Therefore

$$z = \left(\frac{a+b}{2} \right) z_1 + \left(\frac{a-b}{2} \right) \frac{1}{z_1}$$

The derivative, $\frac{dF(z)}{dz}$, may be written

$$\frac{dF(z)}{dz} = \frac{dF(z)}{dz_1} \frac{dz_1}{dz} \tag{37}$$

where the mapping function is

$$z = f(z_1)$$

and

$$\frac{dz}{dz_1} = \frac{df(z_1)}{dz_1} = f'(z_1) \tag{38}$$

From Equations (35) and (36)

$$\frac{dF(z)}{dz_1} = i \sum_{j=1}^{n} K_j \left[\frac{1}{z_1 - z_{1j}} - \frac{\bar{z}_{1j}}{z_1 \bar{z}_{1j} - 1} + \frac{1}{z_1} \right] + U_o \cos\alpha \left(1 - \frac{1}{z_1^2} \right) - i U_o \sin\alpha \left(1 + \frac{1}{z_1^2} \right) - \frac{i K_m f'(z_1)}{f(z_1) - f\left(z_{1_m}\right)} \tag{39}$$

Thus,

$$\left.\frac{dF(z)}{dz}\right|_{z=z_m} = \left[i \sum_{j=1}^{n} K_j \left(\frac{1}{z_1 - z_{1j}} - \frac{z_{ij}}{z_1 \bar{z}_{1j} - 1} + \frac{1}{z_1} \right) + U_o \cos\alpha \left(1 - \frac{1}{z_1^2} \right) - i U_o \left(1 + \frac{1}{z_1^2} \right) - \frac{i K_m f'(z_1)}{f(z_1) - f(z_{1m})} \right]_{z_1 = z_{1m}} \times \left(\frac{1}{f'(z_1)} \right)_{z_1 = z_{1m}} \tag{40}$$

The first and last terms in the brackets have singularities when $z_1 = z_{1m}$, but the other terms are regular if $|z_1| > 1$. Rewriting Equation (40)

$$\left.\frac{dF(z)}{dz}\right|_{z=z_m} = F'(z_m)$$

$$= \frac{1}{f'(z_{1m})} \left\{ i \sum_{\substack{j=1 \\ j\neq m}}^{n} \frac{K_j}{z_{1m}-z_{ij}} - i \sum_{j=1}^{n} \frac{K_j}{z_{1m}(z_{1m}\bar{z}_{1j} - 1)} \right.$$

$$+ U_o \cos\alpha \left(1 - \frac{1}{z_1^2}\right) - i U_o \sin\alpha \left(1 - \frac{1}{z_1^2}\right) \tag{41}$$

$$\left. + i K_m \left[\frac{1}{z_1 - z_{1m}} - \frac{f'(z_1)}{f(z_1) - f(z_{1m})} \right]_{z_1=z_{1m}} \right\}$$

Expanding $f(z_1)$ in a Taylor's series about the point $z_1=z_{1m}$ results in

$$\left[\frac{1}{z_1 - z_{1m}} - \frac{f'(z_1)}{f(z_1)-f(z_{1m})} \right]_{z_1=z_{1m}} = \frac{1}{2} \frac{f''(z_{1m})}{f'(z_{1m})} \tag{42}$$

Finally

$$(u-iv)_m = F'(z_m)$$

$$= \frac{1}{f'(z_m)} \left[i \sum_{\substack{j\neq m \\ j=1}}^{n} \frac{K_j}{z_{1m}-z_{ij}} - i \sum_{j=1}^{n} z_{1m} \frac{K_j}{(z_{1m}\bar{z}_{ij}-1)} \right. \tag{43}$$

Continued on next page

$$+ U_o \cos\alpha \left(1 - \frac{1}{z_1^2}\right) - iU_o \sin\alpha \left(1 + \frac{1}{z_1^2}\right)$$

$$+ \frac{iK_m}{2} \frac{f''(z_{1m})}{f'(z_{1m})}\Bigg]$$

Forces

The steady forces were found earlier from Lagally's theorem.

$$D_1 = -2\pi\rho \sum_{j=1}^{n} K_j (U_o \sin\alpha - v_j)$$

$$L_1 = 2\pi\rho \sum_{j=1}^{n} K_j (U_o \cos\alpha - u_j) \qquad (44)$$

The unsteady forces are found in the same way. From Equation (22) the unsteady components D_2 and L_2 are

$$D_2 + iL_2 = i\rho \oint \frac{\partial w}{\partial t}\, dz \qquad (45)$$

Unlike the steady forces, the unsteady effects must be evaluated in the z-plane, since the operator, $\partial/\partial t$, is not transformed in a one-to-one way in any conformal transformation (Reference 12). The complex potential in the z_1-plane is

$$w(z_1) = -i \sum_{j=1}^{n} K_j \Big[\log (z_1 - z_{1j}) - \log (z_1 - z'_{1j})$$

$$+ \log z_1 - \log \bar{z}_{1j}\Big] - U_o \left[z_1 e^{-i\alpha} + \frac{1}{z_1} e^{i\alpha}\right]$$

where

$$z'_{1j} \equiv \frac{1}{z_{1j}} \tag{46}$$

The inverse of the Joukowski transformation is

$$z_1 = \frac{1}{2}\left[z \pm \sqrt{z^2 - C^2}\right] \tag{47}$$

where

$$C^2 = a^2 - b^2$$

and

$z_1 = \frac{1}{2}\left[z + \sqrt{z^2 - c^2}\right] \sim$ maps points outside the circle into points outside the ellipse

$z_1 = \frac{1}{2}\left[z - \sqrt{z^2 - C^2}\right] \sim$ maps points inside the circle into points inside the ellipse

making the substitutions into Equation 46

$$w(z) = -i \sum_{j=i}^{n} K_j \log\left[\frac{1}{2}\left(z \pm \sqrt{z^2 - C^2}\right) - \frac{1}{2}\left(z_j + \sqrt{z_j^2 - C^2}\right)\right]$$

$$+ i \sum_{j=i}^{n} K_j \log\left[\frac{1}{2}\left(z \pm \sqrt{z^2 - C^2}\right) - \frac{1}{2}\left(z_j' - \sqrt{z_j^2 - C^2}\right)\right] \tag{48}$$

Continued on next page

$$- i \sum_{j=i}^{n} K_j \log \left[\frac{1}{2} \left(z \pm \sqrt{z^2 - C^2} \right) \right]$$

$$+ i \sum_{j=i}^{n} K_j \log \left(\frac{1}{2} \left(z_j + \sqrt{z_j^2 - C^2} \right) \right.$$

$$- U_o \left[\frac{1}{2} \left(z + \sqrt{z^2 - C^2} \right) e^{-i\alpha} + \frac{1}{\frac{1}{2} \left(z + \sqrt{z^2 - C^2} \right)} e^{i\alpha} \right] \qquad (48)$$

Differentiating w(z) with respect to time with z fixed gives

$$\left. \frac{dw}{dt} \right|_z = - i \sum_{j=i}^{n} K_j \frac{\left[- \frac{dz_j}{dt} - z_j \frac{dz_j}{dt} \Big/ \sqrt{z_j^2 - C^2} \right]}{\left[(z - z_j) - \left(\sqrt{z^2 - C^2} + \sqrt{z_j^2 - C^2} \right) \right]}$$

$$+ i \sum_{j=i}^{n} K_j \frac{\left[- \frac{dz'_j}{dt} + z'_j \frac{dz'_j}{dt} \Big/ \sqrt{z'^2_j - C^2} \right]}{\left[(z - z'_j) - \left(\sqrt{z_i^2 - C^2} - \sqrt{z_j^2 - C^2} \right) \right]} \qquad (49)$$

$$+ \left\{ \begin{array}{l} \text{terms which do not contribute singularities to} \\ \text{the derivative, i. e., analytic inside the} \\ \text{ellipse} \end{array} \right\}$$

Thus

$$D_2 + i L_2 = i\rho \oint \frac{\partial w}{\partial t}\, dz$$

$$D_2 + i L_2 = -\rho \sum_{j=1}^{w} K_j \oint \left\{ \frac{\left((1 + z_j / \sqrt{z_j^2 - c^2} \right) \frac{dz_j}{dt}}{\left[(z - z_j) - \left(\sqrt{z^2 - c^2} - \sqrt{z_j^2 - c^2} \right) \right]} \right. \tag{50}$$

$$\left. - \frac{\left(1 - z_j' / \sqrt{z_j'^2 - c^2} \right) \frac{dz_j'}{dt}}{\left[(z - z_j') - \left(\sqrt{z^2 - c^2} - \sqrt{z_j'^2 - c^2} \right) \right]} \right\} dz$$

The force contribution arising from growth rate of the feeding point vortex, and feeding sheet are not derived for the elliptical cylinder.

FUNDAMENTAL INVESTIGATIONS

SHEAR LAYER INSTABILITY

One of the most important practical problems in numerical computer studies is the control of machine time consumption. In the analytical approach chosen for our study, the machine time consumption increases exponentially with the number of vortices in the flow field. It is therefore, desirable to obtain the maximum information from the least number of vortices (least machine time consumption) with acceptable accuracy.

Vorticity Transport Rate

The parameter which defines a particular flow condition is the vorticity transport rate:

$$\frac{dk}{dt} = \frac{\Lambda}{2\pi} \tag{51}$$

In the actual flow, vorticity is transported into the flow field from the solid boundaries in the form of shear layers. By approximating the shear layer by discrete vortex filaments, Equation (51) may be rewritten,

$$\frac{k}{\Delta t} = \frac{\Lambda}{2\pi} \tag{52}$$

where

k = strength of vortex filament - nondimensionalized by $U_o L$.

$\frac{1}{\Delta t}$ = frequency at which vortices are introduced into the flow field - nondimensionalized by $\frac{L}{U_o}$.

L = characteristic length.

U_o = free stream velocity.

It follows immediately from Equation (52) that for a fixed transport rate (Λ = constant) any value of vortex strength (k) may be chosen. But for a given transport rate the number of vortices necessary to approximate the total circulation in the flow field after an elapsed time, $t = t^*$, given by

$$\text{(total circulation) } \Gamma = 2\pi \int_o^{t^*} \left(\frac{dk}{dt}\right) dt \tag{53}$$

is inversely proportional to the vortex strength, k. Stated otherwise, the higher the frequency ($1/\Delta t$) the greater the number of incremental vortices necessary to reach a particular elapsed time, $t = t^* = n \Delta t$.

In order to investigate this problem without expending a great deal of computer time, an analysis for flow over an infinite half-plane with vortices was programmed for the IBM 7094. The configuration is shown below.

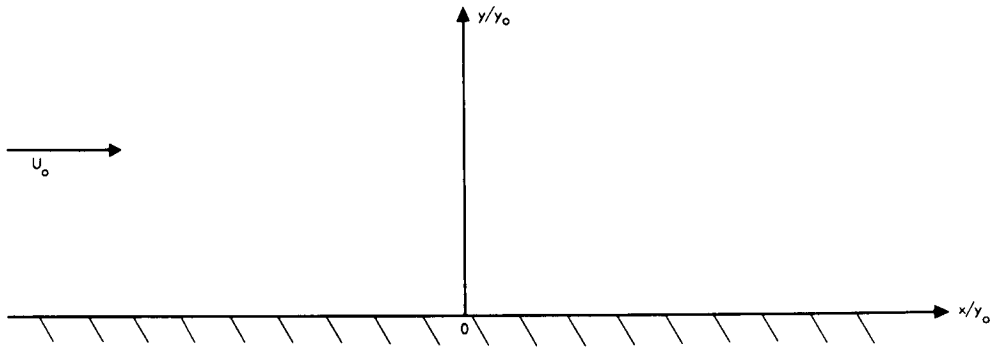

The complex potential for a system of n vortices and uniform flow in the upper half plane is given by

$$w(z) = -i \sum_{j=1}^{n} K_j \log (z - z_j) + i \sum_{j=1}^{n} K_j \log (z - \bar{z}_j) - U_o z$$

The induced velocity at the m^{th} vortex is

$$(U - iv)_m = U_o + i \sum_{\substack{j=1 \\ j \neq m}}^{n} \left(\frac{K_j}{z - z_j} \right) - i \sum_{j=1}^{n} \left(\frac{K_j}{z - \bar{z}_j} \right)$$

For this study a vorticity transport rate was chosen and discrete vortex filaments were introduced into the flow at a prescribed position; e.g., coordinates (0, 1) in the results presented.

Assuming a shear layer at the boundary, the vorticity transport rate consistent with zero surface velocity, $U = U(x)$, and U_o the free stream velocity is

$$\frac{dk}{dt} = \frac{1}{2\pi} \left(\frac{U_o^2}{2} \right) \text{ or } \frac{K/U_o y_o}{\frac{U_o \Delta t}{y_o}} \cong 0.1$$

Location of the feeding point was arbitrarily fixed at $\left(\frac{y}{y_o}\right) = 1.0$. Under these assumptions it was reasoned that this flow solution should be carried out until the vortices moved downstream a distance $x = ny_o$, where $n >> 1$. The implied analogy here is that the feeding point height represents some boundary layer thickness.

Vortex Strength

At first glance, the only variable to be considered is the vortex strength, $\frac{K}{U_o y_o}$. That is, for the given vorticity transport rate and feeding point height, the representation of a continuous shear layer by discrete vortices becomes progressively worse as the strength, hence the period of successive vortices, increases.

What is the criterion for judging whether the vortex strength is or is not too great? If the half-plane were removed (viz., the problem of shear layer feeding point in an unbounded region of uniform flow), even the parameter $\frac{K}{U_o y_o}$ would no longer be a variable, since y_o would be undefined.

Stated in other words, the problem of a shear layer growing from a single point in an unbounded region of uniform flow has only one analytical solution. This solution would consist of an inward spiral from the feeding point.

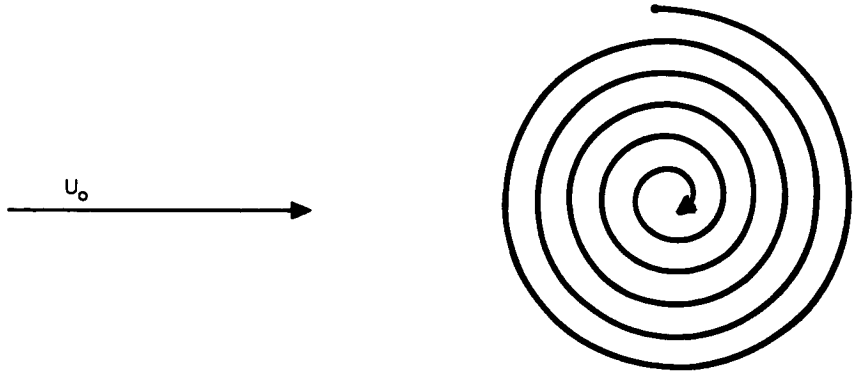

When the solution is obtained numerically, however, the discrete vortices representing the shear layer are finite in number; consequently, the spiral has limited definition in the center. The greater the number of vortices, the greater the definition of the core, obviously. That this statement should be true even when total vorticity is held constant, i.e.,

$$\sum_{i=1}^{n} \frac{Kj}{U_o y_o} = \text{constant},$$

is not quite so obvious. It might thus be argued that one criterion for setting the strength of a discrete vortex might be based upon the degree of exactness desired in representing a Kármán vortex.

The preceding discussion has been based on the presumption that once the change has been made from continuous shear layer to vortex filaments, the solution may be obtained in a straightforward manner. Actually, the instability of numerically computed vortex motions has been the subject of study for many years (see Reference 13). Such instability was encountered in the half-plane study. Invariably this instability results in a relatively rapid randomization of vortices from their smooth, initially line nature into one wherein the vortices assumed positions laterally displaced from the original sheet in a random manner, often at distances of several times the original spacing. Once having spread out, the solution appeared to proceed at a more regular pace. It was reasoned that a sinusoidal motion of the feeding point in time would spread the vortices, thus possibly precluding this type of breakup.

The relationship

$$\frac{y}{y_o} = 1 + \epsilon \sin\left(\frac{n}{N}(360)\right)$$

thus introduces two additional parameters: ϵ , the sinusoidal amplitude, and N, the number of vortices per cycle.

FORMATION OF A GROWING SHEAR LAYER IN FLOW PAST A HALF-PLANE

Table I summarizes eight cases investigated in studying the motion of a growing shear layer in otherwise uniform flow past a half-plane. These results were obtained in an effort to isolate basic characteristics encountered in the numerical technique of approximating a continuous shear layer by discrete vortices, and using finite difference methods to determine their motion. Of primary interest were the effects of vortex strength and integration accuracy. Computer plots of the vortex patterns are presented in Figures 1 through 5.

In all cases, the vorticity feeding rate, $\frac{dk}{dt} = 0.1$, simulated the strength distribution necessary to reduce velocity along the boundary to zero.

It is first pointed out that vortex strength is important only in relation to some characteristic dimension of the problem; in this case, the dimension is height of feeding point above the half-plane. This is made clearer by noting that the nondimensional form of vortex strength is $k/U_o y_o$, where y_o is some characteristic dimension.

Table I. Growth of Shear Layer

Case Number	Figure Number	Discrete Vortex Strength $\frac{K}{U_o y_o}$	Vortex Feeding Period $\frac{U_o \Delta t}{y_o}$	Time Period of Numerical Integration $\frac{U_o \Delta t_I}{y_o}$	Type of Integration	Sinusoidal Amplitude of Feeding Point	No. of Vortices Per Cycle
1	1	0.005	0.05	0.05	A*	0	-
2	2	0.01	0.10	0.10	A	0	-
3	3	0.01	0.1	0.01	A	0	-
4	4	0.01	0.1	0.01	B**	0	-
5	-	0.01	0.1	0.01	B	0.05	8
6	-	0.1	1.0	0.02	B	0	0
7	5	0.1	1.0	0.02	B	0.05	4
8	-	1.0	10.0	0.001	B	0	0

*Type A integration consists of multiplying Δt_I by the velocity components existing at a time break, t_j, to find the change in vortex position at the next time break, t_{j+1}.

**Type B integration is a refinement of Type A in which the vortex velocity computed at the next time break, t_{j+1}, is averaged with the previous one, at t_j, and the change in vortex position is recalculated with this average velocity. Vortex velocity at this new location is not determined. Relative increase in computer time using this refinement is considered negligible.

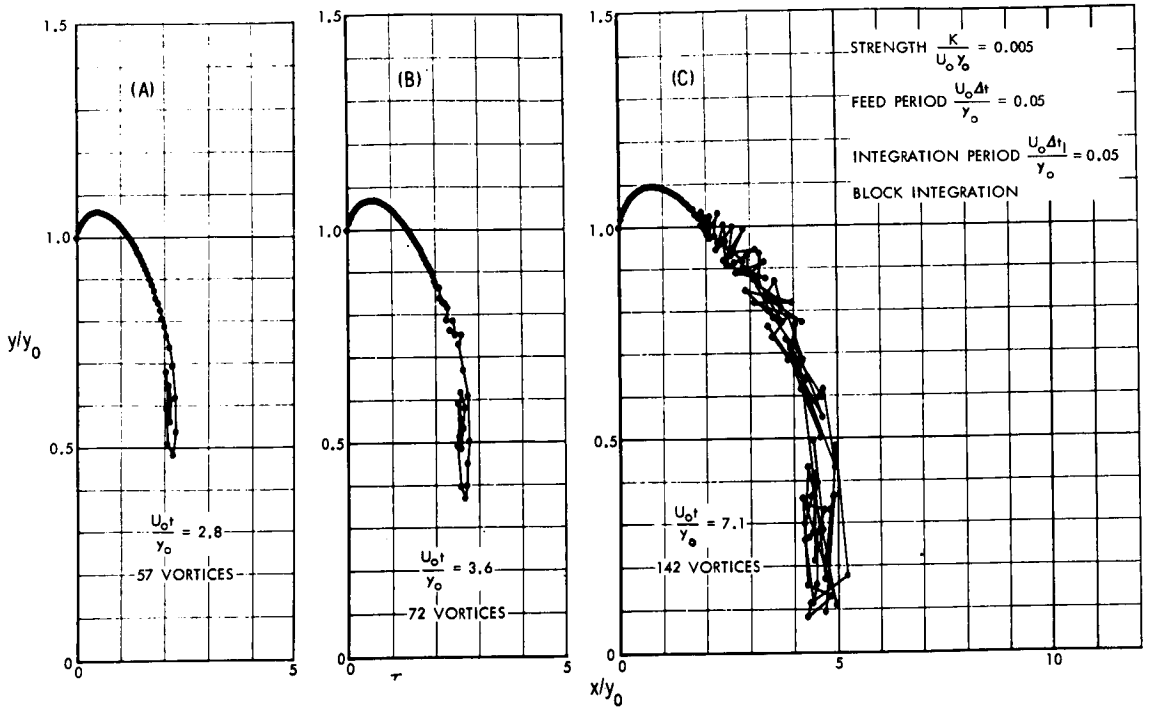

Figure 1. Formation of Shear Layer in Flow Past Half-Plane (Case 1)

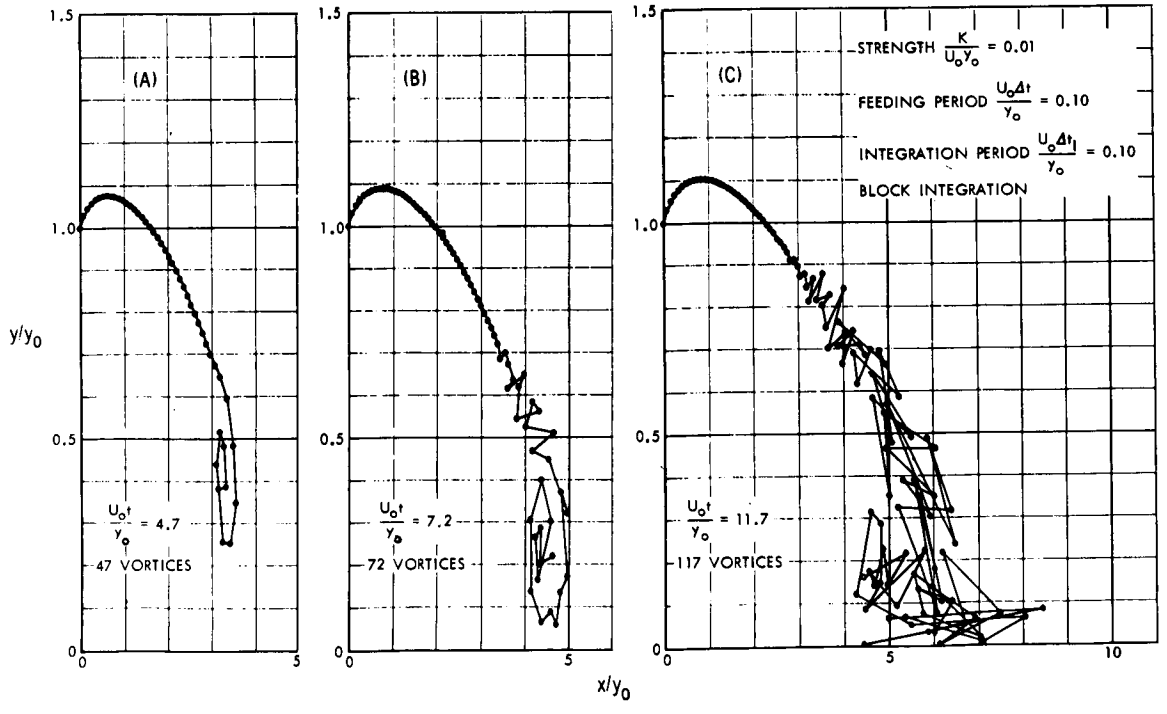

Figure 2. Formation of Shear Layer in Flow Past Half-Plane (Case 2)

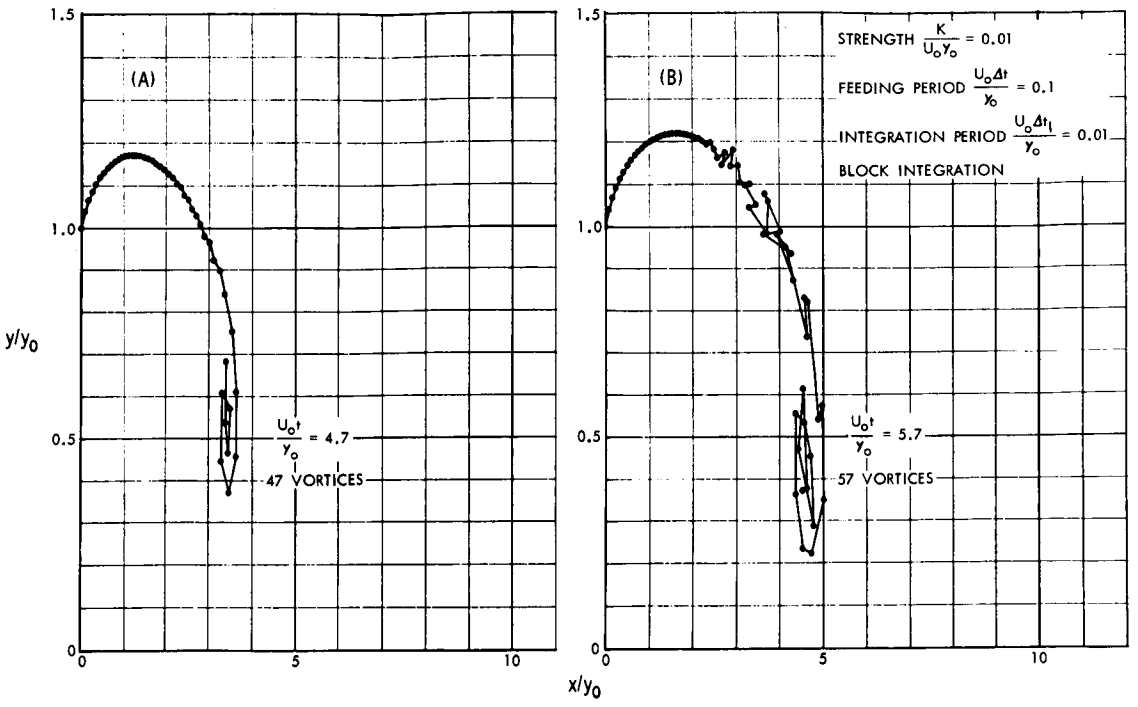

Figure 3. Formation of Shear Layer in Flow Past Half-Plane (Case 3)

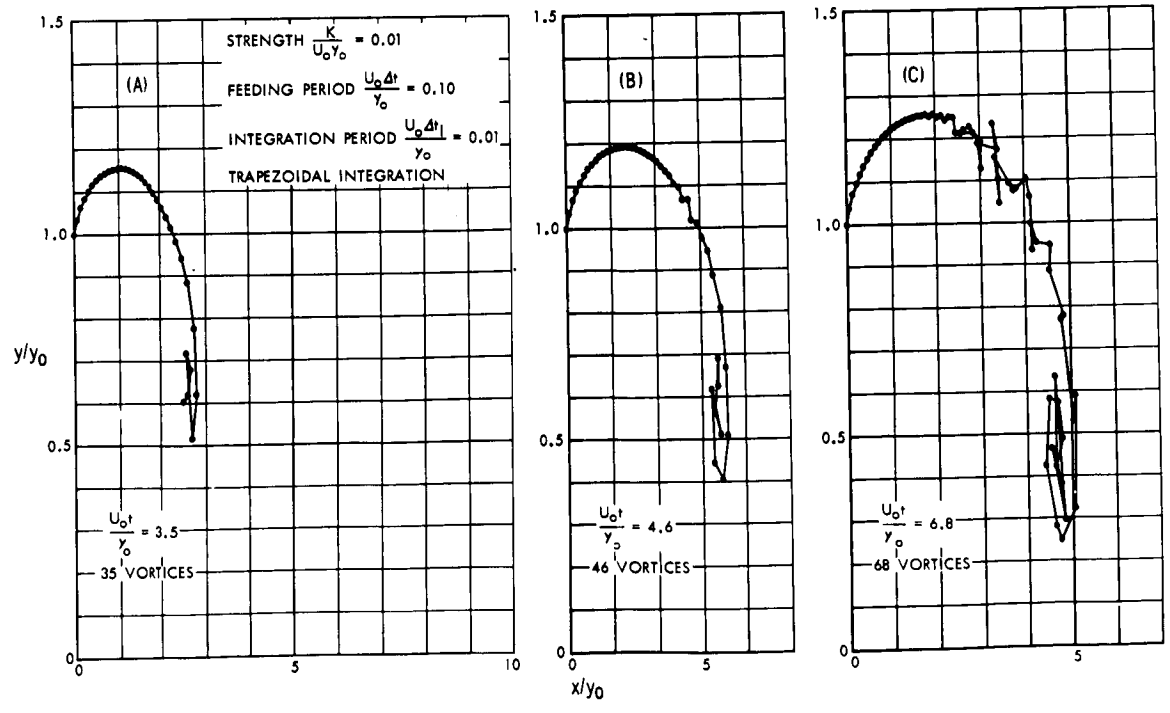

Figure 4. Formation of Shear Layer in Flow Past Half-Plane (Case 4)

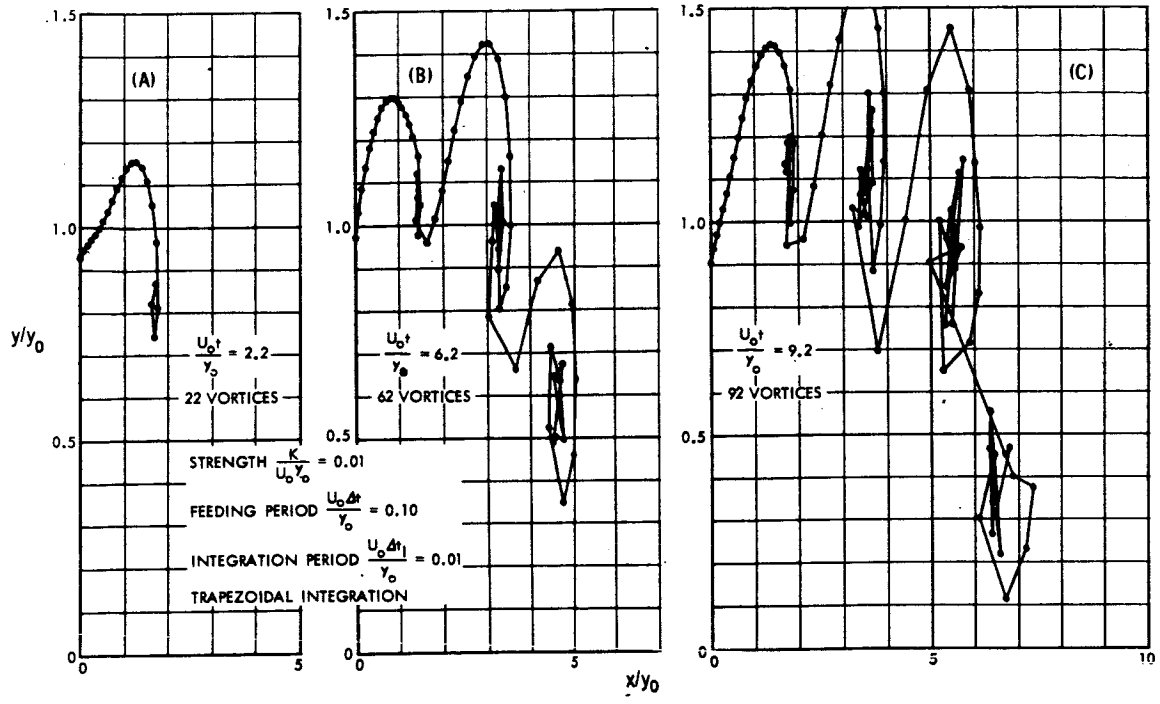

Figure 5. Formation of Shear Layer in Flow Past Half-Plane (Case 7)

It is found that the discrete vortex approximation of a continuous shear layer produces very similar results for a wide range of vortex strengths. For example, Figures 1(C), 2(B), 3(B), and 4(C), show the state of shear layer development at a nondimensional time of $U_o t/y_o \cong 7.0$ but with vortex strengths varying from 0.005 to 0.1. Shear layer length in the x-direction is the same in all cases; however, the maximum height varies from $y/y_o = 1.1$ to 1.2 with the type of numerical integration. The more accurate integration produces greater maximum height. In general, the greater the number of vortices, the more advanced the state of core development. As an extreme case, a solution using $K/U_o y_o = 1.0$, $U_o \Delta t_F / y_o = 10$, and $U_o \Delta t_I / y_o = 0.001$ was attempted (Case 8). Results were completely divergent with vortices scattered in negative as well as positive directions. Shear layer development was not evident. This type of divergence is simply caused by excessive sparseness of the vortices. Each vortex behaves as if it were influenced only by its image, and its velocity of approach toward the symmetrical boundary is not eliminated. Consequently, the image velocity contribution becomes excessive.

It is concluded that the boundary between stable and unstable solution lies in the region of vortex feeding periods $1.0 < U_o \Delta t/y_o < 10.0$. Furthermore only relatively small differences in shear layer configuration results from decreasing the vortex strength much below the marginal value. The

primary differences appear to be in the maximum height attained by the shear layer, and in the state of development of the core at a given value of time elapsed from initiation of the first vortex.

The analogy between the vortex feeding height above the plane of symmetry and distance from the circular cylinder in the vortex shedding problem should be valid only in determining the detail flow whose scale of motion is small compared to cylinder radius. This is important in the "starting" problem wherein vortices which are initially too strong will not form smoothly into a wake cavity, but will instead interact strongly with their image vortices while being moved by convection around the cylinder. The result is an unstable solution very similar in nature to that obtained in Case 8 (Table I). Such results were obtained in previous company-funded studies of this problem. The technique devised at that time to surmount this local instability was to incorporate a time-variable feeding rate wherein the initial vortices had low strength but succeeding vortices were introduced at increasing strengths until the desired feeding rate was reached. This technique was utilized to obtain the Model I computer program results shown in Figures 6 and 7.

It is informative to make the analogy between height of vortex feeding point and radial distance from circular cylinder in the vortex shedding problem. If this distance is set to 0.1 radius, the corresponding boundary between stable and unstable solutions would be $0.1 < U_o\Delta t/a < 1.0$.

Solutions for the circular cylinder shown in the last frame of Figure 6(A) and the first frame of Figure 6(B) were obtained with $U_o\Delta t/a = 0.0710$ and 0.174 respectively and represent the same state of development ($U_o t/a = 7.1$). Their close agreement is strong evidence of a numerically accurate solution. Tentatively, $U_o\Delta t/a$ may be increased still further before this local type of instability might begin to appear. If the above prediction is valid, such instability should occur at $U_o\Delta t/a < 1.0$.

A further analogy may be implied between height of feeding point, y_o, above the plane of symmetry in uniform flow, and the corresponding distance to the feeding point outside a circular cylinder in symmetrical flow also measured from the plane of symmetry. Such an analogy would permit an inference regarding the maximum magnitude of $U_o\Delta t/a$ that might be used to adequately represent flow characteristics away from the immediate cylinder area, but possibly within the region of Kármán vortex formation. Thus, based upon this one-to-one analogy, the nondimensional time, $U_o\Delta t/a$, might be as high as 1.0 without significant loss in accuracy. If so, the real time capability for the same computer machine time could be extended by a factor of five over that presented in Figure 6(B). It is suspected that local instability in regions close to the cylinder would manifest itself in some form at smaller values of $U_o\Delta t/a$.

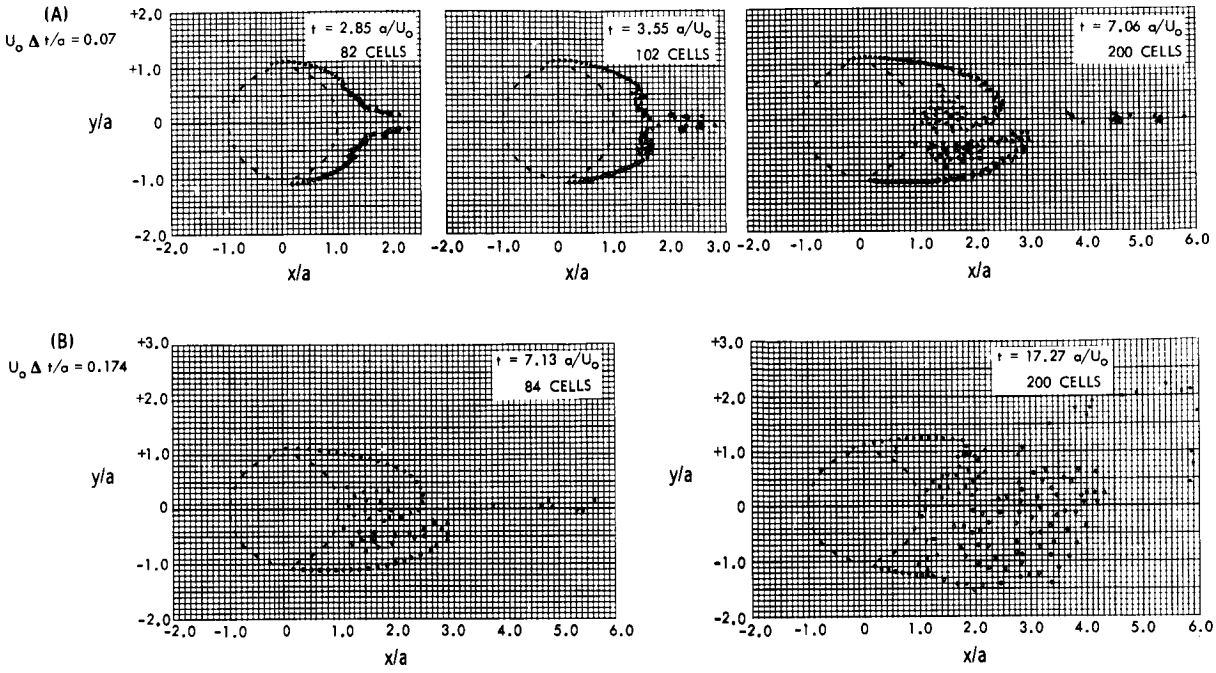

Figure 6. Computed Plots of Vortex Development (Model I)

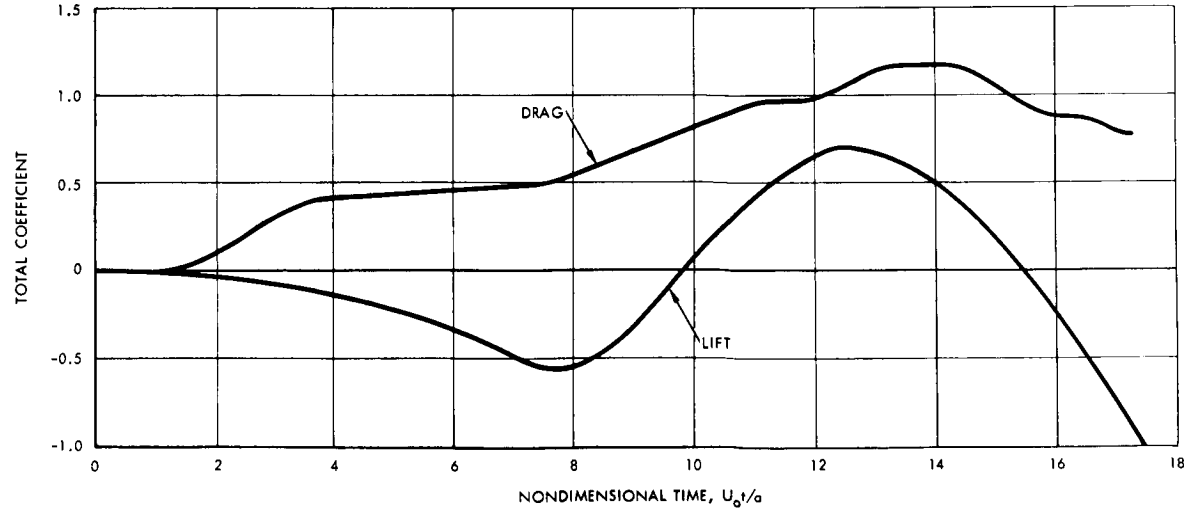

Figure 7. Lift and Drag Time Histories

The above inference, while probably over-optimistic, does contribute to a better understanding of the problem of obtaining stable solutions and indicates that the vortex distribution may be made significantly coarser than that of Figure 6(B) without appreciable loss in accuracy.

Effects of Changing Integration Mode

As previously mentioned, a persistent instability has been encountered in the numerical solutions of a growing shear layer in flow past a half-plane. Invariably this instability manifests itself after a spiral loop has formed in the vortex sheet roll-up. At inception, one or more vortices near the upper edge of the spiral suddenly commence orbiting about their adjacent vortices. This disturbance to the erstwhile smooth consecutive train of vortices is propagated in both directions. As a result, the vortices are displaced laterally by distances which are on the same order of magnitude as their original spacing. Once spread out, the vortices appear to regain some measure of stability.

If this instability is caused by the grossness of numerical integration techniques, it would appear that a refinement of the numerical integration should retard its onset until later real time. That this is not so can be seen by comparing Figures 2(A), 3(A), and 4(B). Figure 3(A) represents results obtained with ten times smaller integration intervals than were used to obtain Figure 2(A), while all other parameters remain unchanged. Yet the shear layer configuration of Figure 3(A) shows signs of breakup while that of Figure 2(A) is still smooth. Figure 4(B) represents results of an improved integration scheme as described in Table I, yet here the breakup is in an even more advanced state than in Figure 3(A)! On this basis it would seem that this instability is not due to grossness of the integration method nor, by the same token, to truncation errors of the digital computer. The randomness of vortex motion encountered by Takami (Reference 13), appears to be of this same nature.

In a further effort to control this instability, it was reasoned that sinusoidal motion of the feeding point could cause initial dispersal sufficient to preclude the unstable randomization. Figures 5(A), (B), and (C) show the results of this investigation. With twenty-four vortices per cycle (Figures 5(A), (B), and (C)), the sinusoids initially crest, then roll up in small vortex groupings. Without further investigation it is concluded that vortex cores will form in concert with any given frequency of feeding point oscillation. Considerably more thought should be directed toward this phenomenon because of its possible effect on numerical results.

This same type of instability is evidenced in flow about the circular cylinder. Its onset may be noticed in Figure 6(A). In a more advanced state, shown in the last frame of Figure 6(A), both vortex sheets depart from the single train configuration at 1.5 radii downstream. The first frame in Figure 6(D), which is at the same nondimensional time but represents a much coarser distribution of vortices (approximately 2-1/2 times coarser), the instability is not evident. Yet the overall flow configurations are essentially the same, and only small differences appear in computed pressure distributions (not shown). It is tentatively concluded that this type of instability is unimportant to the primary flow characteristics of interest in this problem. As a precautionary note, however, mention is made of the similar nature of this instability to transition of an initially laminar shear layer to turbulence. It may be that comprehensive correlation with supercritical Reynolds number effects by the approach taken in this study will require further understanding of this instability phenomenon.

Cylinder Forces Due to Vortex Growth Rate

The relationship for cylinder forces, based upon the impulse of a vortex pair, is given in Equation 32.4. It is repeated here for convenience.

$$(D - i\,L) = i\,2\,\pi\rho \left[\sum_{j=1}^{n} K\,(\dot{z}_j - \dot{z}_j^i) + \sum_{j=1}^{n} \frac{\partial K}{\partial t}\,(z_j - z_j^i) \right] \qquad (32.4)$$

The first summation is in agreement with the corresponding term derived from the Blasius theorem. Furthermore it agrees exactly with results obtained by numerically integrating cylinder pressures computed from Equation (17), minus the pressure term containing $\frac{\partial K}{\partial t}$. Therefore, those terms in the pressure equation (17), the force equation (29), and the force equation (32.4) which do not contain $\frac{\partial K}{\partial t}$ may be considered substantially correct.

The second term in Equation (32.4) requires further consideration to define its correlation with the pressure equation. (The terms involving $\frac{\partial K}{\partial t}$ in Equation (29) are considered inapplicable to the problem at hand, as previously explained.)

In order to isolate as much as possible the particular effect symbolized by the second term, an idealized situation was assumed. Flow conditions are symmetrical about the x axis. Twin vortices are located on the y axis at a distance, ΔR, from the cylinder surface. These vortices are stationary in space, but growing in strength with a nondimensional growth rate of

$$\frac{1}{2\pi}\left(\frac{\dot{\Gamma}}{U_o^2 a}\right) = \frac{\partial\left(\frac{K}{U_o a}\right)}{\partial\left(\frac{U_o t}{a}\right)} = 0.86$$

They are always of equal but opposing strength.

For values of ΔR equal to 0.1, 1.0, and 10.0, pressures on the cylinder surface based on Equation (17) were determined by computer.

Numerical integration of these pressures result in incremental drag coefficients of 0.981, 5.4, and 9.81, respectively. Drag coefficients obtained in this manner appear proportional to the image vortex distance from the cylinder 90-degree position, for this particular vortex configuration.

Thus

$$\Delta C_D = \frac{2}{U_o^2 a}\dot{\Gamma}(z_c - z_k^i) = 4\pi\left|\frac{\partial\left(\frac{K}{U_o a}\right)}{\partial\left(\frac{U_o t}{a}\right)}\right|(z_c - z_k^i)$$

where z_k^i is the position of the upper vortex image, z_c is that point on the cylinder along the radius vector through z_k^i.

It is further noted that the pressure discontinuity at the 90-degree position is a direct consequence of the $\tan^{-1}$ terms of Equation (17). Actually this discontinuity could be made to occur at any position along the surface, simply by choosing a desired direction for the branch cut. Thus, there seems to be no specific criterion for its location, except that it must occur somewhere on the cylinder.

Without formal proof, it is considered that this discontinuity may be made physically consistent by assuming a feeding shear layer connecting the growing vortex to the cylinder at the points of pressure discontinuity.

To incorporate these observations, the second term of Equation (32.4) is written

$$\sum_{j=1}^{n}\frac{\partial K}{\partial t}(z_j - z_j^i) = \sum\frac{\partial K}{\partial t}\left[(z_j - z_c) + (z_c - z_j^i)\right]$$

On the basis of observed correlation, the term

$$\Sigma \frac{\partial K}{\partial t}(z_c - z_j^i)$$

is now taken to define the effect of vorticity growth rate of the growing vortices.

The remaining term

$$\Sigma \frac{\partial K}{\partial t}(z_j - z_c)$$

evidently describes the force contribution due to the radially connecting feeding shear layer.

The following conceptual visualization clarifies the physical significance of this term. First, the impulse concept of defining force due to a vortex pair requires some contour connecting the vortices. Impulsive pressure differential across this contour integrates out to the impulsive force generating the vortex pair.

In the case at hand, the feeding shear layer of length ΔR may be considered part of the contour. Barring computer limitation, ΔR would ideally be zero, so that each vortex would grow to full strength on the circle before separating (becoming free). In this sense, the feeding shear layer may be visualized as a sort of protuberance attached to the circle. Its main purpose is to permit vortex growth at a point sufficiently removed from the circle to preclude computational instabilities. With this in mind, the feeding shear layer is considered to be a bound vortex sheet whose strength, U_s, is such that $U_s^2/2$, the vorticity transport rate, satisfies some specified criterion. With this concept, the term

$$\Sigma \frac{\partial K}{\partial t}(z_j - z_c)$$

does indeed define the force effect of the feeding shear layer. Its counterpart in the pressure equation, if exactly defined, would require an integral term. But since its effect is expected to be only secondary upon overall flow mechanics, the representation is simplified. Conceptually, the discrete vortex approximation treats the feeding sheet as a train of equally spaced, bound, discrete vortices of equal and constant strength. Obviously, the greater this number, the better will be the approximation. For practical reasons, the feeding sheet is approximated by a single discrete bound vortex. Its velocity, if free, would be one-half the strength of the equivalent sheet $\frac{U_s}{2}$.

The product of the strength of this single vortex and this velocity is therefore

$$K\,(\text{velocity}) = \frac{U_s}{2\pi}\,(\Delta R)\left(\frac{U_s}{2}\right)$$

$$= \frac{U_s^2}{4\pi}\,(\Delta R)$$

$$\frac{K}{U_o a}\,\frac{U}{U_o} = \frac{\alpha 2}{2\pi}\,\left(\frac{\Delta R}{a}\right)$$

where ΔR is the length of the feeding sheet. While requirements could be developed for improving the rigor of this derivation, such detailed consideration is felt to be unwarranted in view of its anticipated secondary influence on the flow solution. In general, ΔR should be kept sufficiently small that the assumption of second order importance is not violated.

The influence of the terms representing the feeding sheet may be estimated. Experimentally, $\alpha^2 \cong 2$, and if $\frac{\Delta R}{a}$ is taken equal to 0.1 radius

$$\Delta C_D = \frac{\alpha^2}{2\pi}\left(\frac{\Delta R}{a}\right) = \frac{2}{2\pi}\,(0.1) \cong .03$$

Since the force coefficients are on the order of 1.0, this influence should be less than three percent. To incorporate this effect, the pressure equation (17) should have an additonal term of the form

$$+\ \frac{K_s}{U_o a}\,\frac{(y_k - y_s)\,u_s - (x_k - x_s)\,v_s}{(x_k - x_s)^2 + (y_k - y_s)^2}$$

where the subscript s denotes the bound vortex representing the shear layer. But because of its negligibly small effect, the correction was not applied in this study.

FLOW MODELS

Preliminary investigations have been conducted on two different potential flow models. For brevity the two models will be denoted Model I and Model II. Since the chief criticism of the use of a potential flow model for the vortex shedding problem has been the arbitrary selection of the flow separation point on the cylinder, both models incorporate self-consistent methods for determining "separation" points.

FLOW MODEL I

Having an expression for the velocity field, the non-steady problem of vortex shedding about a circular cylinder will be approximated by a finite difference technique. At a given time (t) the velocity of the m^{th} vortex will be given by Equations (5) and (6). The new coordinates of the m^{th} vortex will then be found from the solution of the differential equations,

$$\frac{dx_m}{dt} = u_m (x_1, x_2, \ldots x_n, y_1, y_2, \ldots y_n)$$

$$\frac{dy_m}{dt} = v_m (x_1, x_2, \ldots x_n, y_1, y_2, \ldots y_n)$$

or written as difference equations

$$x_m (t+\Delta t) = x_m (t) + u_m (t) \Delta t$$

$$y_m (t+\Delta t) = y_m (t) + v_m (t) \Delta t$$

This procedure applied to all vortex filaments outside the circular cylinder will give a time history of their displacements. Once the velocity is known, the pressure distribution on the cylinder and the resultant forces may be found for each time increment.

Model I approximates the phenomenon of vortex shedding by the following considerations. Initially, there exists a system of n vortex filaments outside the circular cylinder. At some characteristic frequency new vortices are introduced into the flow at predetermined positions near the cylinder. The velocity of each vortex filament is found, subsequently giving new positions. This procedure is repeated until terminated by

choice or by computer time consumption. It is expected that at some distance downstream of the cylinder, the flow in the near wake will become fully developed. This flow configuration is further expected to resemble a vortex street where the discrete vortex elements have "rolled up" into clouds of vorticity. The initial condition, i. e., the original number of vortices, may be chosen arbitrarily.

One of the chief difficulties in an analysis of flow over blunt bodies, the problem of vortex formation, has heretofore been neglected. Here the question is whether boundary layer theory can account for the circulation of one vortex; i. e., the strength of a vortex filament.

From boundary layer theory, the rate at which vorticity in the form of vortex sheets is generated at the cylinder is given by

$$\frac{d\Gamma}{dt} = \frac{d}{dt} \int_A \xi d_x d_y = \Lambda U_o^2 \tag{54}$$

where

$$\Lambda = \frac{1}{U_o^2} \frac{d}{dt} \int_A \xi d_x d_y \tag{55}$$

$$\xi = \text{vorticity} = \frac{\partial u}{\partial y} - \frac{\partial v}{\partial x} \tag{56}$$

$$K = \frac{\Gamma}{2\pi} = \text{strength of vortex filament}$$

It is easily shown that $\Lambda = 1/2$ if $v = 0$.

Roshko (Reference 17) postulates that

$$\Lambda = \frac{\epsilon \alpha^2}{2} \tag{57}$$

where

α^2 = base pressure parameter

$$\alpha^2 = 1 - C_p = 1 - \frac{p - p_o}{\frac{1}{2}\rho U_o^2} = \left(\frac{U_s}{U_o}\right)^2$$

U_s ≡ velocity outside boundary layer at separation point

ϵ ≡ fraction of the original vorticity which remains in the fully developed wake (experimentally found to be about 0.50)

For Model I, α^2 introduces a Reynolds number effect into the problem as shown in Figure 8 (reproduced from Reference 17). It is shown in Figure 8 that $\alpha^2 = (U_s/U_o)^2$ is always greater than unity. Also if we consider potential flow over a circular cylinder $(U_s)_{max} = 2\,U_o$, therefore it is reasonable to assume that the following inequality is true

$$1 \leq \alpha^2 \leq 4$$

The model is now complete. Equation (54) may be written in the form

$$f \cdot 2\pi K = \Lambda U_o^2 \tag{58}$$

where

f = characteristic frequency

Thus for a given value of Λ we have a simple relation between the vortex filament strength, K, and the frequency of introduction of new vortices, f. The determination of the correct combination of these parameters to simulate the actual flow completes the solution.

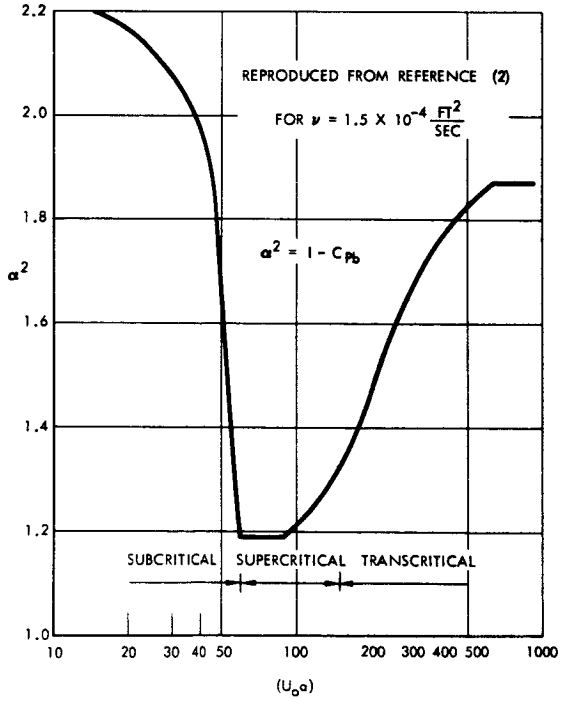

Figure 8. Vorticity Transport Rate

Effect of Vortex Feeding Period

More than any other single parameter, the vortex feeding period determines the total time solution that can be reached by the computer in a reasonable computation time. Computer time consumption depends primarily upon the total number of vortices in the field, and of course the larger the strength of each incremental vortex, the greater time span of vorticity generation represented by that vortex.

The permissible degree of coarseness in discrete vortex approximation of a vortex sheet was investigated by comparing time solutions from the Model I program leaving all parameters unchanged except the vortex feeding period. Figure 9 compares the solutions obtained for feeding periods of 0.071, 0.174, and 0.5 a/U_o respectively. (The integration periods were 0.071, .0435, and 0.05 a/U_o).

Peripheral Position of Feeding Point

Peripheral position of the feeding point was, for the Model I program, the primary means of inducing asymmetrical flow (periodic vortex shedding). If the peripheral position of the feeding points are symmetrically located, the resulting flow field is also symmetrical.

While a 1.0-degree asymmetry in peripheral position did induce asymmetrical flow, the buildup in asymmetry was considered too slow for practical investigation of periodic vortex shedding because of computer limitations. Feeding points located 10 degrees ahead of and behind that ±90-degree point were found to result in an acceptably rapid onset of periodic shedding.

This asymmetry was maintained for all Model I solutions for unsymmetrical flow presented in this report.

Radial Position of Feeding Point

With the objective of simulating actual boundary layer separation as closely as possible, it would appear that the feeding point should be located close to the cylinder surface. Initial attempts to locate the vortices as close as 0.01 radius from the surface invariably resulted in strong interaction between the vortex and its image, resulting in wild, completely random vortex displacements. (Keep in mind that vortex strength has been determined by specifying vorticity transport rate and feeding period.) Relaxing this distance to 0.1 radius permitted a regular solution. While this was not as close as desired, it was considered a reasonable compromise and was used in all solutions of cylinder flow.

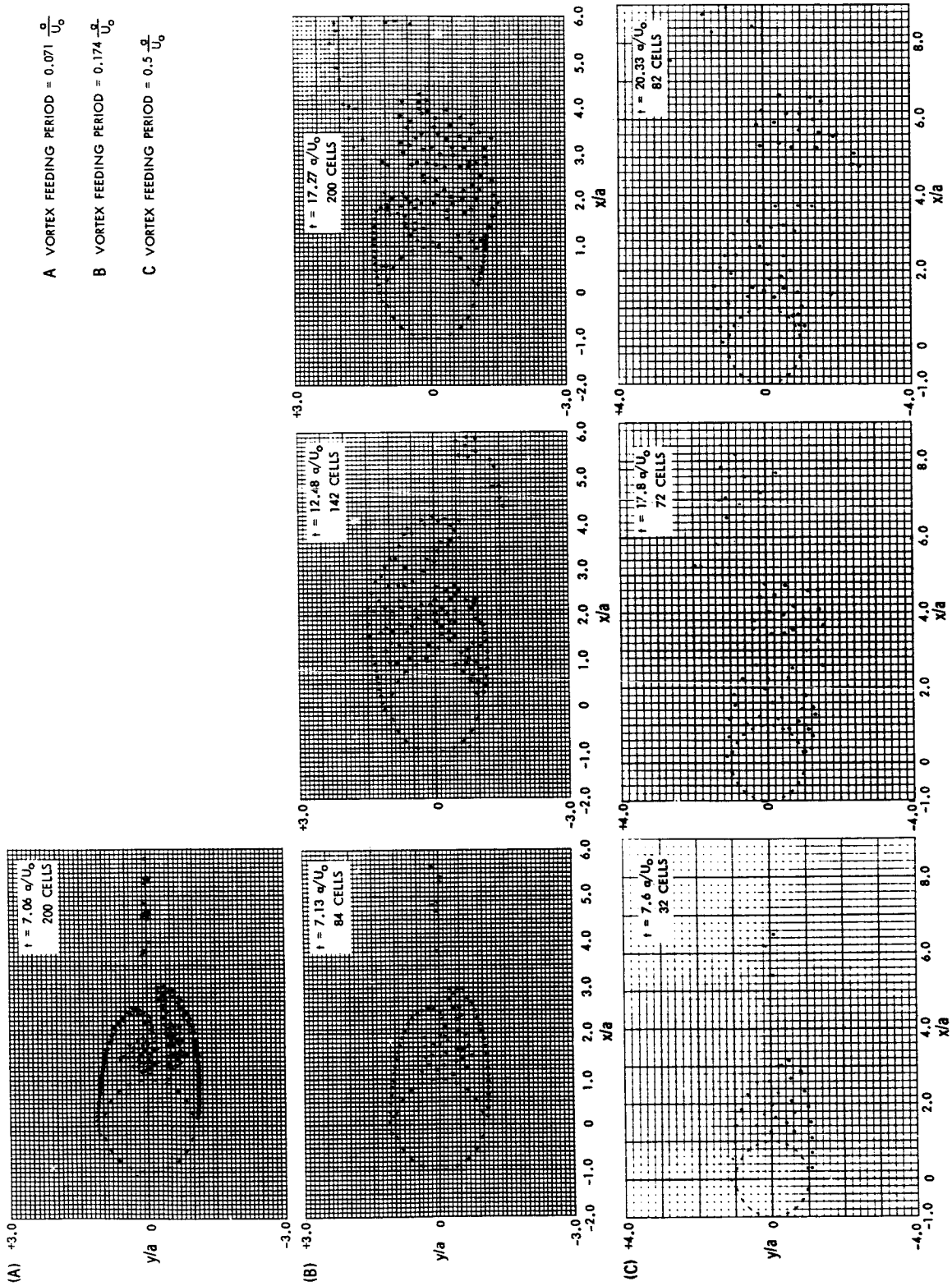

Figure 9. Comparison of Effects of Vortex Feeding Period on Flow Development

Effect of Incremental Integration Time Period

Vortex displacements were obtained by integrating vortex velocities by elementary block integration. As explained earlier, this integration method was considered satisfactory on the basis of results obtained analyzing vortex sheet development in flow past a half-plane. The term "satisfactory" is qualitative, in the sense that a single solution did not result as the integration time interval was made smaller (holding the incremental vortex feeding period constant). Instead, shear layer instability appeared as the integration was made finer. Also, appreciable differences were evident in motion of the overall vortex sheet configuration within the range of integration time periods and total flow development times investigated.

These results, coupled with results given in the literature (References 13 and 14), led to a qualitative conclusion that a unique solution using the discrete vortex approximation probably does not exist, and that a regular solution showing a smooth flow development would be satisfactory for the exploratory purpose of this study. On this basis, an incremental integration time period of between 0.04 and 0.05 a/U_o was observed on all numerical computations for the flow about a circular cylinder except for those of Figure 9(A). The integration period for Figure 9(A) was set equal to the vortex feeding period of 0.071 a/U_o.

FLOW MODEL II

The previously described Model I approach is basically limited in its applicability because of the necessity for explicitly specifying the vorticity transport rate and the vorticity feeding point locations. Implicit determination of these quantities by a potential theory approach to calculation of separated flow would be highly desirable. Recognizing this, possible criteria for determining those quantities were investigated.

Initially it was believed that the feeding point should be located at the separation point. According to classical theory, the separation point is that point at which the boundary layer velocity profile has zero slope in the radial direction. Thus, tangential velocities near the surface on either side of this point are in opposite directions. With this point defined instantaneously, incremental vortices could be introduced there with strengths corresponding to the tangential velocity some specified distance forward of the separation point.

However, examination of tangential velocity profiles on the cylinder from solutions with the Model I program showed that the separation point

as defined above was not easily detected. In some cases there appeared to be a "dead" region wherein essentially zero velocity was uniformly prevalent. Furthermore, no convenient criterion was apparent whereby the vorticity transport rate could be specified.

Another approach, along the lines of the free streamline theory adopted by Roshko (Reference 15), appeared to provide a better solution. For instance, the vortex feeding point would now be located well ahead of any separation point, and vortex strength could be determined by the tangential velocity at that selected point. In the free streamline theory, the point of flow separation is called the detachment point. It is different from the separation point defined above in that it is based upon potential theory, and permits neither a stagnation point nor pressure discontinuity there (Reference 16). It should be noted that there is a pressure discontinuity in going across the free streamline.

In studying pressure distribution from the Model I program it was noted that a pressure minimum invariably occurred near the region where the free streamline detachment point would be expected to lie. This appeared also to be the case in the data presented in Figures 6 and 7 of Reference 16. Intuitively, this agrees with the notion that flow detachment must occur near that point where the pressure gradient becomes positive. Such a pressure minimum, fortunately, appears to be relatively well defined in results obtained with the Model I program. For programming, it was therefore decided to use the first pressure minimum encountered aft of the forward stagnation point. Following this approach, a Model II program was formulated. The criteria for implicit determination of vortex feeding point and vorticity transport rate was simple:

> The feeding point is located at the first pressure minimum aft of the forward stagnation point. Vorticity transport rate is $(U_T/V_o)^2/2$ where U_T is the tangential velocity at that minimum pressure point.

A computer program with this formulation was written and checked out in both the symmetrical and general (unsymmetrical) form. Unfortunately, insufficient time was available for its application to the ellipse (i.e., primarily flat plate).

Initially, the total instantaneous pressure from the unsteady pressure equation was used. Those pressures were determined starting from a point near the forward stagnation point and well ahead of the probable pressure minimum point. Successive pressure computations were then

made at uniform, angular intervals around the cylinder until the pressure minimum was reached. An incremental vortex would then be introduced at this point for the ensuing velocity integration of the vortex field.

Use of a single vortex sheet in the region of boundary layer separation introduces a pressure discontinuity on the cylinder at the point of vortex sheet attachment. As noted by Bryson (Reference 10), this jump has a magnitude of $\rho\dot{\Gamma}$. Because of this, the determination of pressure minima using the total instantaneous pressure imposed some numerical difficulty. Hence the terms contributing to this discontinuity were removed from this technique of determining the feeding points. This was accomplished by dropping out the term multiplied by $\frac{\partial K}{\partial t}$ in the pressure equation (17).

COMPUTER PROGRAMS

The flow Models I and II were programmed in Fortran IV for the IBM 7094 coupled computing system and the peripheral system which reads magnetic tape output from a computer program and produces graphic and alphanumeric tabular output. The major items of peripheral equipment are the SC 4020 optical plotter and the IBM highspeed digital printer. The obvious application of this combination is the rapid production of tabulated data and labeled graphs which for this analysis is essential.

The flow chart of the main program for both models is presented in Figure 10. The block data, IPVAL, initially sets all logical controls false, and precedes all decks in machine load. True inputs of control items in the name list, FLOW, decide the path through the flow chart for each case.

The main programs, KT1M and KT2M, are for Models I and II respectively. The basic concept in these programs is to provide common communications between subroutines and call subroutines, and to control the computation and output time cycles. A blank common area establishes NN, the number of cells in the field; NØ, half the number of cells in the field; NØM, NØ-1, NØP, NØ+1, and the B matrix. Several labeled commons establish communication to various subroutines.

Both the Model I and II decks and many subroutines have been modified for the symmetric case. The computer run time of the symmetric case is approximately one-third of the nonsymmetric case. The elliptical rather than cylindrical cases are run with the same Model I and II decks but use appropriately modified subroutines.

The B matrix contains vectors of locations (X and Y), velocities (U and V), strength (AUK), and radii (ARAD) which are shifted for each new cell and recomputed for each integration interval. The columns 8 through 13 are computed values of steady and total lift and drag coefficients, etc., for selected times (TCL) which provide time history graphs at the termination of a run.

Input data consist of two standard name list arrays, FLOW and DATA, and the initial cell locations. These are defined in Table II. The single initial cell case applies to Model I only. The multi-cell initial condition can be standard input for a given case or read from Tape 10 for continuation

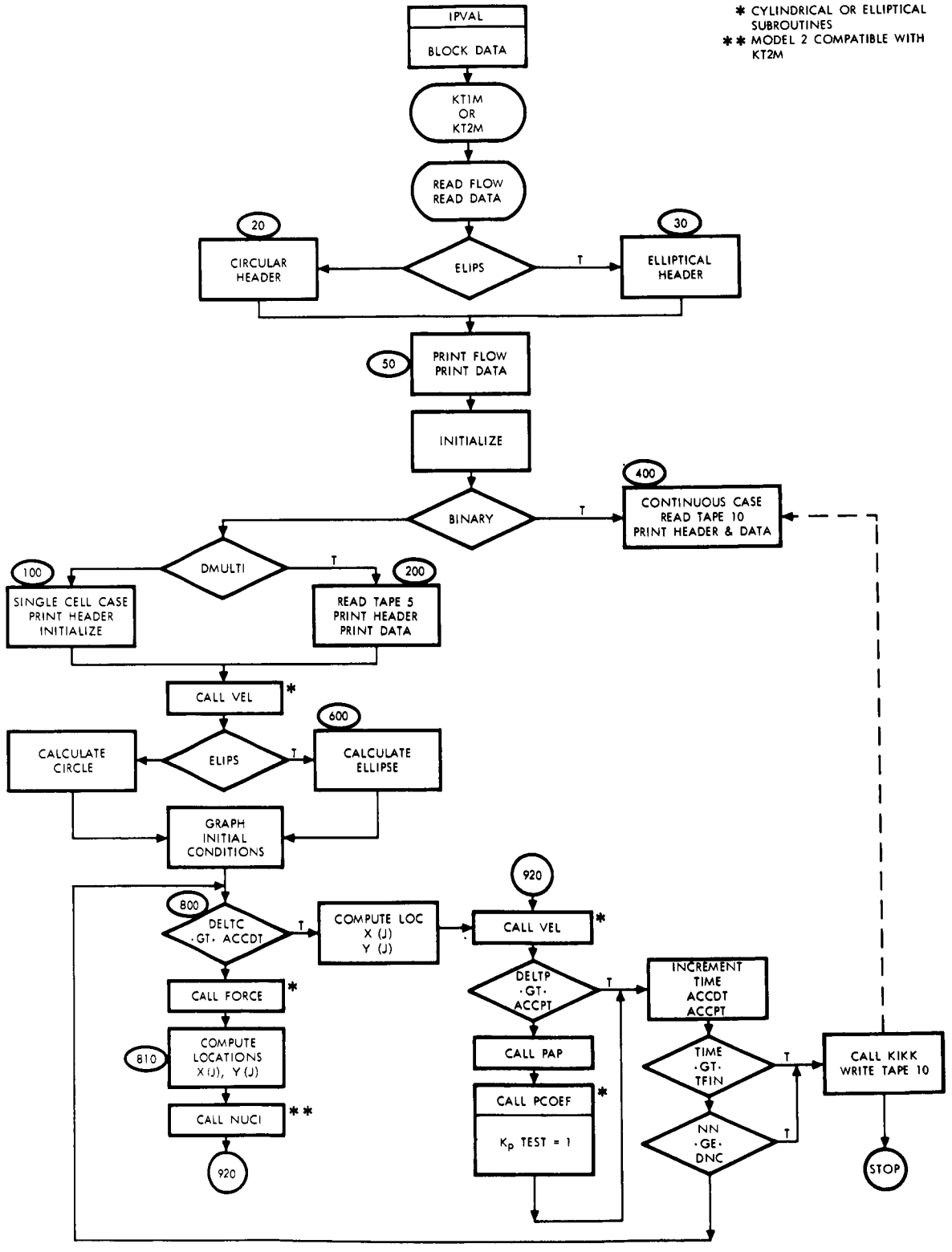

Figure 10. Computer Program Flow Chart

of a previous case. The frequency of printed and graphed output and the economy of each run is controlled by judicious selection of DELTP, which is input datum.

Subroutine VEL is called originally to compute the velocity vectors for the initial condition cells, and subsequently to compute velocity vectors within the basic time increment (DELT) loop.

The input DELTC determines the incremental time for introducing a pair of new cells to the field. This loop consists of two subroutines and the computation of the X and Y location vectors. The FORCE subroutine calculates the steady and total lift and drag forces and stores them in the B matrix. FØR2 is a Model II deck required because of the redimensioning of the B matrix. The NUC1 or NUC2 subroutines introduce the new cells for Models I or II, respectively. The first seven columns of the B matrix are shifted to make room for the new pair, one cell in the lower field and one cell in the upper field. The X, Y, U, and V components and the strength for the new cells are introduced, and the counters adjusted.

Within the DELT loop, the subroutine VEL is called, followed by the output time test. Whenever DELTP is exceeded, subroutine PAP is called and normal field information from B matrix at a given time is printed, graphed and written on Tape 8. The graphing provides for three consecutive graphs defined by the XR input. Additional output from subroutine PCØEF consists of the printed and graphed steady and total pressure coefficients and total lift and drag coefficients with and without the $\dot{\Gamma}$ term.

The program is terminated by either of two conditions controlled by input variables DNC, desired number of cells in field or TFIN, final time. Both tests call subroutine KIKK which writes terminating case data on Tape 10, calls PAP, PCOEF and PAPF, a subroutine for printing and plotting the steady and total, lift and drag coefficient time histories as computed throughout the run in subroutine FORCE.

In the event the requested final machine time is exceeded, a drop-in package to modify the Fortran IV system permits a KIKOFF subroutine to be called which in turn calls KIKK and a normal case exit is executed.

Table II. Computer Program Input Definition

Name list FLOW

BINARY	True to read Tape 10 input and continue case.
DMULTI	True for multi-cell initial condition. Reads NN cards of ITH, X, Y and AUK values on (I12, 3E12.0) format.
ELIP$	True for elliptical case.
VARAL	True for variable alpha computation, false uses input constant values of CØNAS for α^2.
CALCG	Currently not used.

Name list DATA

TIME	Non-dimensional current analysis time, initial case = 0.
DELTC	Increment for introducing new pair of cells.
CONKC	Factor to compute DELT from input DELTC.
DELTP	Increment to call for print and graph output.
TFIN	Final computation time.
TPO	Error control on output time = 0.000001.
TCO	Error control on new cell time = 0.000001.
NN	Number of cells in field for initial condition; number of pairs for symmetric case.
DNC	Desired number of cells to complete run.
ETAU	Angle for location of single upper cell. (Model I only)
ETAL	Angle for location of single lower cell. (Model I only)
DELR	Increment beyond unit radius for initial cell location.
TK	Table of strength values. (Model I only)

Table II. Computer Program Input Definition (Cont)

ALFA	Variable alpha values vs. TK. (Model I only)
BETA	Elipse definition = a-b/a+b. (Model I only)
CØNA$	Constant α^2 value, required for initializing even if VARAL true. (Model I only)
MESHNØ	Argument of MESHI subroutine which adjust grid on graph for PAP output.
XXL YR YB YT	Arguments of LIMITI subroutine which define limits of graph scale for X left, X right, Y bottom, and Y top.
IUP IBOT	Character code for identifying upper and lower cells on graph.
MESHCP	Argument of MESHI subroutine which adjust graph grid for PCØEF output.
PMAX PMIN	Arguments of LIMITI subroutine which defines limits of graph scale for PCØEF output.
YYBOT YYTOP	Arguments of LIMITI subroutine which defines limits of graph scale for PAPF outputs.
CASENØ	Case number (Format F 10.4), suggested AABB.CCDD where AA month, BB date, CC year and DD run number.

SOLUTIONS WITH MODEL I PROGRAM

UNSYMMETRICAL SEPARATED FLOW AROUND A CIRCULAR CYLINDER

Principal limitations of the Model I computer program are that vorticity transport rate and feeding point locations must be specified on the basis of experimental data. Nevertheless, brief exploratory computer solutions obtained with this program indicated surprising similarity to physical flow in the eddy formation and shedding. Computed cylinder pressure distributions and force coefficients appeared to be of the expected order of magnitude. Time limitations imposed by a six-month study were rather severe. The tight schedule did not permit delay in favor of improved solutions at a later date before making comprehensive correlation studies of pressure and velocity distributions on the cylinder and in the wake. Therefore, in spite of these limitations, it was decided to make an extended computer run with the Model I program in order to determine cylinder pressure and wake characteristics in a fully developed flow.

Cylinder Pressure Distributions

Pressure distributions around the cylinder at approximately the time of maximum and minimum lift coefficient are shown in Figure 11. The circular symbols outline the total pressure distribution. Discontinuous behavior of the total pressure distribution in the vicinity of 90 and 270 degrees is caused by the proximity of local vortices, and by vortex feeding sheets radially connecting the feeding points to the cylinder. The curves outlined by the asterisks constitute partial pressures which do not include the effect of vorticity growth rate at the feeding points.

Pressure distributions around the cylinder, of the type shown in Figure 11, were computed at time intervals of $2.5\ a/U_o$ and displayed in both tabular and graphic form. Concurrently, these pressures were integrated by Simpson's rule to obtain cylinder force coefficients. These force coefficients were displayed in digital form, and served as convenient checks on the cylinder forces obtained by the generalized Blasius theorem.

Using these pressure distributions, pressure coefficient time histories were plotted for eleven points on the wake-exposed portion of the cylinder. They are shown in Figure 12. These pressure time histories were made to observe any characteristic time behavior, and permit an estimate of the average pressure at these points over the time period of well developed flow. Such average pressures would presumably be comparable to those that might be obtained by a pressure manometer in physical flow.

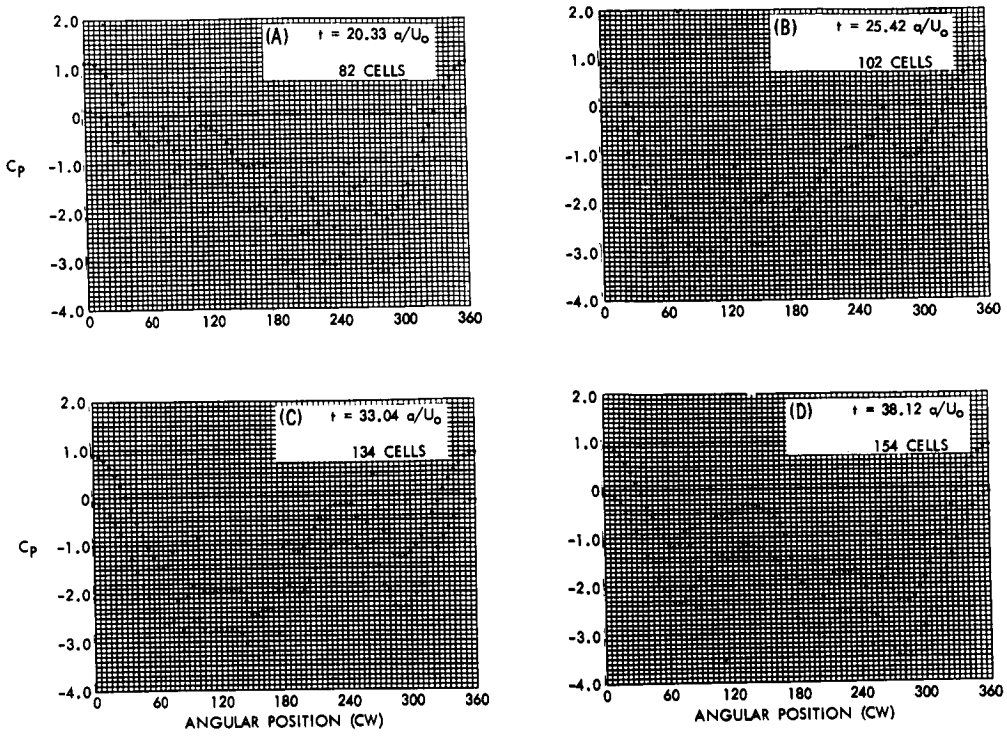

Figure 11. Cylinder Pressure Distributions at Times of Max and Min C_L

Average pressure coefficient values were obtained in this manner at ten-degree intervals around the cylinder and are shown in Figure 13. The values at 100 degrees and 280 degrees were found to be singularly displaced from those nearby. Therefore average pressures were determined at 95, 105, 275, and 285 degrees and used in defining the curve in this area. The values at 100 degrees and 280 degrees were ignored. The reason for these sharp peaks is not clear. Grossness in mathematical simulation of vorticity generation effects in this region is probably the basic cause.

Force Computation

Time histories of instantaneous forces on the cylinder were computed by the generalized Blasius theorem. Mathematical development of the force equations are given in a previous section. As initially derived, these equations did not include the contribution due to rate of change in vorticity at the feeding points. Some difficulty was encountered in correctly defining the mathematical model from which this particular force contribution could be determined. As a result, the correct force expression including the effect of vorticity growth rate at the feeding point could not be incorporated into the computer program in time for the force computations presented in this study. Comparison of these initial force values with those obtained by

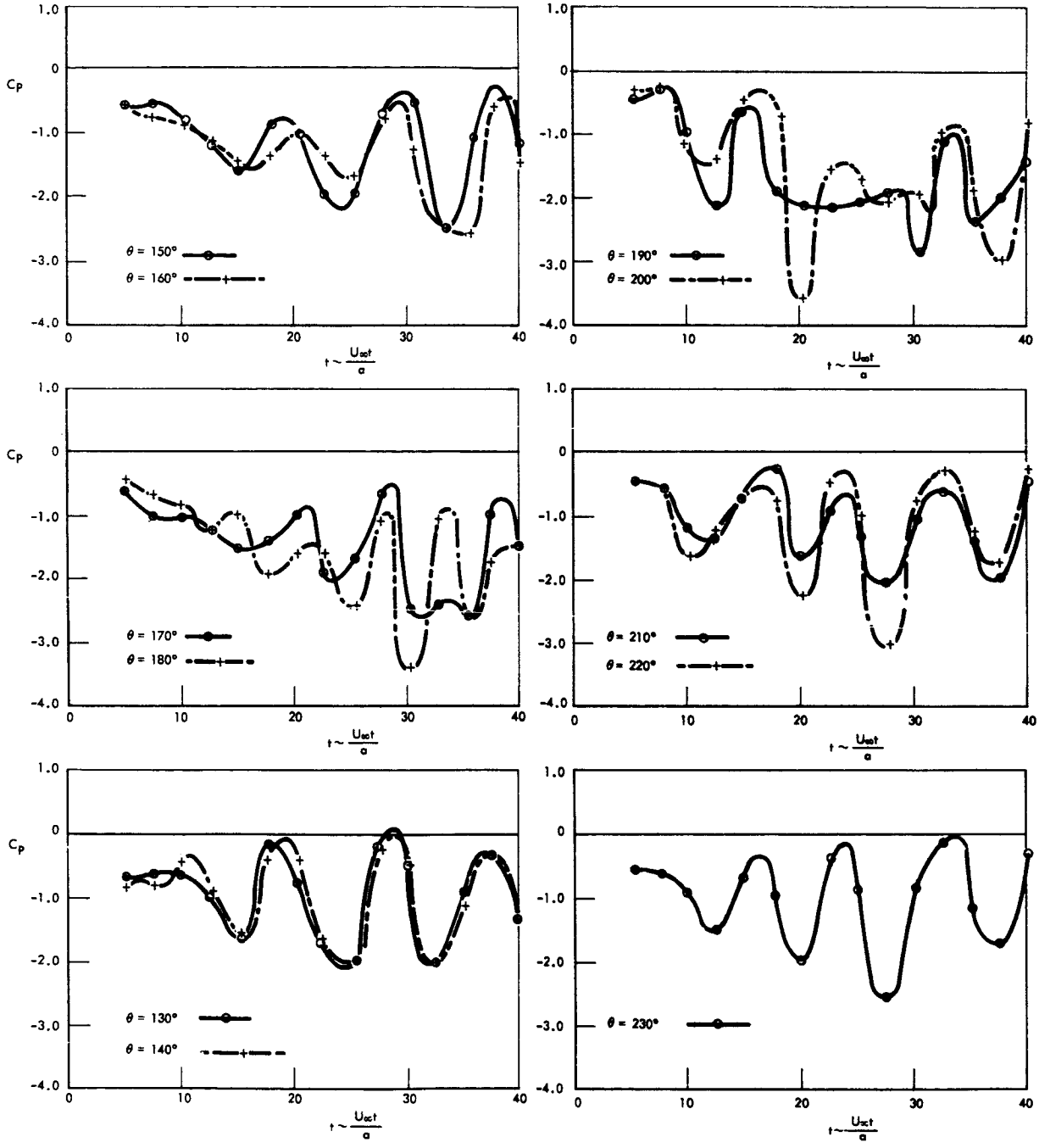

Figure 12. Pressure Coefficients for 11 Points on Wake-Exposed Portion

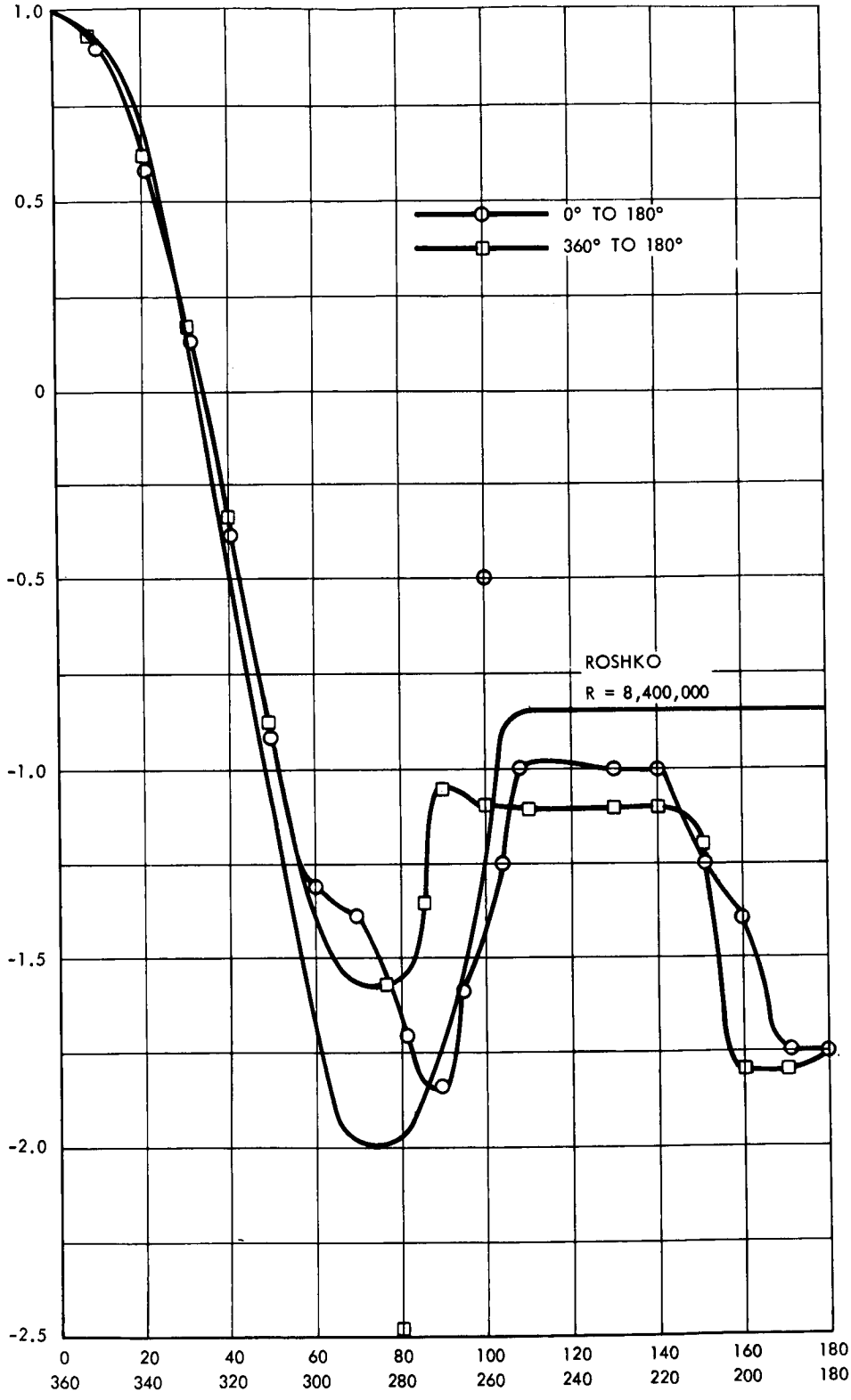

Figure 13. Time-Averaged Distributions of Cylinder Pressure Coefficient

pressure integration showed the error to be small. Therefore, since this computation method is much faster than numerical pressure integration, these force equations were used to determine the detail force time histories shown in Figure 14.

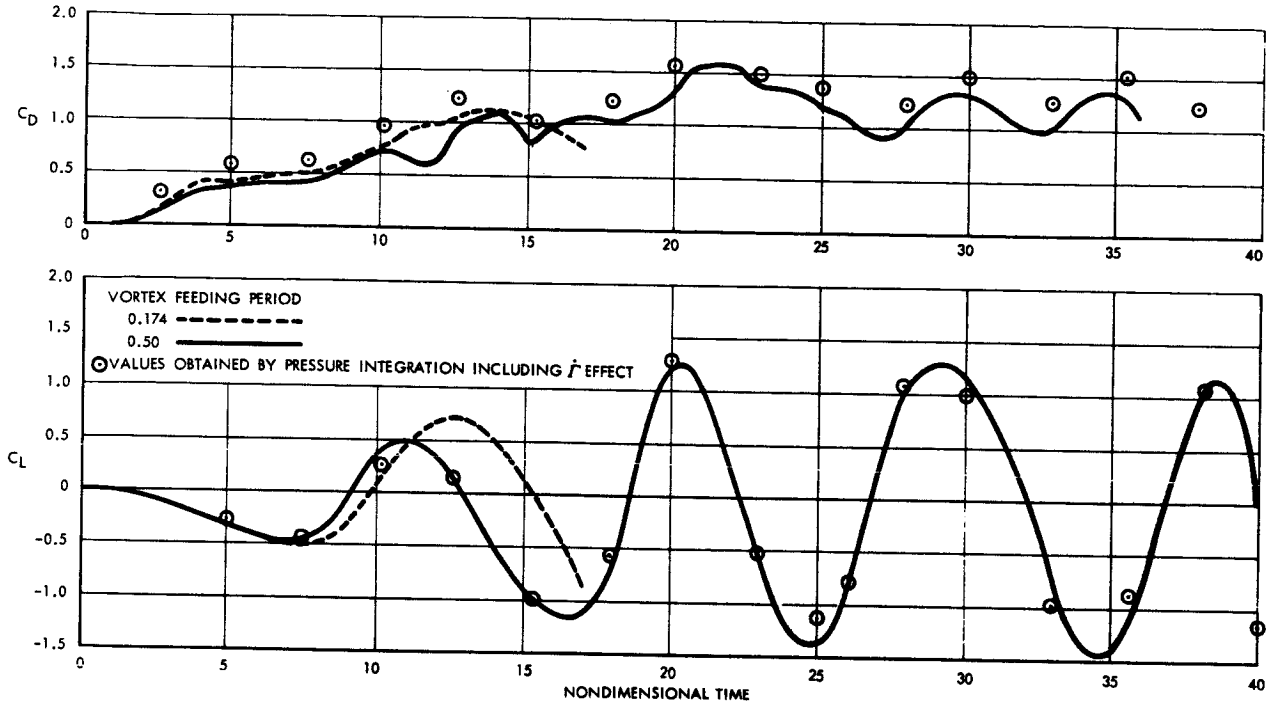

Figure 14. Effects of Vortex Feeding Period on Lift and Drag

Cylinder force time histories for two cases are shown. The one extending to a nondimensional time of 17 was obtained with a vortex feeding period of 0.174 and contained a total of 200 vortices in the field at the final time. This shorter time history of lift and drag corresponds with the flow development shown in Figure 9(B).

The longer time history extending to a nondimensional time of 40 corresponds to the flow development shown in Figures 9(C) and 15. This solution culminated in 160 vortices generated with a feeding period of 0.5 between successive pairs. For this longer run, pressure distributions on the cylinder were determined periodically at a time interval of 2.5 a/U_o. At the same time these pressures were integrated with Simpson's rule to determine lift and drag coefficients. Determination of force coefficients in this manner is mathematically straightforward, being based only upon the unsteady pressure equation. Effect of growth rate at the vortex feeding points are thus included in these coefficients. The circle points shown in Figure 14 are force coefficient values obtained by pressure integration.

Wake Characteristics

The correlation of computed cylinder pressures and forces with experimental data provide the most critical evaluation of applicability of potential flow theory to analysis of separated wake flows. A second but nonetheless important area of further correlation for which experimental data exists are the pressure and velocity profiles of the near wake. Roshko in Reference 17 presents averaged pressures along the wake centerline. Kovásznay (Reference 18) and Spitzer (Reference 4) present data on wake velocity profiles. To obtain results comparable to these data, wake pressure and velocity profiles were computed at various downstream sections in the near wake during the extended Model I solution. At each of these sections, average velocity profiles across the wake were determined by averaging nine instantaneous velocity profiles sampled uniformly over the time period from 17 to 40 a/U_o. Solutions at earlier times were considered to be affected by the starting transient, and were not included. While a more accurate approach would be to obtain average velocities by plotting velocity time histories at each point considered, sufficient time was not available to permit this amount of detail. Pressures along the wake centerline, however, were obtained in this manner. The general shape and smoothness characteristics of instantaneous wake profiles, is illustrated by the flow configuration for $t = 40.66a/U_o$. The vortex arrangement is shown in Figure 15 with vertical lines superimposed to indicate the downstream wake sections that were used in the computation.

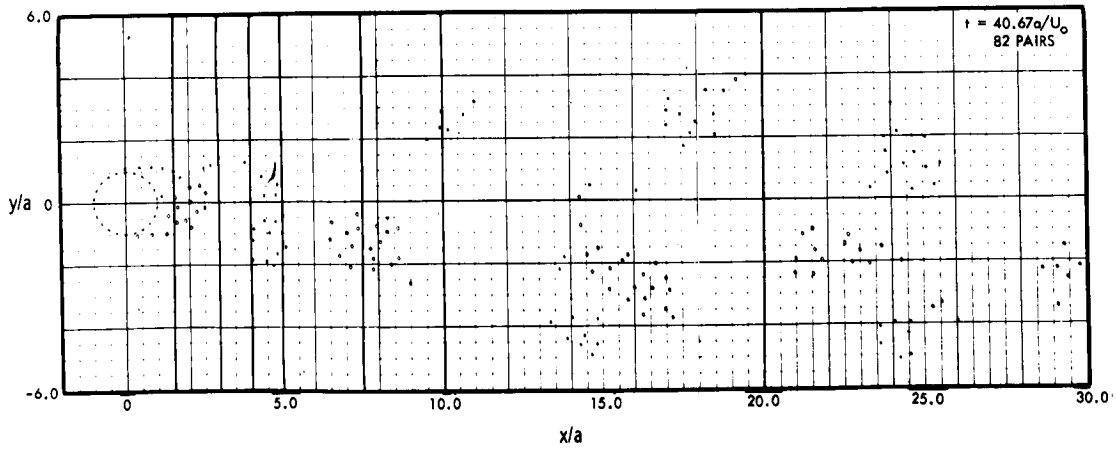

Figure 15. Characteristic Vortex Configuration (Model I). (Vertical Lines Indicate Section Where Instantaneous Wake Pressure and Velocity Profiles were Computed. See Figures 16 and 17)

The corresponding velocity and pressure profiles are shown in Figures 16 and 17. The circled points represent total pressure, while the starred points reflect pressures which do not include the effect of vorticity growth at the feeding points. The profiles are generally smooth except when discrete vortices are close enough to cause significant local distortion. One discrepancy has been noted. The asymptotic value of pressure coefficient far from the wake appears to be slightly biased from zero. In this case the asymptote appears to be about -0.1. Without certainty, it is believed that this may be associated with the fact that cylinder pressure distributions at the forward stagnation point in Figure 15 also are not precisely 1.0. Interestingly enough, an examination of the unsteady pressure equation (17) shows that for pressure coefficient to approach zero as y becomes large,

$$-\sum_{j=1}^{N} \frac{\partial K_j}{\partial t} \tan^{-1}\frac{y_j}{x} + \sum_{j=1}^{N} K_j \frac{x_j v_j - y_j u_j}{x_j^2 + y_j^2} \rightarrow 0$$

In the Model I solution, the discrete vortices are of constant strength except at the feeding points. Furthermore, the vorticity growth at the lower feeding point is the negative of that at the upper feeding point, with their locations 10 degrees forward and aft of the 90-degree axis, respectively.

Hence $$\sum_{j=1}^{N} K_j \frac{x_j v_j - y_j u_j}{x_j^2 + y_j^2} - \frac{\partial K}{\partial t} (100 \text{ degrees} + 80 \text{ degrees})$$

or $$\sum_{j=1}^{N} K_j \frac{x_j v_j - y_j u_j}{x_j^2 + y_j^2} \rightarrow \pi \frac{\partial K \text{ upper}}{\partial t} = \pi \frac{\alpha^2}{4\pi} = 0.462$$

On a physical basis, the reason for this particular relationship is not apparent. Superficially, at least, it might be conceded that the time <u>average</u> value of the term $\sum_{j=1}^{N} K_j \frac{x_j v_j - y_j u_j}{x_j^2 + y_j^2}$ might be some constant value. But that its instantaneous value should be invariant implies a condition not understood. Yet the fact that it is being satisfied to within the magnitude of the bias (approximately 0.1) is clear from the computations. As a matter of interest, the magnitude of this bias, i.e., the asymptotic pressure coefficient at large values of y, observed in the nine time samplings of wake pressure are shown in Table III.

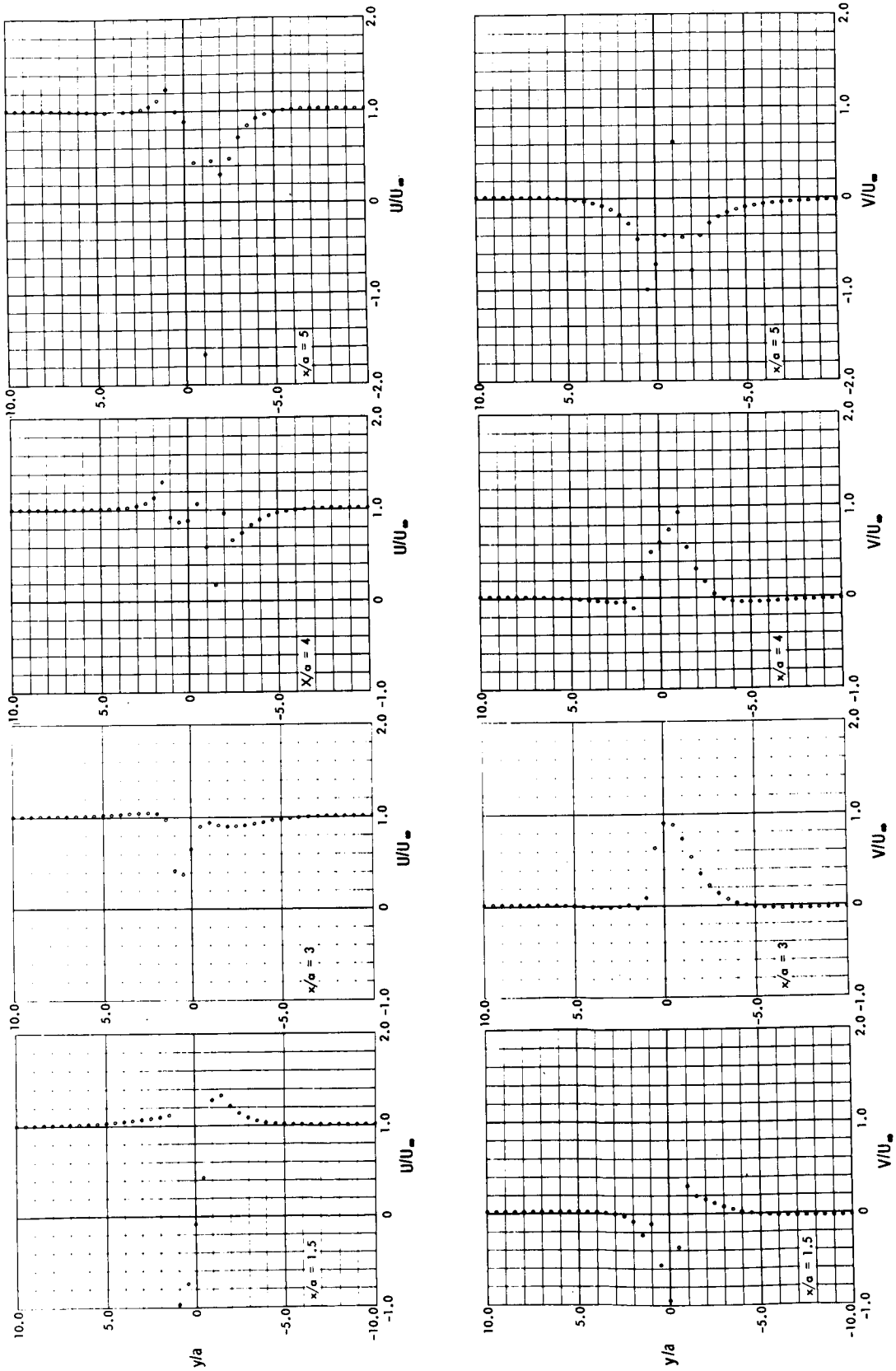

Figure 16. Instantaneous Wake Velocity Profiles (Sheet 1 of 2)

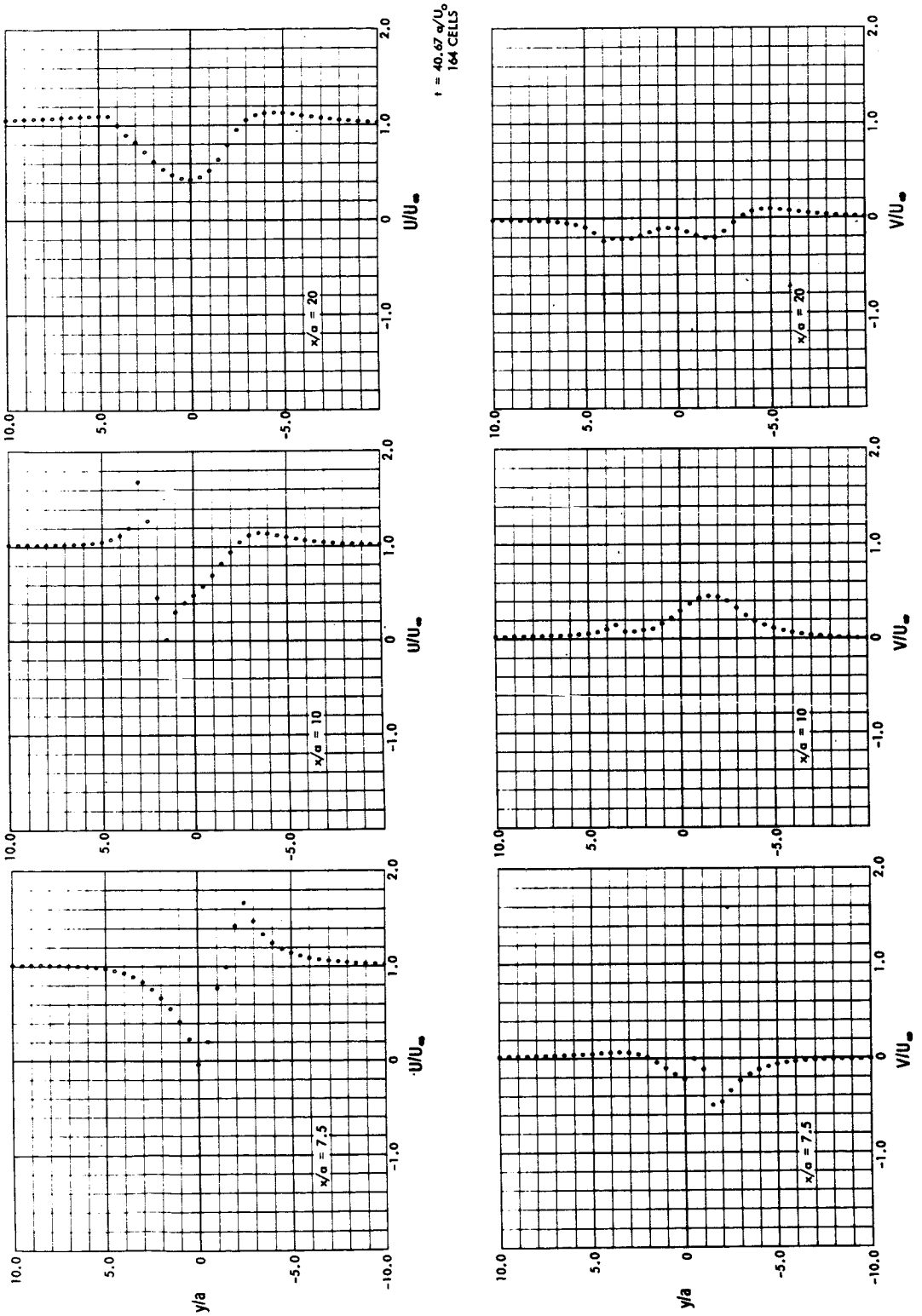

Figure 16. Instantaneous Wake Velocity Profiles (Sheet 2 of 2)

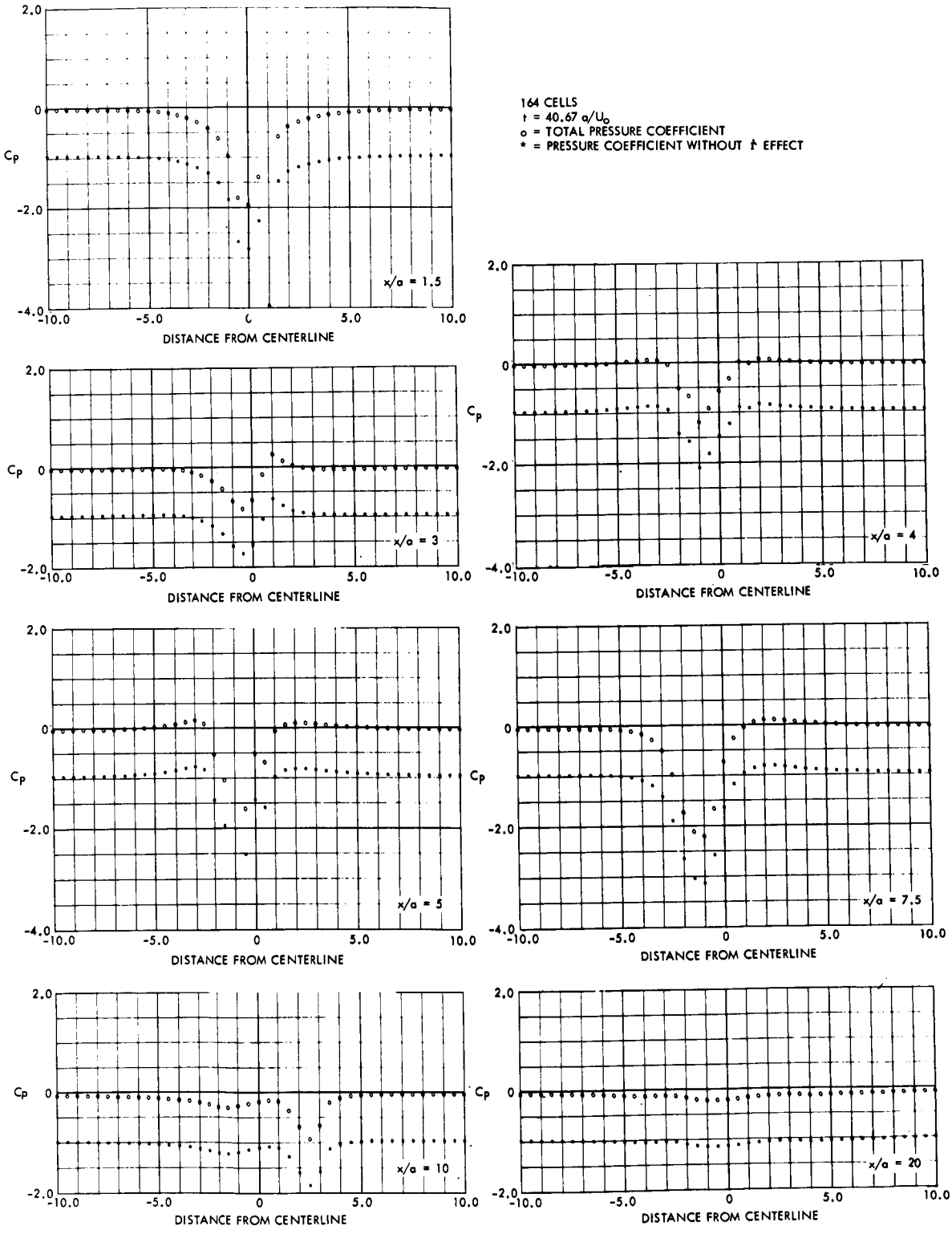

Figure 17. Instantaneous Wake Pressure Profiles

Table III. Wake Pressure Bias From Zero

$\frac{U_o t}{a}$	(C_p) at $\frac{x}{a} = 20.0$	
	y/a = +10	y/a = -10
17.26	-0.11	-0.09
22.87	-0.022	-0.012
25.42	-0.12	-0.10
27.96	+0.09	+0.088
30.5	-0.023	-0.012
33.04	-0.19	-0.145
35.5	-0.18	-0.151
38.12	-0.14	-0.143
40.66	-0.075	-0.05

A possible alternative interpretation may be expressed by the following argument. It is noted that the above expressions leading to finite pressure at infinity stem from the inclusion of the term $(\tan^{-1} -y_j/x_j)$ in the potential equation (13). If, at infinity, the condition of $C_p = 0$ is imposed, the right-hand side of the pressure equation (7), namely $\bar{C}(t)$, could be required to cancel out the troublesome term above. In this way, the pressure at infinity could be made exactly zero.

Pressures along the wake centerline were also computed at each of the nine time points tabulated above. The average of these values have been used to construct the average pressure coefficient along the wake centerline. This curve is shown in Figure 18. For comparison, Roshko's data from Reference 17 are also shown. These data were taken at a Reynolds number of 14,500.

The reduction of wake velocity profiles was accomplished in a manner roughly analogous to that described by Kovasznay (Reference 18) and followed by Spitzer (Reference 4). The mean pressure at a point was first determined by averaging the nine wake velocity computations; deviation about this mean was then determined.

Thus $$\sqrt{\overline{V^2}} = \left[\frac{\sum_{i=1}^{9} (V_i - \bar{V})^2}{9} \right]^{1/2}$$

where $$V = \vec{u} + \vec{v}$$

$$\bar{V} = \frac{\sum_{1}^{9} V_i}{9}$$

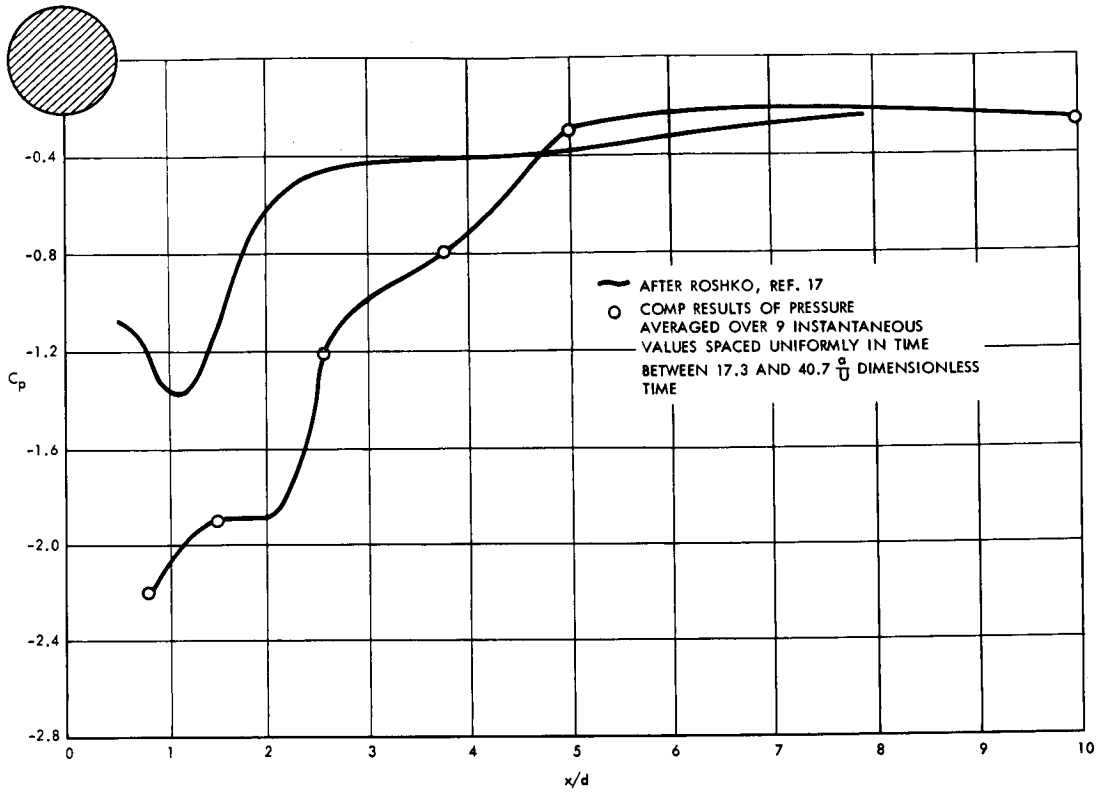

Figure 18. Average Wake Pressure on Center Line

The mean resultant velocity profile for $\frac{x}{a} = 3$ and 7.5 are shown in Figure 19 with Kovásznay's data (Reference 18) near the same downstream distance shown for comparison. The data by Kovásznay were taken at a Reynolds number of 56, just above critical value. The rms deviations for these same downstream points are shown in Figure 20 with Spitzer's data superimposed for comparison. The Reynolds number for the data by Spitzer is given as 2.5×10^5.

Wake Velocities for Vortex Shedding

Average wake velocities related to unsymmetrical flow about a circular cylinder were studied using the wake velocities generated as output from the Model I program. Wake center-line values of horizontal velocity for the nine time points ranging from 17.27 to 40.67 seconds were averaged and the mean velocity for each of seven wake locations are plotted and joined by the continuous curve shown in Figure 21. The mean velocity curve obtained from an investigation of cylinder wake properties by Kovásznay (Reference 18) is represented by the dashed curve of Figure 21.

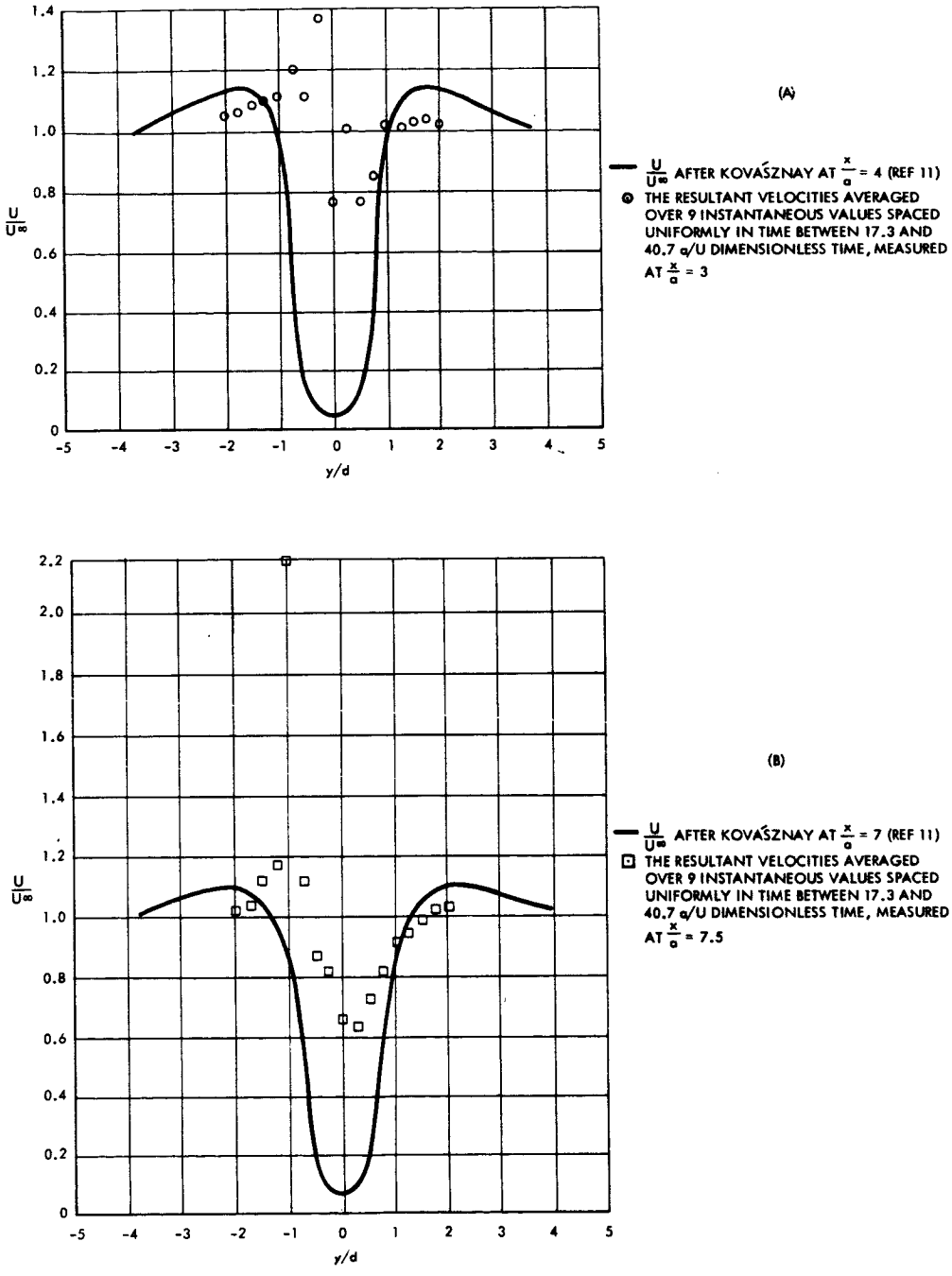

Figure 19. Computed Mean Wake Velocity Compared with Experimental

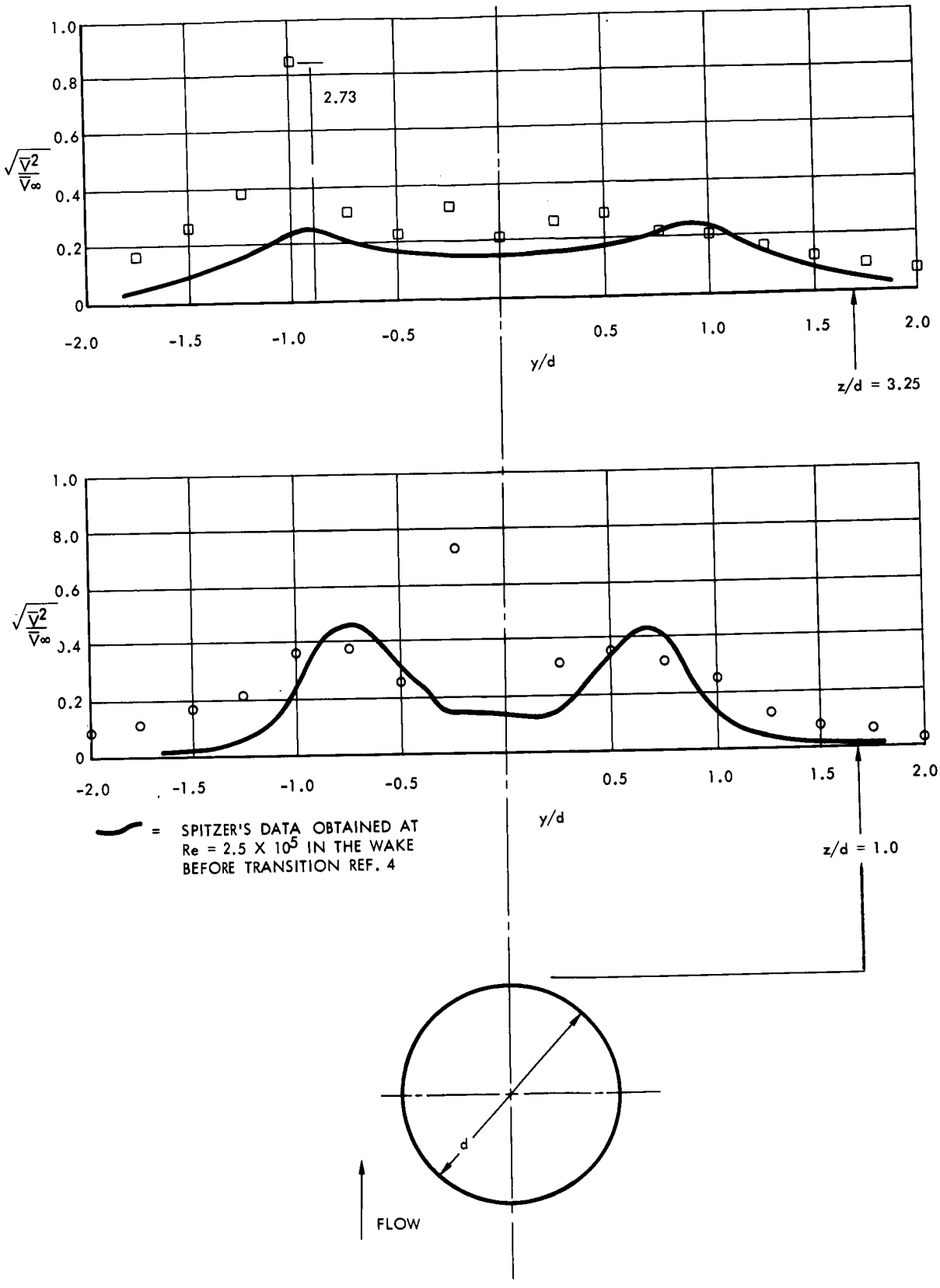

Figure 20. Wake RMS Velocity Fluctuations

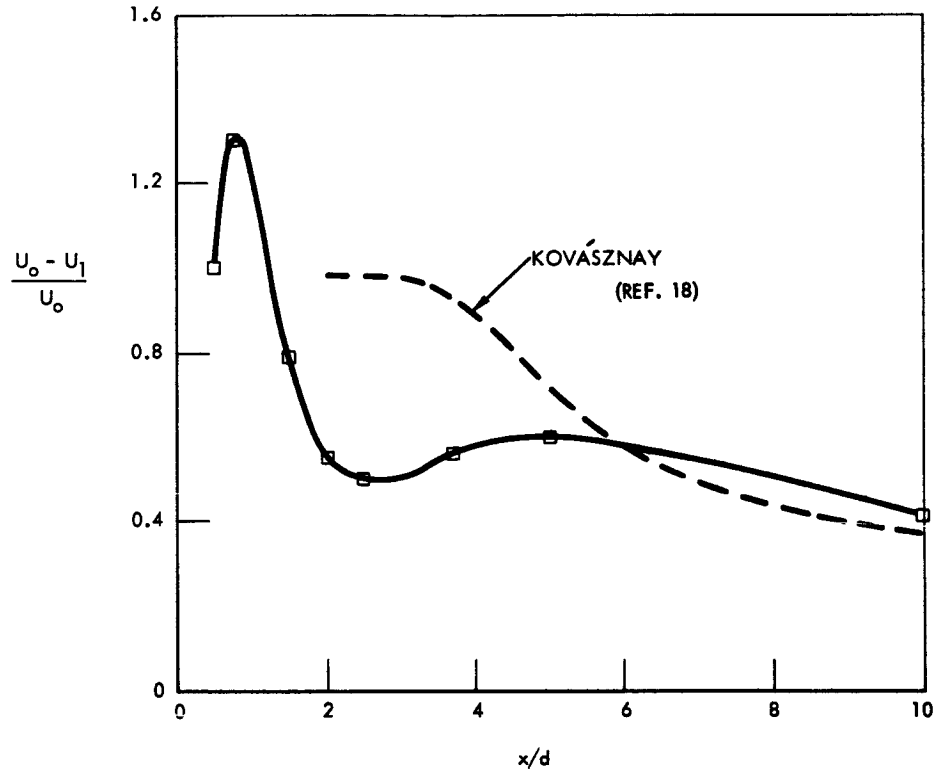

Figure 21. Center-Line Wake Velocity vs Distance Downstream

SYMMETRICAL SEPARATED FLOW ABOUT A CIRCULAR CYLINDER

In physical experimentation involving rectilinear motion of a circular cylinder at Reynolds number above 40, the flow conditions are initially symmetrical. However, inherent turbulence in the flow or asymmetries in the circular shape eventually cause the flow symmetry to break down. The final state, depending upon the Reynolds number, may or may not exhibit

periodic vortex shedding. A well-known experiment involving cylinder flow in the initial symmetrical state is that by Schwabe (Reference 19). The Reynolds number for this experiment was 580. Flow development was recorded to a time of $9a/U_o$. Streamlines were photographed by the aluminum particle technique, and pressure distributions were determined by use of these streamlines. From these data Schwabe determined a C_D time history that reached a value between 1.9 and 2.0 at $U_o t/a = 6.0$.

A simulation of Schwabe's experiment was attempted with the Model I program. Since both vorticity transport rate and feeding point location had to be specified, a unique solution could not be obtained. Therefore the principal objective was to determine the particular vorticity transport function which would produce a drag curve similar to that in Reference 19. If successful, such a reference curve of vorticity transport could be helpful in checking results obtained by a more sophisticated approach wherein the vorticity transport rate and feeding point locations are implicitly determined in the solution. Feeding point location was maintained always at the 90-degree position, and feeding period was $0.52\ a/U_o$. The integration period was $0.0435\ a/U_o$.

Since the condition of flow symmetry considerably simplifies the velocity field computations, a separate Model I program incorporating this simplification was checked out and used for this study. A three or four minute computer run was normally sufficient to obtain a solution out to $17\ a/U_o$ with this "symmetrical" program. An initial estimate of the vorticity transport rate was made from the relationship

$$\frac{d\Upsilon}{U_t} = \frac{1}{2}\frac{U_s^2}{U_o^2} = \frac{1}{2}\alpha^2 = 1 - \overline{C}_{p\ \text{wake}}$$

where $\overline{C}_{pw}$ is the average pressure coefficient over the wake-exposed portion of the cylinder.

Pressure coefficients on the cylinder are given in Reference 19 for various stages in the flow development. These pressures are fairly uniform over the wake portion. Hence, using these average wake pressures in the relationship above, a time variation of vorticity transport rate was derived and is shown as curve 1 in Figure 22. Curve 2 represents an initial approximation which resulted in drag coefficient growth illogically high compared with available references. Curve 3 of this figure depicts a rate

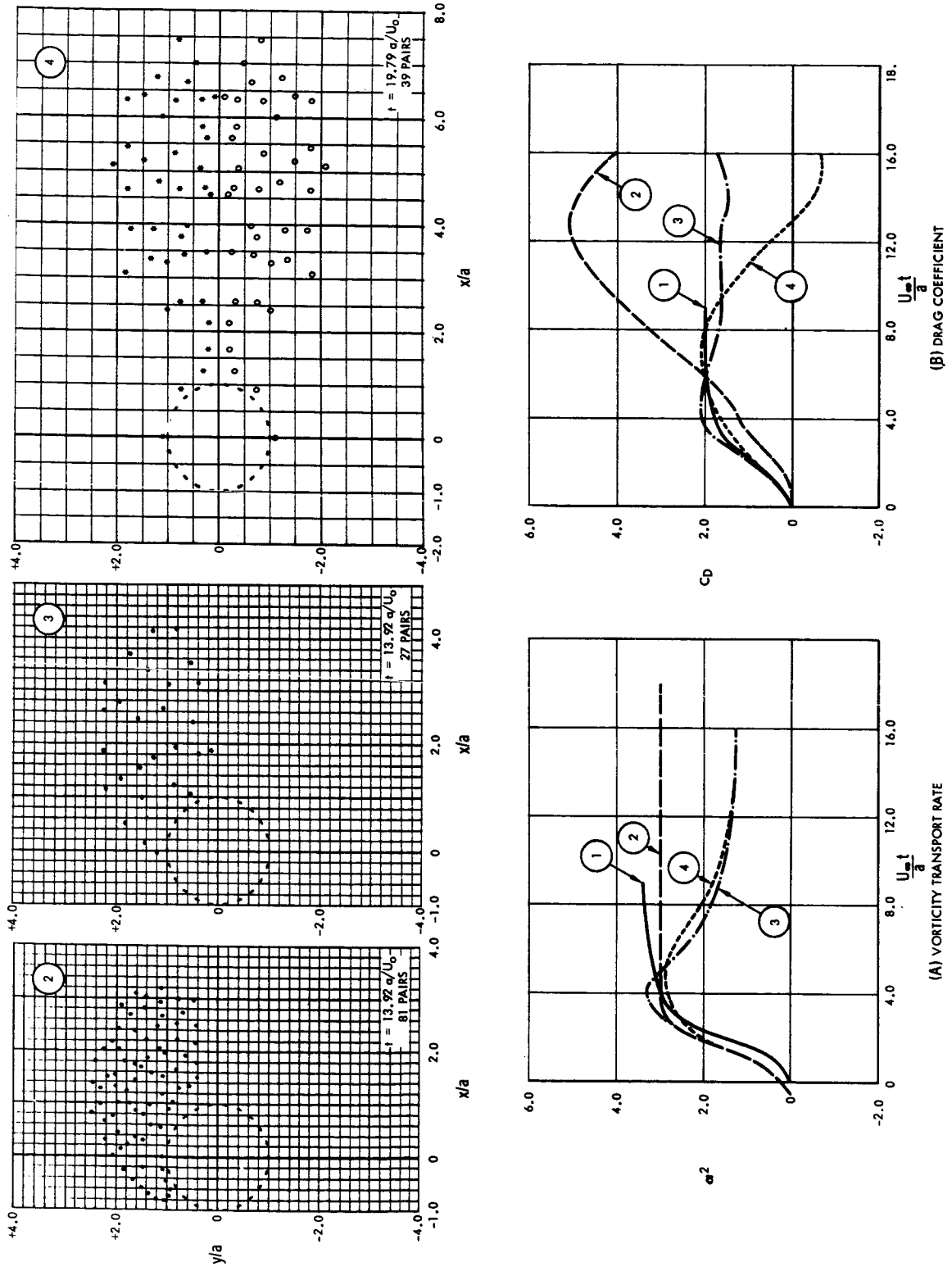

Figure 22. Effects of Variation in Vorticity Transport Rate

which gives reasonable correlation with Schwabe's data, and Curve 4 has good initial agreement but displays a radical departure with vortex growth. Drag coefficient variation curves corresponding to the above vorticity transport curves have like identification numbers in Figure 22 (B) and clearly illustrate the sensitive nature of changes to the vorticity transport rate. Vortex patterns generated for α^2 curves 2, 3, and 4 are presented in Figure 22 (C).

These plots demonstrate a similar sensitivity to variations of the vorticity transport rate. Plot 2 shows a forward motion of the vortices which are introduced at symmetrically located feed-in points of ±90 degrees. This trend is considered to be a result of the vortex build-up without obvious tendency toward shedding. Plot 3 displays the typical shape for one-half of a symmetrical vortex, and Plot 4 shows the symmetrical case for incipient shedding. In this case, the upper vortex is reflected to complete the symmetrical contour. The number of discrete vortices shown varies according to the elapsed time selected and the rate at which additional vortices are introduced.

Repeated attempts at readjusting the vorticity transport curve were made in an effort to establish correlation between input and output. The trend of α^2 with drag coefficient and integrated area of the transport rate curve related to maximum drag coefficient were studied in making alterations to the α^2 time variation. Although some measure of correlation was established, the sensitivity of transport curve changes seems to indicate that transport rate cannot be specified by a general curve but must be determined as an implicit part of the solution.

Computer plots depicting the development of discrete vortices in the flow are shown in Figure 23 for the solution corresponding to curves 3 of Figure 22 (A) and (B).

The distribution of cylinder pressure corresponding to the vortex configuration of Figure 23 (E) is shown in Figure 24. Pressure discontinuity at 90 degrees is due to the single vortex sheet connecting the feeding point radially to the cylinder surface. Magnitude of this discontinuity is α^2. The large variation in pressure between 90 and 180 degrees is indicative of considerable reverse flow in this region. The forward stagnation shows a pressure coefficient of approximately 1.3 whereas experimental data generally shows the pressure there to be 1.0 with possibly 10 percent maximum variation (Reference 20).

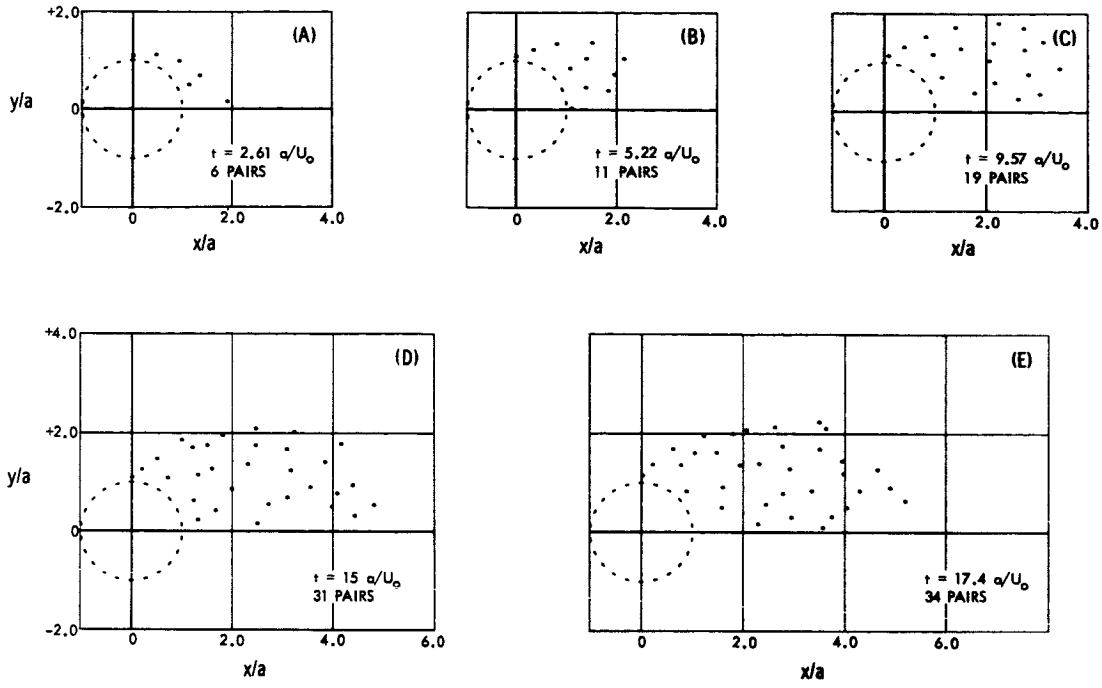

Figure 23. Wake Development for an Impulsively Started Cylinder

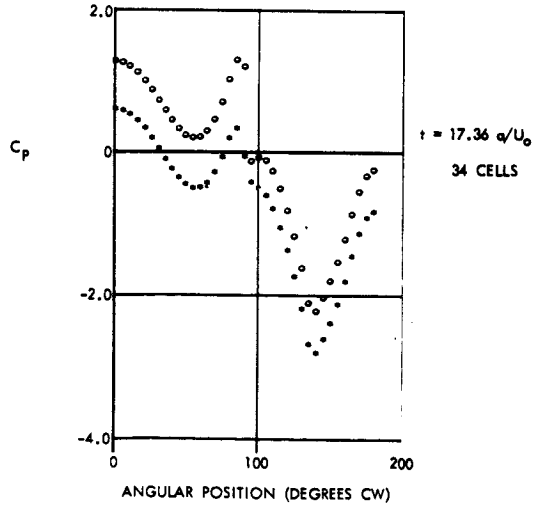

Figure 24. Typical Cylinder Pressure Distribution for Symmetrical Flow

SYMMETRICAL SEPARATED FLOW ABOUT A FLAT PLATE

Separated flow about a flat plate normal to the flow is of interest for the following reason. It is known that, experimentally, the flat plate drag coefficient of 2.0 is nearly independent of Reynolds number. Furthermore, flow separation always occurs at the edge. It would appear then, that vorticity transport is the only major parameter requiring definition. If so, the approach developed in this study should result in a drag coefficient that agrees with experiment if the correct vorticity transport rate can be specified.

With this in mind, the Model I program for symmetrical flow about a circular cylinder was extended to the more general case of symmetrical flow about an ellipse. The special case of flow about a flat plate was then studied by using an ellipse with major-to-minor-axis ratio of 10. It was believed that this ellipticity was sufficiently high to simulate a flat plate, yet avoid the infinite potential velocity at the edge. The vortex feeding point was positioned at 0.02 mean radius from the surface on normal 10 degrees aft of the vertical axis. A constant α^2 value of 1.5 was based upon the data of Reference 17.

Only one computer solution for the flat plate was obtained. The results show characteristic wake development basically similar to that obtained for the Model I solution to symmetrical flow about a cylinder for the case of excessive vorticity transport. (Figure 22(C).) The wake pattern outlined by the vortices at a nondimensional time of 61.72 is shown in Figure 25 (A). Its similarity to Figure 22(C) is evident. The computed rise in drag coefficient is shown in Figure 25 (B).

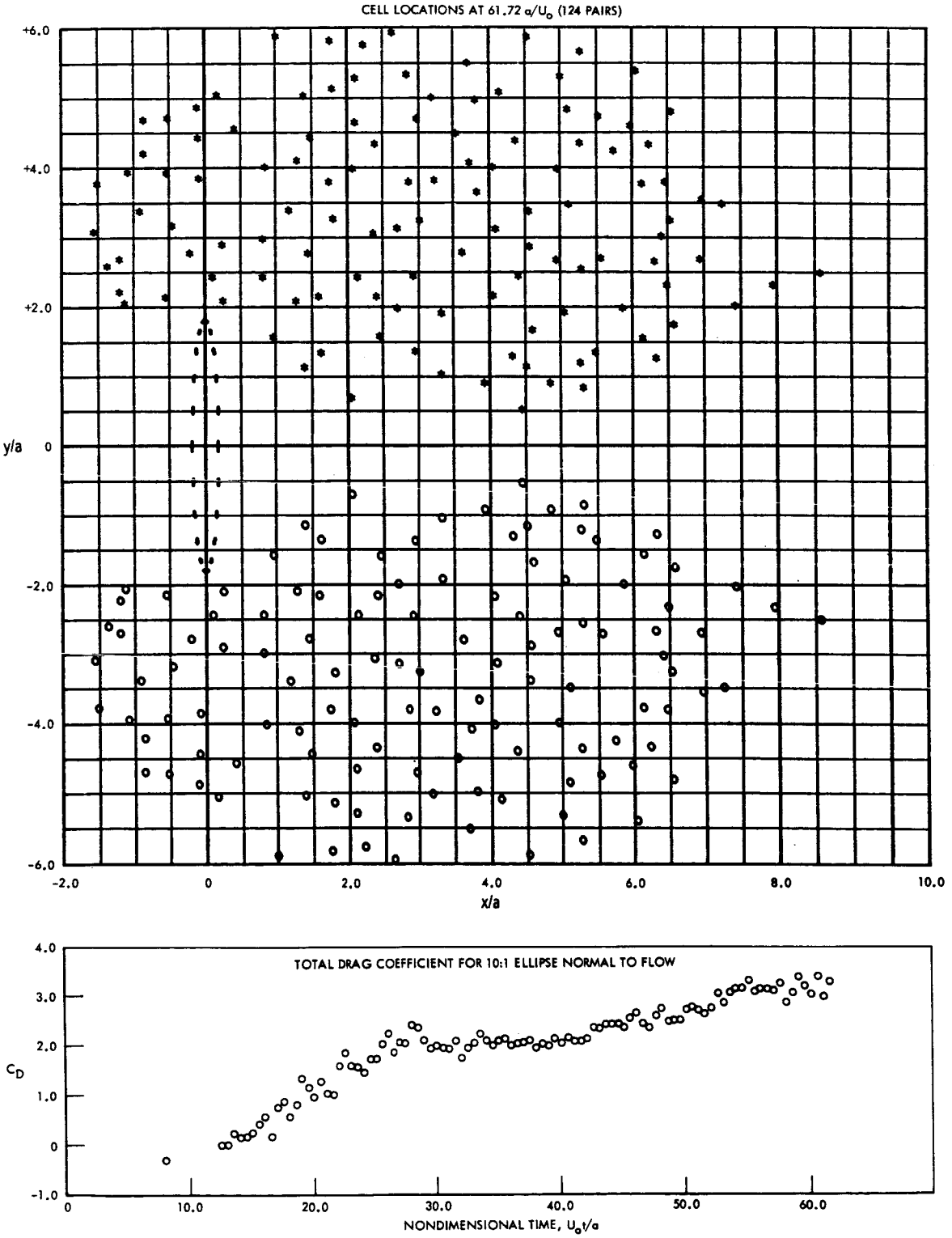

Figure 25. Model I Solution for Flat Plate

SOLUTIONS WITH MODEL II PROGRAM

UNSYMMETRICAL FLOW ABOUT A CIRCULAR CYLINDER

The Model II program for unsymmetrical flow was used with essentially the same integration parameters as for the extended Model I solution. Radial position of the feeding point was kept at 0.1 radius from the cylinder surface. Feeding period was 0.5 a/U_o and integration period was 0.05 a/U_o. Some initial experimentation was made to determine the asymmetry required to achieve rapid onset of periodic shedding. A set of 12 pairs of initial vortices were determined by situating them on the uniform flow streamline passing through 1.1 cylinder radii. Their strengths were determined from the local tangential velocity and a time increment of 0.2 a/U_o during which vorticity at a point was accumulated. It was found that if vortices were used for only one side, the asymmetry was excessive and numerical instability resulted. Using quarter-strength vortices on one side resulted in a stable solution with acceptably rapid onset of periodic shedding. This initial configuration of vortices is shown in Figure 26. A one-hour computer run was made.

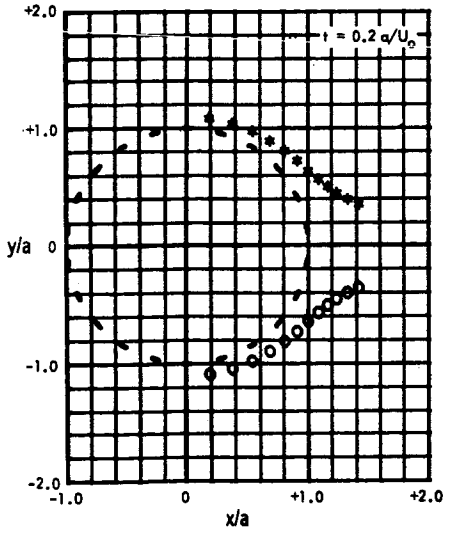

Figure 26. Initial Cell Locations

This run produced 850 graphs of vortex position and time histories of C_L and C_D to a nondimensional time of 40. The graphs of vortex position have

been made into a movie which aids considerably in developing an insight into the flow mechanics. Selected frames from this movie are shown in Figure 27, together with corresponding pressure distributions. The final vortex configuration is shown in Figure 28. Time histories of C_L and C_D are shown in Figure 29. Note is made of the fact that these force time histories do not include an incremental effect due to time rate of change in vorticity at the feeding points. This effect is secondary, as discussed previously, and it is believed that the curves in Figure 29 may be considered computationally correct to within 10 percent.

Pressure distributions are shown for the first three frames in Figure 27 to illustrate their typical appearance. The "steady C_p" and the pressure distributions with and without the effect of vorticity growth rate are shown. Circle points represent total pressure, whereas the starred curve is the one used for determining the minimum pressure point according to the particular Model II approach adopted for this study. The time variation in feeding point peripheral position and vorticity transport rate at the upper and lower vortex feeding points are also shown. The "steady C_p" of Figure 27 is simply $1 - \left(\frac{V_T}{U_o}\right)^2$ hence indicate the magnitude of local tangential velocity.

The force coefficients of Figure 29 are significantly greater than those encountered experimentally. For example, the mean drag coefficient is about 1.6 whereas experimentally this should be 1.2 for subcritical Reynolds numbers (Reference 15). Maximum lift coefficient of over 2.0 shown in Figure 29 compares with 1.1 or 1.2 at subcritical Reynolds numbers, Reference 20. It was concluded from this comparison that vorticity cancellation effects, not included in these results, are important.

In Reference 17 Roshko (after Fage and Johansen) utilizes a parameter, ϵ, which defines the net percentage of the total vorticity generated in the boundary layer that moves downstream by convection in the Kármán vortices. Fage and Johansen (Reference 17) concluded from experimental evidence that ϵ must be 0.5. According to Gerrard (Reference 20), reverse flow velocities in the wake are responsible for a significant amount of counter vorticity.

It is observed that incremental vortices in Figures 27 and 28 do not show a great deal of mixing, certainly not enough to indicate a 50 percent reduction of vorticity. On the other hand, the "steady C_p" curves in Figure 27 show that relatively large reverse velocities exist over some rearward portions of the cylinder. It is reasonable to expect that these areas of high reverse velocity would generate a significant amount of counter vorticity. Such counter vorticity in turn would increase the vorticity cancellation.

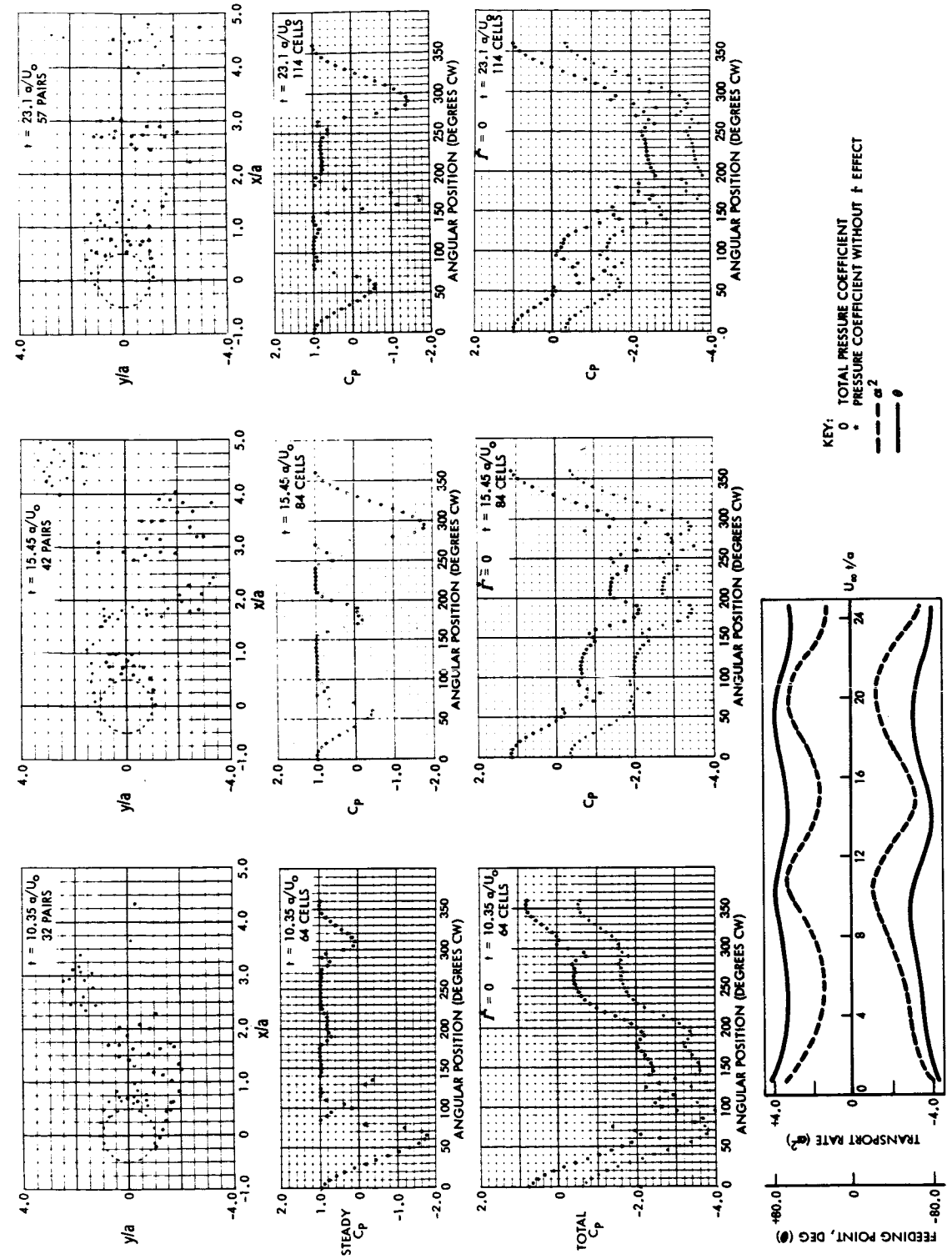

Figure 27. Unsymmetrical Flow About a Circular Cylinder (Model II)

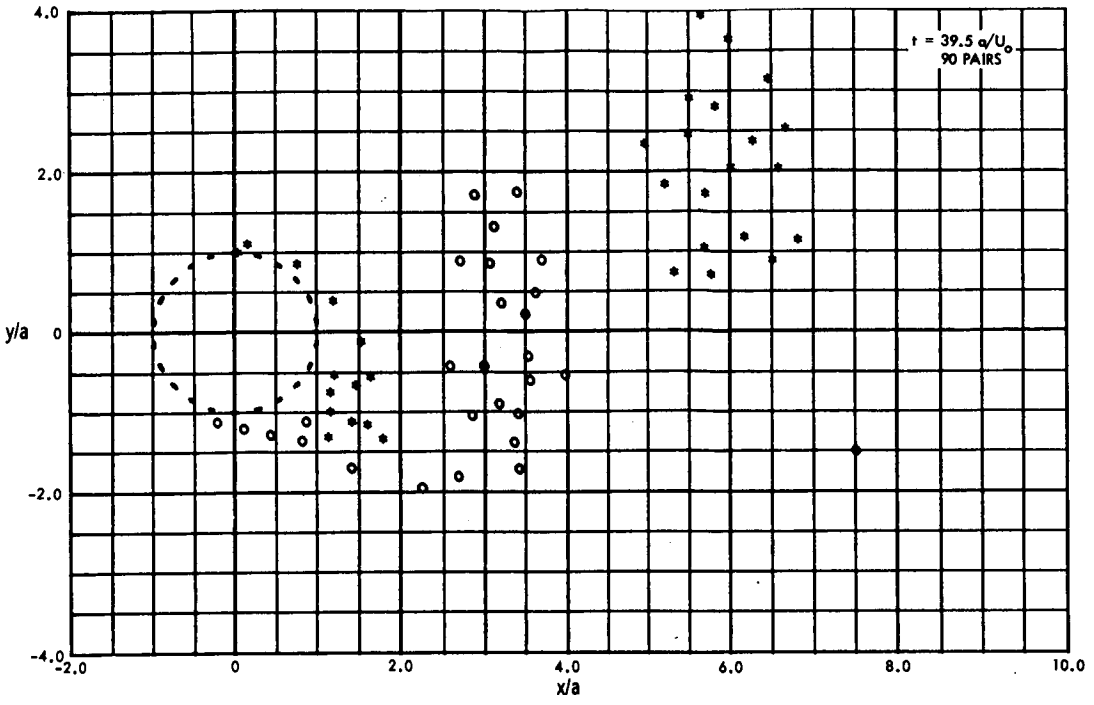

Figure 28. Vortex Configuration for Unsymmetrical Flow

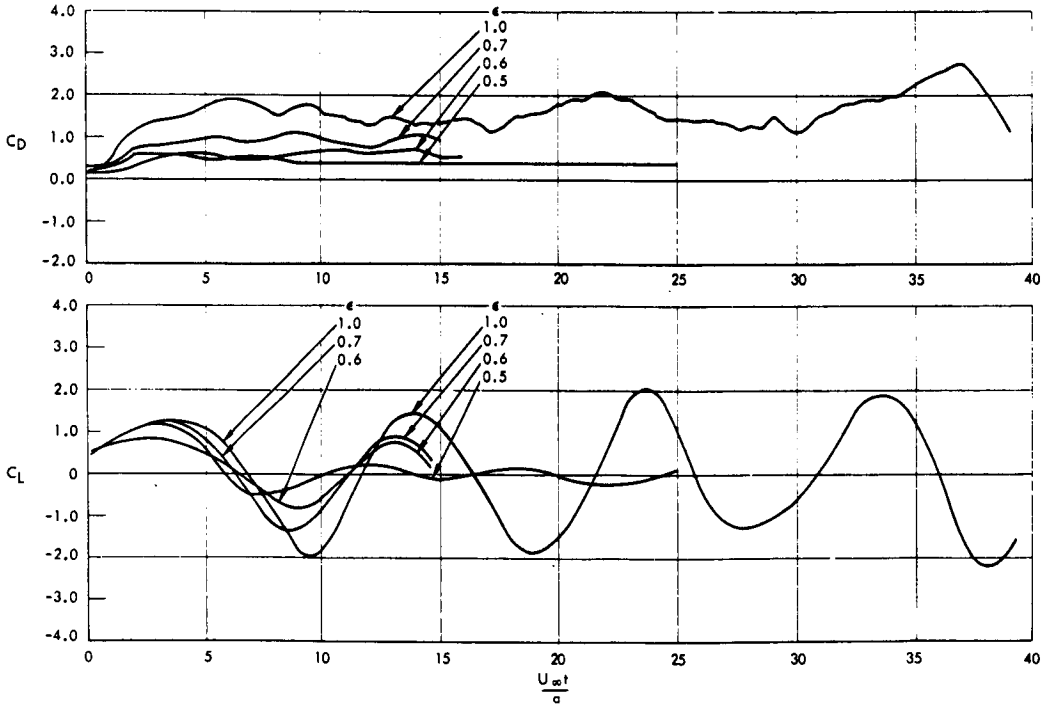

Figure 29. Lift and Drag Time Histories (Model II Unsymmetrical Flow)

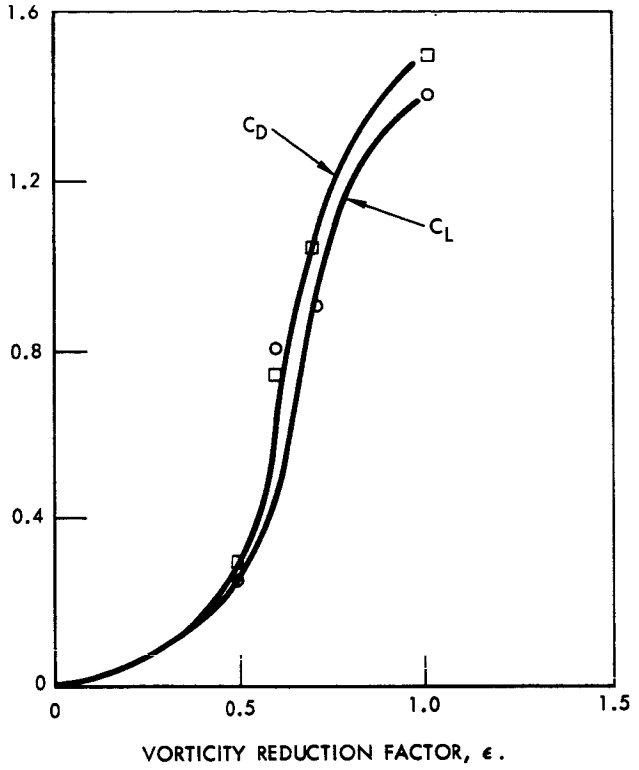

Figure 30. Variation in C_L and C_D at Time of Second Peak in C_L (Ref. Figure 29)

As a first approach in accounting for this counter vorticity and vorticity cancellation, the parameter ϵ was applied directly to the primary vortex feeding points. The value of ϵ was varied between 0.5 and 1.0 and computer solutions were obtained to determine the effect on lift and drag coefficients. The variation of C_L and C_D at time of second peak in C_L in Figure 29 is shown in Figure 30. The solutions for ϵ = 0.5, 0.7 and 1.0 were obtained with identical initial vortices. The solution for ϵ = 0.6 was obtained with the initial vortices reduced in strength by ϵ.

From these results it appears that a value of ϵ between 0.6 and 0.7 results in lift and drag coefficients in agreement with subcritical Reynolds number data. This value is higher than the 0.5 given by Fage and Johansen (Reference 17). It may be noted in Figure 31 that significant reversed velocity still occurs for ϵ as low as 0.6, although the total pressure distribution is now fairly uniform over the wake.

Wake development for ϵ = 0.5 is also shown in Figure 31, together with corresponding cylinder pressures. These results show very little reversed velocity of the cylinder.

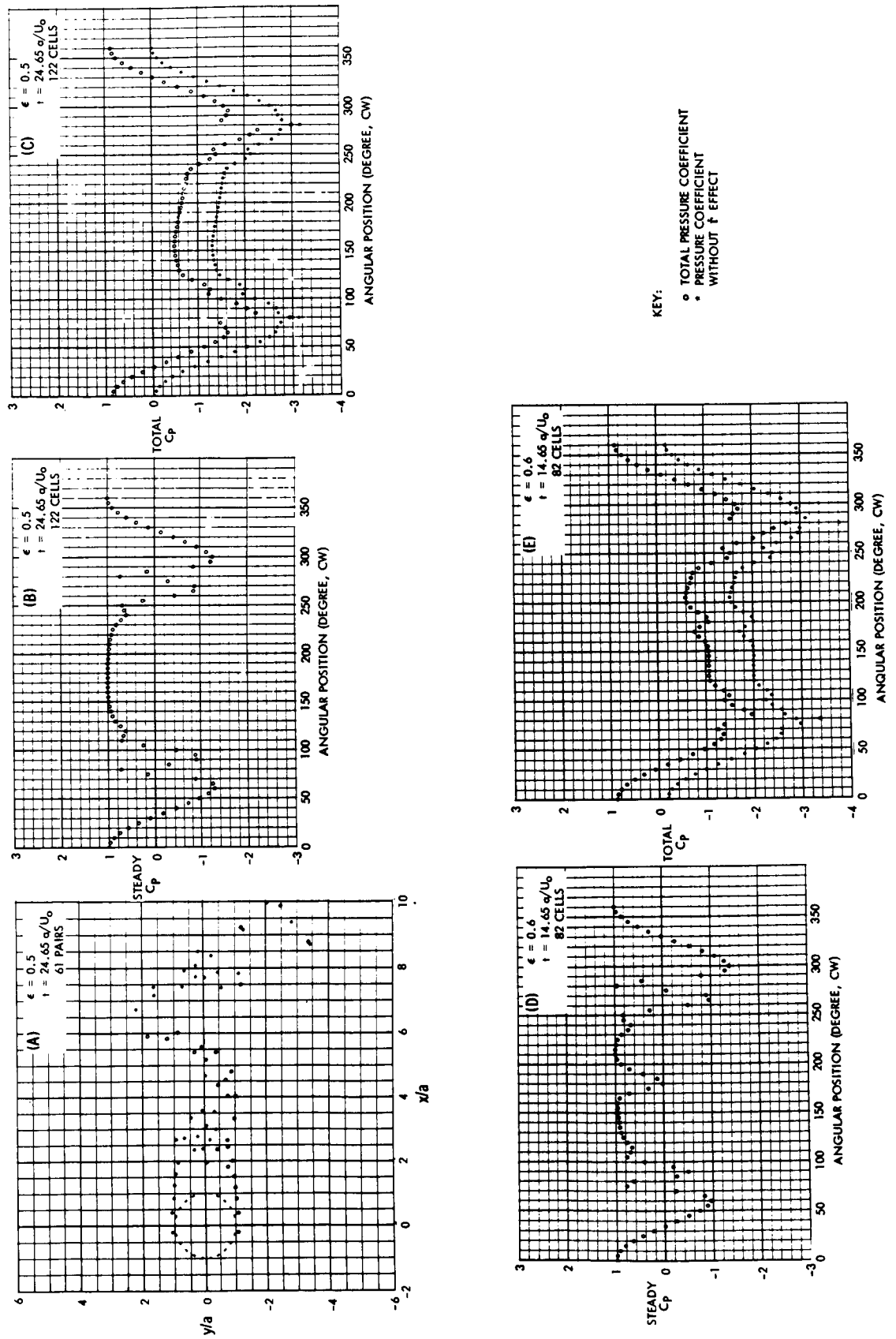

Figure 31. Vortex Patterns and Cylinder Pressures for $\epsilon = 0.5$ and 0.6

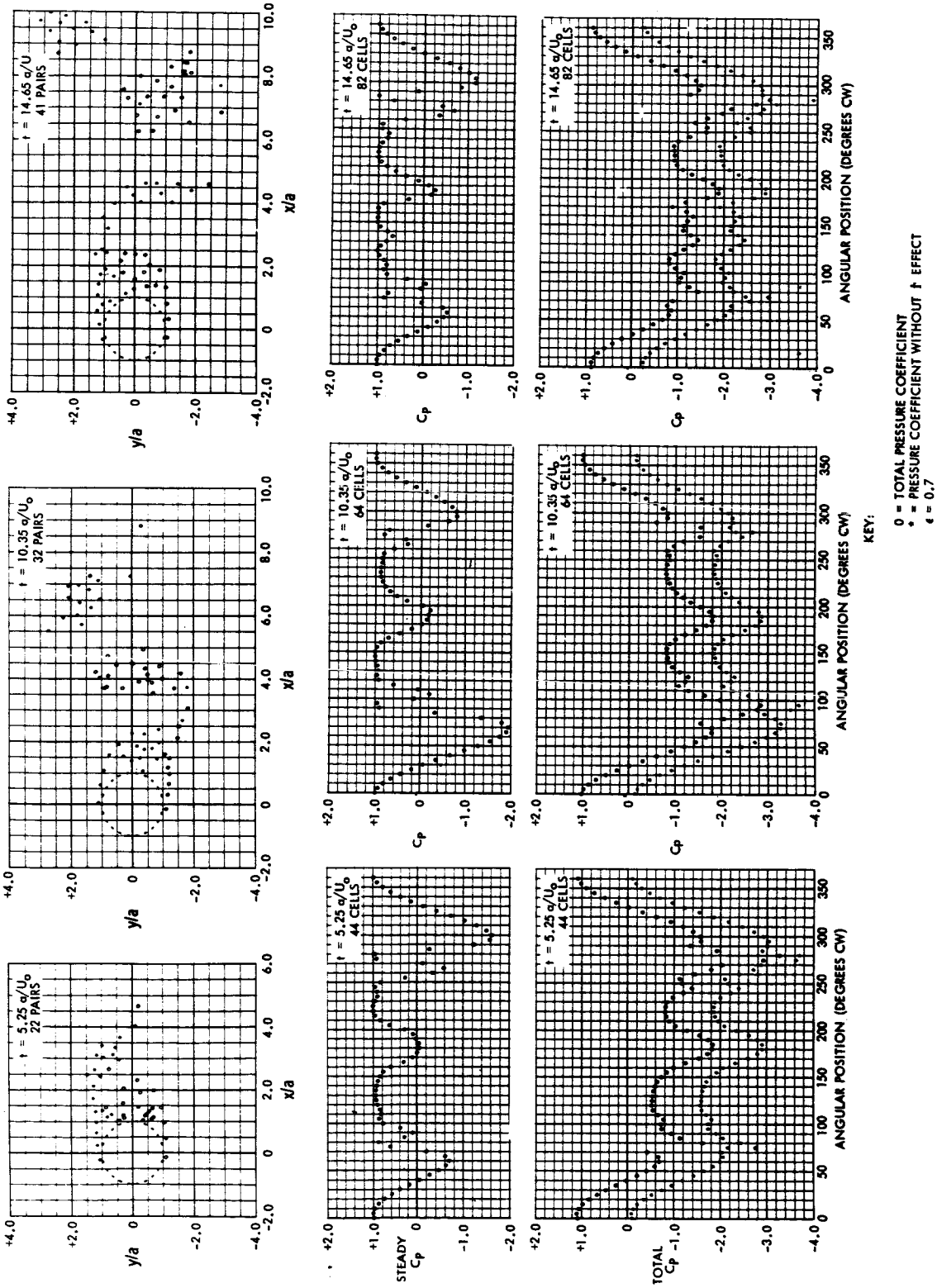

Figure 32. Vortex Patterns and Cylinder Pressures for $\epsilon = 0.7$

For $\epsilon = 0.7$ the Strouhal number is 0.22 from the first cycle of lift force. Flow development is shown by the incremental vortices in Figure 32, for $\epsilon = 0.7$, at three time points in the flow. Curves of $1 - V_T^2$ on the cylinder surface are indicated by asterisks as "steady C_p." Total pressure coefficient is also shown in Figure 32. Partial force time histories for $\epsilon = 0.5$, 0.6, and 0.7 were shown in Figure 29 superimposed on the time history obtained for $\epsilon = 1.0$.

UNSYMMETRICAL FLOW STREAMLINES

Streamlines for certain flow conditions were determined from the stream function represented by the imaginary part of the complex potential, Equations (2) and (3). The particular form programmed for the computer was

$$\frac{\psi(x, y)}{U_o a} = -\frac{y}{a}\left[1 - \frac{1}{\left(\frac{x}{a}\right)^2 + \left(\frac{y}{a}\right)^2}\right]$$

$$+ \sum_{j=1}^{n} \frac{K_j}{U_o a} \log \left[\frac{\left[\left(\frac{x}{a} - \frac{x_j^i}{a}\right)^2 + \left(\frac{y}{a} - \frac{y_j^i}{a}\right)^2\right]^{1/2} \left[\left(\frac{x_j}{a}\right)^2 + \left(\frac{y_j}{a}\right)^2\right]^{1/2}}{\left[\left(\frac{x}{a} - \frac{x_j}{a}\right)^2 + \left(\frac{y}{a} - \frac{y_j}{a}\right)^2\right]^{1/2} \left[\left(\frac{x}{a}\right)^2 + \left(\frac{y}{a}\right)^2\right]^{1/2}}\right]$$

The technique adopted to construct computer plots of flow streamlines uses letters of the alphabet to denote lines of constant ψ. Values of the stream function are initially determined at rectangularly spaced grid points placed uniformly over the field of interest. The stream functions determined at the forward row of grid points are then assigned alphabetical letters. Interpolation is used to locate the position of these latter streamlines in each cross-stream grid point row within the grid system initially determined. Consecutive spacing of the cross-stream grid point rows is made sufficiently close that a clear indication of the streamlines is obtained without connecting them by lines. Figure 33 shows computer plots of streamlines obtained in this manner. For this solution $\epsilon = 0.7$, and the initial vortices were also multiplied by this factor.

Since the technique adopted determines the streamlines passing through preselected points, this method does not permit accurate determination of the zero streamline for unsymmetrical flow. Further iterations could be made to determine this zero streamline accurately, but this was not felt to be warranted.

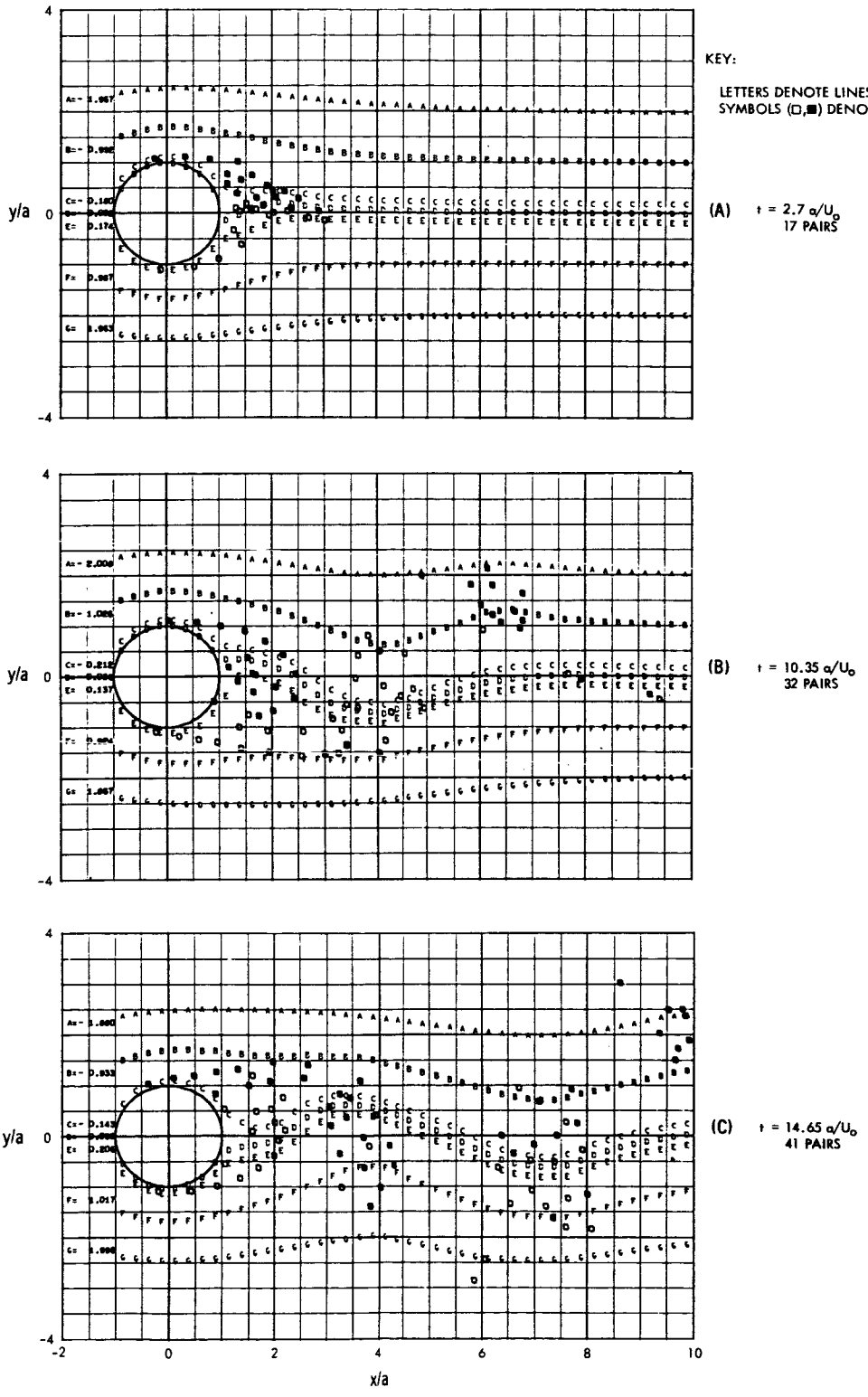

Figure 33. Unsymmetrical Flow Streamlines

SYMMETRICAL SEPARATED FLOW ABOUT A CIRCULAR CYLINDER

Further correlation of computer results with experimental data was made by simulating Schwabe's experiment for symmetrical flow with the symmetrical version of the Model II approach. This program was identical to the Model I "symmetrical" program discussed previously, except for the implicit determination of vorticity transport rate and peripheral location of the vortex feeding point. Radial location of the vortex feeding was maintained at 0.1 radius. Vortex feeding period was 0.5 a/U_o, and integration period was 0.05 a/U_o. An initial group of elemental vortices were arranged along the uniform flow streamline passing through 1.1 radii at the 90-degree point. This was similar to the Model II unsymmetrical problem. For this case, however, the vortex strengths were symmetrical. Flow development shown by the incremental vortex positions in Figure 34 are for one side only. In this particular run the graphic reflection process did not function properly, and the circle points were not correctly plotted. The circle points should be ignored. The "steady C_p" curves of Figure 34 are shown to indicate the magnitude of reverse flow velocities along the cylinder surface. Total pressures are also shown. The pressure discontinuity at approximately 60 degrees in the pressure curve, as previously discussed, is due to a vortex sheet attaching the feeding point radially to the cylinder surface. A one-hour computer solution resulting in a drag time history to a time of approximately 60 a/U_o was obtained for this case, and is also shown in Figure 34. The experimental drag curve by Schwabe (Reference 19) is superimposed for comparison. Points marked by a cross are drag values obtained by pressure integration, and include the effect of vorticity growth rate at the feeding points. The flow configuration at $t = 62.65\ a/U_o$ is shown in Figure 35.

The time variation of vorticity transport rate, Figure 36, is shown for comparison with the estimated curve used for the Model I program (Fig. 22). Feeding point location is also shown in Figure 36 because of its significant difference from the 90 degrees assumed for the Model I solution.

The vorticity reduction parameter, ϵ, applied at the vortex feeding point could possibly produce results more in agreement with experimental data. With this in mind, a computer solution was obtained with $\epsilon = 0.6$.

Position of the incremental vortices at a time of 14.65 a/U_o and the corresponding steady and total pressure distributions for the $\epsilon = 0.6$ solution are shown in Figure 37. Computed time development of drag coefficient is also shown.

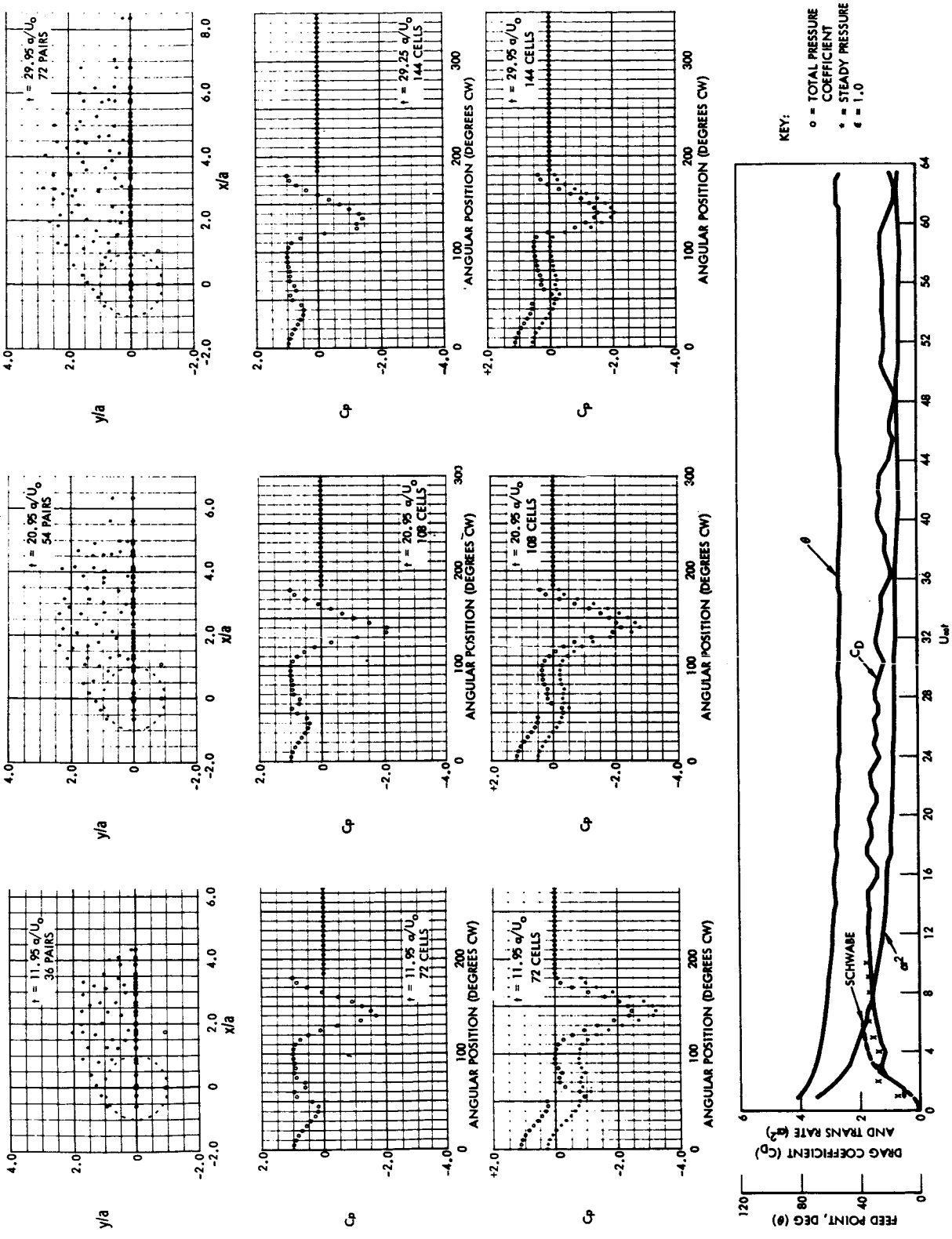

Figure 34. Symmetrical Flow About a Circular Cylinder (Model II)

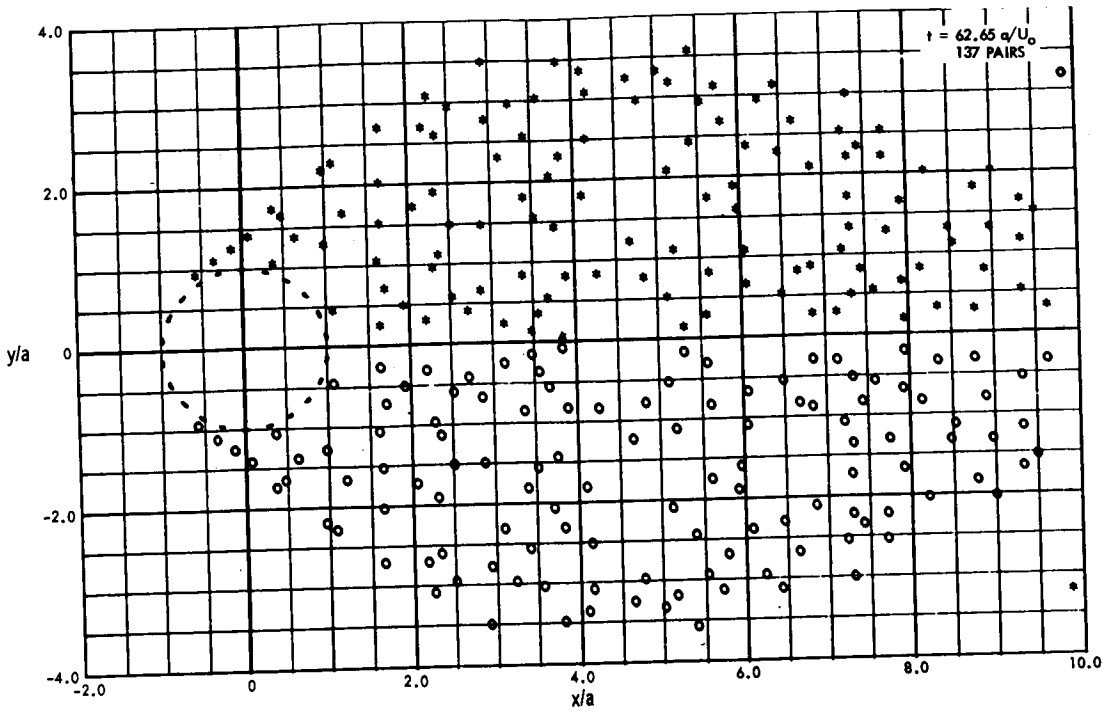

Figure 35. Vortex Configuration at t = 62.65 a/U_o

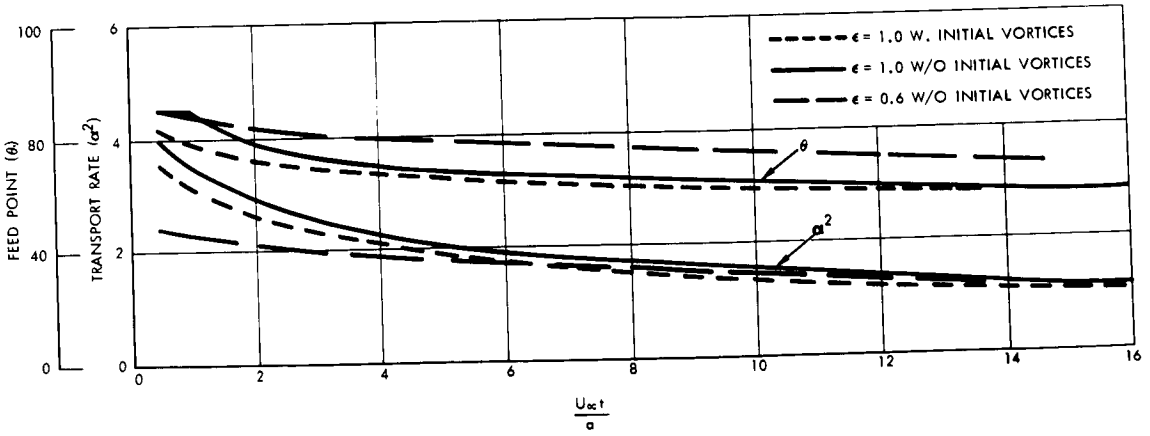

Figure 36. Variation in Feed Point and Transport Rate for Different ϵ

The use of initial vortices to start the solution was based upon experience obtained with the Model I program. The extended time history of C_D in Figure 34 was started with initial vortices. This accounts for the initial value of C_D equal to 0.5 rather than zero. By accident it was discovered that initial vortices were not necessary in the Model II program for preventing vortex instability. Figure 38(A) shows the solution of vortex positions at $U_o t/a = 22.7$ obtained without initial vortices. Figure 38(B) shows drag build-up to this same time. It may be seen that this curve is essentially similar to that shown in Figure 34. Principal differences are that the drag starts from zero, and appears to be slightly higher, reaching $C_D = 2.0$ at $U_o t/a = 18.5$. In Figure 34, maximum C_D following the gradual rise is attained at a time of 12.5 a/U_o; thereafter a gradual decrease results, and beyond a time of about 36 a/U_o the average C_D seems to hold at approximately 1.0.

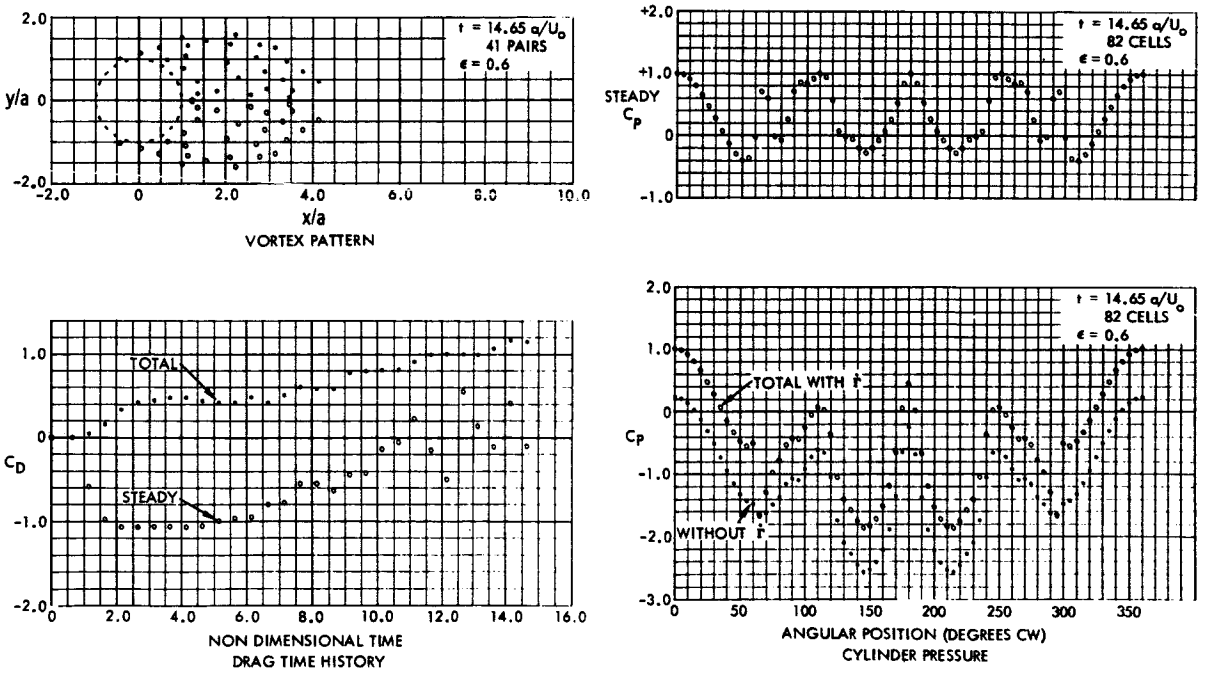

Figure 37. Symmetrical Flow Solution for $\epsilon = 0.6$

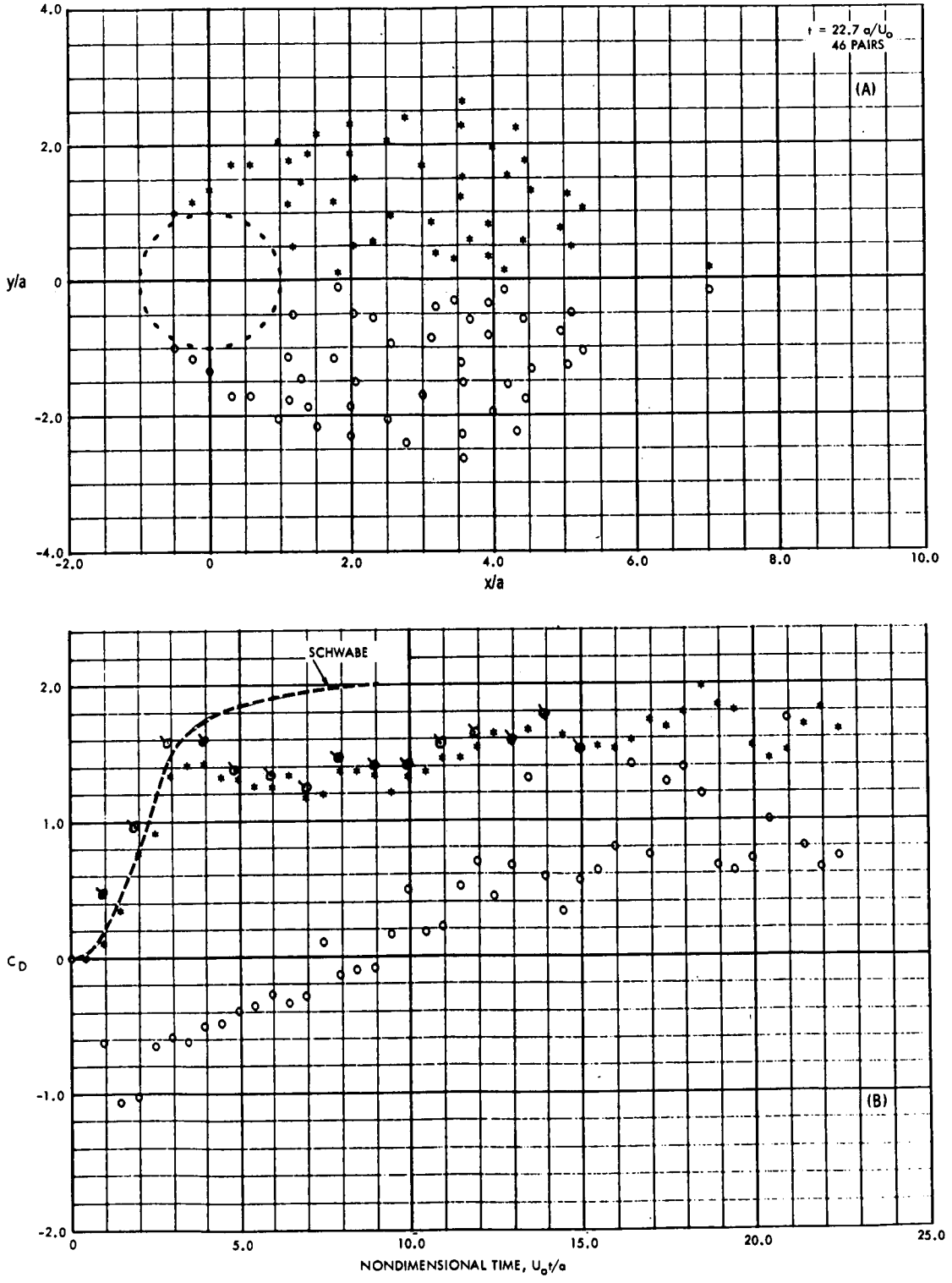

Figure 38. Flow Pattern and Related Drag Time History Without Initial Vortices

SYMMETRICAL FLOW STREAMLINES

Streamlines were determined for the flow solution depicted in Figure 38 and are shown in Figure 39. Examination of the streamlines in Figure 39 shows that they are quite smooth, even in areas where the streamlines pass close to discrete vortices. Superficial consideration of the effects of these vortices indicates that local warpage of the streamlines should occur near the vortices. Part of the smoothness may occur from the coarseness of the interpolation method. But the smoothness of these lines even through the vortex cloud indicates that overall streamlines are actually smooth, except in areas extremely close to the discrete vortices.

Most surprising is the fact that the streamline outlining the wake cavity in symmetrical flow is well inside the reaches of the discrete vortices. It is not difficult, with hindsight, to see that this must be so, since pressure recovery must increase as the streamlines become smoother. A comparison of wake width at $U_o t/a = 6.95$ with the data by Schwabe (Reference 19) shows the computed values to be somewhat narrower.

The zero streamline of Figure 39 is on the order of -1×10^{-6}. This streamline clearly shows the shape of the wake cavity. Its early disappearance near $x = 1$, $y = -1$ is a result of coarseness in the numerical interpolation scheme. A more refined appreciation of its behavior in this region may be gained from the digital printout of stream functions at the indicated grid points (Table IV).

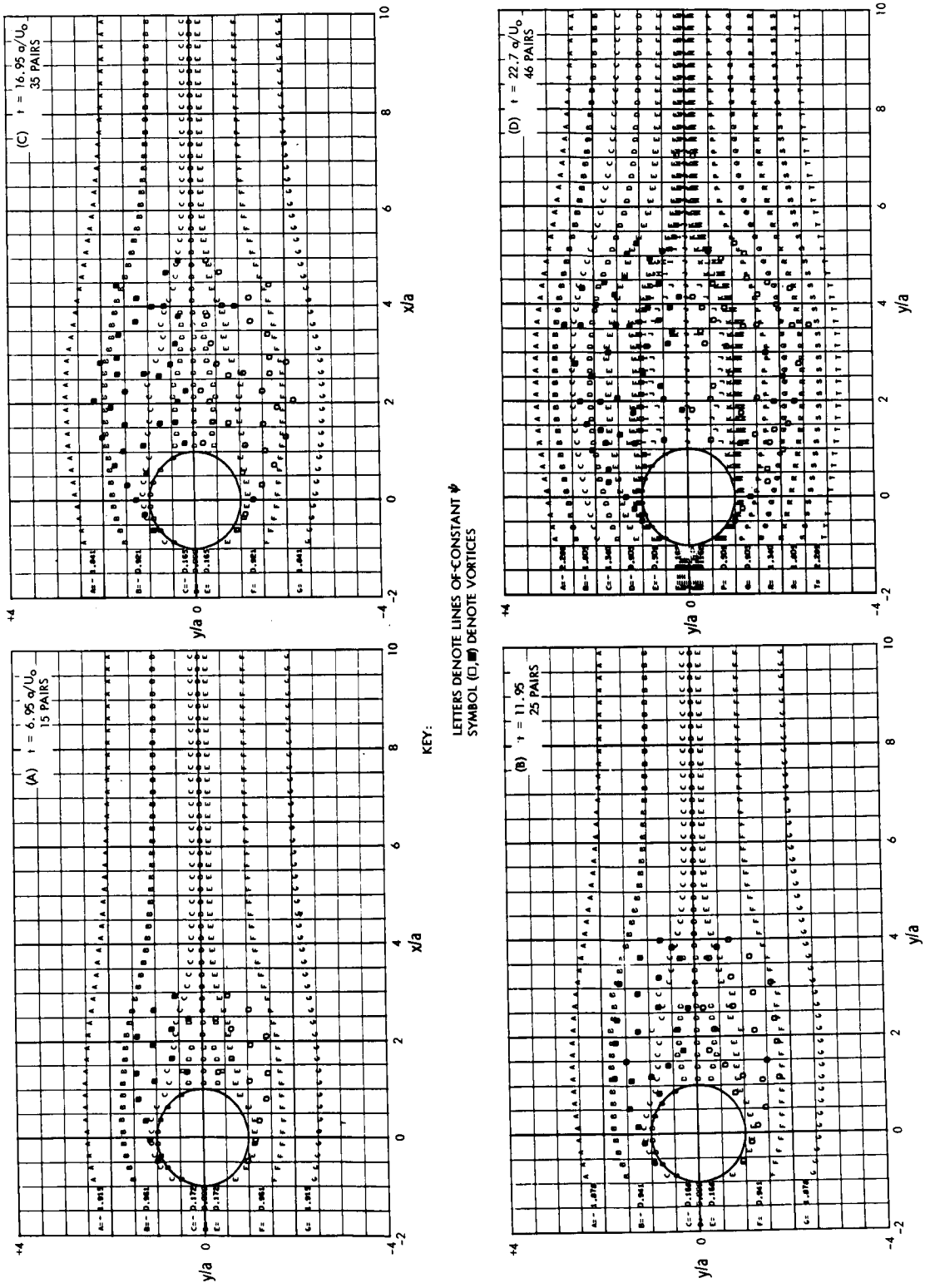

Figure 39. Symmetrical Flow Streamlines

Table IV. Stream Functions

YS	XS = -1.870	XS = -1.620	XS = -1.370	XS = -1.120
6	-5.5905499E 00	-5.5761408E 00	-5.5617751E 00	-5.5475512E 00
2.75	-2.2894266E 00	-2.2501495E 00	-2.2082051E 00	-2.1639631E 00
2.25	-1.8057508E 00	-1.7599817E 00	-1.7098428E 00	-1.6557935E 00
1.75	-1.3404189E 00	-1.2878901E 00	-1.2278319E 00	-1.1604721E 00
1.25	-9.0387425E-01	-8.4698054E-01	-7.7693242E-01	-6.9161118E-01
.75	-5.0949275E-01	-4.5889927E-01	-3.8951959E-01	-2.9193921E-01
.25	-1.6224557E-01	-1.4041809E-01	-1.0739712E-01	-5.2972599E-02
.20	-1.2948500E-01	-1.1179537E-01	-8.4883744E-02	-4.0094443E-02
.15	-9.6930100E-02	-8.3527315E-02	-6.3046481E-02	-2.8694178E-02
.10	-6.4531871E-02	-5.5531108E-02	-4.1732641E-02	-1.8457306E-02
.0001	-6.4360290E-05	-5.5335874E-05	-4.1447799E-05	-1.7896776E-05
- .1	6.4532041E-02	5.5531250E-02	4.1732737E-02	1.8457338E-02
- .15	9.6930274E-02	8.3527458E-02	6.3046576E-02	2.8694214E-02
- .2	1.2948518E-01	1.1179552E-01	8.4883840E-02	4.0094480E-02
- .25	1.6224574E-01	1.4041823E-01	1.0739721E-01	5.2972641E-02
- .75	5.0949296E-01	4.5889944E-01	3.8951970E-01	2.9193929E-01
-1.25	9.0387446E-01	8.4698074E-01	7.7693257E-01	6.9161130E-01
-1.75	1.3404192E 00	1.2878903E 00	1.2278320E 00	1.1604723E 00
-2.25	1.8057511E 00	1.7599820E 00	1.7098431E 00	1.6557938E 00
-2.75	2.2894269E 00	2.2501498E 00	2.2082054E 00	2.1639634E 00
-6	5.5905504E 00	5.5761413E 00	5.5617756E 00	5.5475516E 00

Table IV. Stream Functions (Cont)

XS= -0.870	XS= -0.620	XS= -0.370	XS= -0.120
-5.5335757E 00	-5.5199620E 00	-5.5068286E 00	-5.4942979E 00
-2.1179486E 00	-2.0708007E 00	-2.0232086E 00	-1.9758539E 00
-1.5986847E 00	-1.5396773E 00	-1.4799764E 00	-1.4204744E 00
-1.0871677E 00	-1.0107090E 00	-9.3487555E-01	-8.6259297E-01
-5.9066626E-01	-4.7841248E-01	-3.6903953E-01	-2.9139350E-01
-1.5337020E-01	0.0000000E-39	0.0000000E-39	0.0000000E-39
0.0000000E-39	0.0000000E-39	0.0000000E-39	0.0000000E-39
0.0000000E-39	0.0000000E-39	0.0000000E-39	0.0000000E-39
0.0000000E-39	0.0000000E-39	0.0000000E-39	0.0000000E-39
0.0000000E-39	0.0000000E-39	0.0000000E-39	0.0000000E-39
0.0000000E-39	0.0000000E-39	0.0000000E-39	0.0000000E-39
0.0000000E-39	0.0000000E-39	0.0000000E-39	0.0000000E-39
0.0000000E-39	0.0000000E-39	0.0000000E-39	0.0000000E-39
0.0000000E-39	0.0000000E-39	0.0000000E-39	0.0000000E-39
0.0000000E-39	0.0000000E-39	0.0000000E-39	0.0000000E-39
1.5337023E-01	0.0000000E-39	0.0000000E-39	0.0000000E-39
5.9066635E-01	4.7841255E-01	3.6903957E-01	2.9139351E-01
1.0871678E 00	1.0107092E 00	9.3487564E-01	8.6259304E-01
1.5986849E 00	1.5396774E 00	1.4799765E 00	1.4204745E 00
2.1179488E 00	2.0708010E 00	2.0232088E 00	1.9758540E 00
5.5335762E 00	5.5199624E 00	5.5068291E 00	5.4942983E 00

Table IV. Stream Functions (Cont)

XS= 0.130	XS= 0.380	XS= 0.630	XS= 0.880
-5.4824931E 00	-5.4715373E 00	-5.4615502E 00	-5.4526468E 00
-1.9293955E 00	-1.8844845E 00	-1.8419136E 00	-1.8022902E 00
-1.3617491E 00	-1.3047229E 00	-1.2496268E 00	-1.1941919E 00
-7.9074389E-01	-7.1090218E-01	-6.5279118E-01	-6.3124456E-01
-2.6674897E-01	-2.6778107E-01	-2.5934831E-01	-2.2079590E-01
0.0000000E-39	0.0000000E-39	0.0000000E-39	-1.8158944E-02
0.0000000E-39	0.0000000E-39	0.0000000E-39	0.0000000E-39
0.0000000E-39	0.0000000E-39	0.0000000E-39	0.0000000E-39
0.0000000E-39	0.0000000E-39	0.0000000E-39	0.0000000E-39
0.0000000E-39	0.0000000E-39	0.0000000E-39	0.0000000E-39
0.0000000E-39	0.0000000E-39	0.0000000E-39	0.0000000E-39
0.0000000E-39	0.0000000E-39	0.0000000E-39	0.0000000E-39
0.0000000E-39	0.0000000E-39	0.0000000E-39	0.0000000E-39
0.0000000E-39	0.0000000E-39	0.0000000E-39	0.0000000E-39
0.0000000E-39	0.0000000E-39	0.0000000E-39	0.0000000E-39
0.0000000E-39	0.0000000E-39	0.0000000E-39	1.8158903E-02
2.6674897E-01	2.6778106E-01	2.5934827E-01	2.2079585E-01
7.9074394E-01	7.1090219E-01	6.5279114E-01	6.3124450E-01
1.3617492E 00	1.3047230E 00	1.2496268E 00	1.1941919E 00
1.9293956E 00	1.8844846E 00	1.8418138E 00	1.8022903E 00
5.4824936E 00	5.4715378E 00	5.4615507E 00	5.4526473E 00

Table IV. Stream Functions (Cont)

XS= 1.130	XS= 1.380	XS= 1.630	XS= 1.880
-5.4449339E 00	-5.4385085E 00	-5.4334561E 00	-5.4298478E 00
-1.7670054E 00	-1.7367429E 00	-1.7119818E 00	-1.6929002E 00
-1.1493529E 00	-1.1089585E 00	-1.0827359E 00	-1.0614680E 00
-5.4347550E-01	-5.4560784E-01	-5.5504120E-01	-5.3430409E-01
-1.5287704E-01	-1.7630397E-01	-1.7576344E-01	-1.8212516E-01
-6.2254071E-04	-9.0177245E-03	-1.9043166E-02	-1.1104591E-02
2.2441630E-02	2.5192257E-02	2.5810149E-02	3.9988397E-02
1.6067092E-02	2.0208593E-02	2.3707654E-02	3.9083378E-02
1.1009628E-02	1.5184303E-02	2.0222856E-02	3.8668988E-02
6.8640676E-03	1.0139115E-02	1.4996043E-02	3.3692610E-02
6.4751139E-06	1.0107971E-05	1.6375410E-05	3.7311172E-05
-6.8641074E-03	-1.0139212E-02	-1.4996196E-02	-3.3692807E-02
-1.1009666E-02	-1.5184404E-02	-2.0222997E-02	-3.8669184E-02
-1.6067139E-02	-2.0208698E-02	-2.3707807E-02	-3.9083567E-02
-2.2441684E-02	-2.5192367E-02	-2.5810298E-02	-3.9988590E-02
6.2244385E-04	9.0176463E-03	1.9043010E-02	1.1104375E-02
1.5287690E-01	1.7630384E-01	1.7576330E-01	1.8212499E-01
5.4347543E-01	5.4560774E-01	5.5504108E-01	5.3430400E-01
1.1493529E 00	1.1089585E 00	1.0827358E 00	1.0614679E 00
1.7670054E 00	1.7367430E 00	1.7119819E 00	1.6929003E 00
5.4449342E 00	5.4385089E 00	5.4334564E 00	5.4298482E 00

Table IV. Stream Functions (Cont)

XS= .2.130	XS= 2.380	XS= 2.630	XS= 2.880
-5.4277389E 00	-5.4271677E 00	-5.4281533E 00	-5.4306952E 00
-1.6804979E 00	-1.6739857E 00	-1.6723733E 00	-1.6789604E 00
-1.0513090E 00	-1.0417928E 00	-1.0384155E 00	-1.0625977E 00
-5.3442495E-01	-5.5218017E-01	-5.4817618E-01	-5.0425622E-01
-2.0839252E-01	-2.1630131E-01	-2.1320599E-01	-2.0774098E-01
3.1144544E-03	9.6211657E-03	-4.5333058E-04	3.8213283E-04
3.8029194E-02	2.8383480E-02	1.9038431E-02	2.2439452E-02
3.0471699E-02	2.2723297E-02	1.5847098E-02	1.8828182E-02
2.3016681E-02	1.7066031E-02	1.2237497E-02	1.4614236E-02
1.5482754E-02	1.1393440E-02	8.3235037E-03	9.9706016E-03
1.5550577E-05	1.1281028E-05	8.3270934E-06	1.0016794E-05
-1.5482947E-02	-1.1393691E-02	-8.3237514E-03	-9.9708475E-03
-2.3016886E-02	-1.7066271E-02	-1.2237739E-02	-1.4614487E-02
-3.0471906E-02	-2.2723537E-02	-1.5847344E-02	-1.8828416E-02
-3.8029406E-02	-2.8383713E-02	-1.9038683E-02	-2.2439705E-02
-3.1146854E-03	-9.6213892E-03	4.5308471E-04	-3.8232654E-04
2.0839234E-01	2.1630114E-01	2.1320583E-01	2.0774079E-01
5.3442484E-01	5.5218009E-01	5.4817607E-01	5.0425601E-01
1.0513090E 00	1.0417928E 00	1.0384155E 00	1.0625976E 00
1.6804979E 00	1.6739867E 00	1.6723733E 00	1.6789604E 00
5.4277394E 00	5.4271681E 00	5.4281537E 00	5.4306957E 00

Table IV. Stream Functions (Cont)

XS= 3.130	XS= 3.380	XS= 3.630	XS= 3.880
-5.4347721E 00	-5.4403416E 00	-5.4473407E 00	-5.4556862E 00
-1.6912259E 00	-1.7018265E 00	-1.7197106E 00	-1.7698828E 00
-1.0879230E 00	-1.0979516E 00	-1.1021832E 00	-1.1699404E 00
-5.1524661E-01	-5.8099313E-01	-6.1415246E-01	-6.5115687E-01
-2.0000783E-01	-1.8232147E-01	-1.7722002E-01	-2.7275948E-01
3.6449261E-02	6.9845393E-03	-4.7167465E-03	-1.6218364E-02
4.4344163E-02	7.2524359E-02	5.0376583E-02	4.5612486E-02
3.5350345E-02	5.6061743E-02	4.2109538E-02	3.6689123E-02
2.6520295E-02	4.0697034E-02	3.2362122E-02	2.7978305E-02
1.7702704E-02	2.6512227E-02	2.1853259E-02	1.8993008E-02
1.7586360E-05	2.5922656E-05	2.1897942E-05	1.9196867E-05
-1.7702962E-02	-2.6512494E-02	-2.1853501E-02	-1.8993238E-02
-2.6520559E-02	-4.0697303E-02	-3.2362426E-02	-2.7978562E-02
-3.5350621E-02	-5.6061991E-02	-4.2109793E-02	-3.6689397E-02
-4.4344412E-02	-7.2524654E-02	-5.0376840E-02	-4.5612710E-02
-3.6449477E-02	-6.9847703E-03	4.7165304E-03	1.6218156E-02
2.0000766E-01	1.8232129E-01	1.7721978E-01	2.7275931E-01
5.1524635E-01	5.8099304E-01	6.1415242E-01	6.5115675E-01
1.0879230E 00	1.0979515E 00	1.1021831E 00	1.1699404E 00
1.6912259E 00	1.7018265E 00	1.7197106E 00	1.7698828E 00
5.4347725E 00	5.4403421E 00	5.4473411E 00	5.4556866E 00

Table IV. Stream Functions (Cont)

XS= 4.130	XS= 4.380	XS= 4.630	XS= 4.880
-5.4652767E 00	-5.4759954E 00	-5.4877122E 00	-5.5002888E 00
-1.8194626E 00	-1.8728079E 00	-1.9318754E 00	-1.9926404E 00
-1.2152488E 00	-1.2476526E 00	-1.3699799E 00	-1.4568533E 00
-6.9036604E-01	-7.5058659E-01	-8.5818522E-01	-9.5730821E-01
-3.2598278E-01	-3.7691285E-01	-4.3812966E-01	-5.1040770E-01
-6.1474897E-02	-8.0157213E-02	-1.3672715E-01	-1.6166459E-01
3.8787551E-02	1.1956720E-02	-1.6563207E-02	-4.2653477E-02
4.5397980E-02	1.0735163E-02	-1.3061725E-02	-3.3958100E-02
6.0478223E-02	9.0413261E-03	-9.6806008E-03	-2.5392316E-02
3.7567672E-02	6.6169398E-03	-6.3947225E-03	-1.6897962E-02
3.2374288E-05	7.0308070E-06	-6.4175883E-06	-1.6939258E-05
-3.7567905E-02	-6.6171233E-03	6.3945809E-03	1.6897852E-02
-6.0478449E-02	-9.0415254E-03	9.6804369E-03	2.5392190E-02
-4.5398198E-02	-1.0735366E-02	1.3061568E-02	3.3957988E-02
-3.8787782E-02	-1.1956910E-02	1.6563047E-02	4.2653361E-02
6.1474688E-02	8.0156989E-02	1.3672697E-01	1.6166445E-01
3.2598262E-01	3.7691268E-01	4.3812954E-01	5.1040762E-01
6.9036601E-01	7.5058652E-01	8.5818515E-01	9.5730817E-01
1.2152488E 00	1.2476525E 00	1.3699799E 00	1.4568533E 00
1.8194627E 00	1.8728079E 00	1.9318755E 00	1.9926405E 00
5.4652772E 00	5.4759958E 00	5.4877127E 00	5.5002893E 00

Table IV. Stream Functions (Cont)

XS= 5.130	XS= 5.380	XS= 5.630	XS= 5.880
-5.5135818E 00	-5.5274469E 00	-5.5417429E 00	-5.5563346E 00
-2.0515796E 00	-2.1073347E 00	-2.1594395E 00	-2.2077219E 00
-1.5332937E 00	-1.6022556E 00	-1.6648153E 00	-1.7213425E 00
-1.0426322E 00	-1.1216619E 00	-1.1941952E 00	-1.2585566E 00
-5.6775237E-01	-6.6687703E-01	-7.5962898E-01	-8.3190694E-01
-2.4596740E-01	-3.3176419E-01	-4.0557430E-01	-4.6289362E-01
-6.6101776E-02	-9.8418977E-02	-1.2632694E-01	-1.4749573E-01
-5.3378334E-02	-7.8501253E-02	-1.0074224E-01	-1.1773981E-01
-4.0280545E-02	-5.8755597E-02	-7.5372423E-02	-8.8154593E-02
-2.6958212E-02	-3.9118337E-02	-5.0161358E-02	-5.8698004E-02
-2.7076001E-05	-3.9098330E-05	-5.0096682E-05	-5.8627300E-05
2.6958136E-02	3.9118301E-02	5.0161355E-02	5.8698040E-02
4.0280459E-02	5.8755557E-02	7.5372418E-02	8.8154631E-02
5.3378250E-02	7.8501211E-02	1.0074223E-01	1.1773984E-01
6.6101709E-02	9.8418929E-02	1.2632694E-01	1.4749576E-01
2.4596732E-01	3.3176415E-01	4.0557432E-01	4.6289366E-01
5.6775229E-01	6.6687702E-01	7.5962901E-01	8.3190701E-01
1.0426322E 00	1.1216620E 00	1.1941953E 00	1.2585568E 00
1.5332938E 00	1.6022557E 00	1.6648155E 00	1.7213427E 00
2.0515798E 00	2.1073349E 00	2.1594397E 00	2.2077222E 00
5.5135823E 00	5.5274475E 00	5.5417434E 00	5.5563352E 00

Table IV. Stream Functions (Cont)

XS= 6.130	XS= 6.380	XS= 6.630	XS= 6.880
-5.5710960E 00	-5.5859115E 00	-5.6006777E 00	-5.6153041E 00
-2.2521429E 00	-2.2927639E 00	-2.3297329E 00	-2.3632647E 00
-1.7720384E 00	-1.8172013E 00	-1.8572651E 00	-1.8927447E 00
-1.3143263E 00	-1.3621662E 00	-1.4031499E 00	-1.4383820E 00
-8.8882741E-01	-9.3451709E-01	-9.7180039E-01	-1.0027863E 00
-5.0634763E-01	-5.3946234E-01	-5.6488965E-01	-5.8510663E-01
-1.6330886E-01	-1.7461000E-01	-1.8083650E-01	-1.7631730E-01
-1.3042971E-01	-1.3943807E-01	-1.4406929E-01	-1.3730158E-01
-9.7694247E-02	-1.0442767E-01	-1.0766315E-01	-1.0035062E-01
-6.5068059E-02	-6.9544612E-02	-7.1574658E-02	-6.5630009E-02
-6.4988602E-05	-6.9430592E-05	-7.1340210E-05	-6.4640785E-05
6.5068129E-02	6.9544717E-02	7.1574801E-02	6.5630193E-02
9.7694323E-02	1.0442776E-01	1.0766328E-01	1.0035081E-01
1.3042978E-01	1.3943818E-01	1.4406942E-01	1.3730177E-01
1.6330892E-01	1.7461011E-01	1.8083663E-01	1.7631750E-01
5.0634772E-01	5.3946246E-01	5.6488980E-01	5.8510682E-01
8.8882754E-01	9.3451722E-01	9.7180058E-01	1.0027865E 00
1.3143264E 00	1.3621663E 00	1.4031501E 00	1.4383822E 00
1.7720385E 00	1.8172014E 00	1.8572654E 00	1.8927449E 00
2.2521431E 00	2.2927642E 00	2.3297332E 00	2.3632650E 00
5.5710965E 00	5.5859119E 00	5.6006782E 00	5.6153046E 00

RESULTS OF INVESTIGATION

VORTEX INSTABILITY

The investigation of flow past a half-plane was made with the intent of determining, if possible, some of the limitations that may be inherent in approximating a continuous shear layer by a continuous arrangement of discrete vortices. Schindel* indicated that, based upon his results, a discrete vortex approximation to a continuous shear layer could not satisfactorily be made in analyzing shear layer motion. However, results of this facet of the investigation show that a discrete vortex approximation to a continuous shear layer may be accomplished without sacrificing any characteristics essential to analysis of continuous shear layer motion. True, unstable vortex motion can be encountered due to interaction with its image vortex. Such instability was produced in this shear layer study, using $K/U_oL_o = 1.0$, $U_o\Delta t_F/L_o = 10$ and $U_o\Delta t_I/L_o = 0.001$

where

Δt_F = feeding period

Δt_I = integration period

In this case, the vortices were so far apart that they were essentially isolated. Each vortex behaved in a manner largely uninfluenced by the others. Expressed differently, the angular change of the vortex sheet element represented by the discrete vortex was insufficient to remove the velocity component normal to the half-plane. As a result, the velocity vector of the approaching vortex always retained a component directed towards the half-plane. A quantitative criterion could no doubt be derived on a rigorous basis. For the purpose of this study, it was sufficient to recognize the nature of this instability, and to avoid it by using vortex feeding periods sufficiently small to preclude its occurrence. In the analysis of flow about a cylinder and a flat plate, it was found that a non-dimensional feeding period of $U_ot_F/a = 0.5$ appeared to be a reasonable compromise between solution accuracy and extent of real time solution.

A second objective, equally important, was to determine the inaccuracies arising from employment of numerical techniques in integrating the

*Personal communication.

motion of discrete vortices to determine their displacements. In this connection it was found that a type of internal shear layer instability invariably occurred after the solution had been carried beyond a certain point. Generally, the onset of this internal instability occurred after one or two whorls had formed. The point of inception was usually in that part of the shear layer connecting the straight portion to the convolution. This instability may be noticed in Figures 1 through 5.

The peculiar fact about this internal instability is that it is not caused by the crudeness of numerical integration. On the contrary, the finer the integration method and/or the discrete vortex representation of the vortex sheet, the more rapidly the whorled configuration and this instability appear. The obvious conclusion is that a continued refinement of the discrete vortex approximation would eventually lead to instantaneous occurrence of this instability at the feeding point. Similarity of this effect to the natural transition of a laminar physical shear layer to turbulence is evident. Furthermore, this immediate transition to turbulence is precisely what should occur for the infinite Reynolds number case.

If the postulation of nonviscous wake flow should be pursued to its logical end, it appears reasonable to assume that the present technique, based on potential theory, could reproduce the random type of shedding characteristically associated with supercritical Reynolds number.

To explain how this type of instability might become applicable to random vortex shedding, recourse is made to the explanation offered by Roshko (Reference 2). In this explanation, the randomness of the shedding at supercritical Reynolds number is caused by the shear layer transition from laminar to turbulent flow at a point very close to the shear layer separation. Due to minor pressure fluctuations and other possible effects, the transition point can momentarily move forward of the separation point. When this happens, the relatively increased energy of the fluid near the surface causes the boundary layer to become reattached, thus creating what is known as a "separation bubble." Because the motion of this separation bubble is extremely sensitive to pressure fluctuations, the separation point is forced to move erratically in a random manner. To simulate this phenomenon analytically would require an investigation of microscopic flow mechanics in the separation region. Qualitatively it would require that the instability referred to above be made to occur in a manner similar to the separation mechanics described.

SYMMETRICAL FLOW

The most significant results obtained from simulation of Schwabe's experiment for symmetrical flow about an impulsively started cylinder are that

(1) The vorticity transport rate during the transient period of symmetrical flow development cannot be related to the base pressure coefficient using the relationship $\alpha^2 = 1 - \overline{C}_{pw}$. Thus it is mandatory, for symmetrical flow, to use an approach wherein vorticity transport rate and feeding point location are implicitly defined.

(2) Model II results for the drag coefficient (Figure 38) show maximum C_D to be in agreement with Schwabe's data. The drag build up curve also correlates well. The extended solution shows a drop to an average C_D near 1.0 for time beyond 35 a/U_o. At a Reynolds number near 10,000 the drag coefficient for the cylinder with splitter plate is given as 0.72, and that for the cylinder alone as 1.15 (Reference 17).

The present solution does not include any counter vorticity and vorticity cancellation effects. It is, therefore, somewhat surprising that this agreement should be obtained. A more detailed study of the Models I and II solutions, however, has led to the following explanation.

It was shown by the Model I investigation, Figure 22, that the drag coefficient is highly sensitive to small changes in vorticity transport rate. If α^2 is too high, the vortices begin to move forward of the cylinder. If too low, the symmetrical vortex arrangement completely detaches, leaving no wake cavity at all.

Therefore, the formation of a symmetrical separated wake is primarily governed by stability criteria that require the wake cavity to remain attached, and at the same time restrain it from becoming too large. With the Model II approach, these criteria govern the vorticity transport in such a way that stability is maintained. For example, if the wake cavity becomes too large, the feeding point (i.e., minimum pressure point) moves forward and the tangential velocity, hence vorticity transport rate, is reduced. Conversely, if the cavity tends to separate, the feeding point moves farther aft where the tangential velocity is greater, thus providing an increase in vorticity transport rate. This interplay between drag coefficient, vorticity transport rate and feeding point location is evident in Figure 34.

Because of this stability criterion, the vorticity transport rate is automatically reduced by an amount that should be the same as that produced by vorticity cancellation. On this basis, then, an estimate of ϵ, the net fraction of boundary layer vorticity which remains in the far wake, can be made by comparing the average value of α^2 in the steady state. From Figure 34, α^2 is taken to be 0.65. The value of α^2 from Reference 17 for the cylinder with splitter plate is 1.45 and for cylinder alone, is 1.7.

Corresponding values of ϵ are then $\frac{0.65}{1.45} = 0.45$ and $\frac{0.65}{1.45} = 0.38$ respectively. These values are less than the 0.5 found by Fage and Johansen. Assuming the splitter plate produces symmetrical flow, $\epsilon = 0.45$ should be the more accurate value of the two.

It was partly in an attempt to verify this hypothesis that an additional solution was obtained for $\epsilon = 0.6$. If the hypothesis were correct, the feeding point should move farther aft in an attempt to make up for the decreased vorticity transport. While this does happen to a certain extent, the vorticity transport rate initially remains lower than the case for $\epsilon = 1.0$. As a result, the buildup rate in drag coefficient is much slower than for $\epsilon = 1.0$ (Figure 37). The long time solution probably would result in much the same drag coefficient, with possibly an improved pressure distribution. For the short time solution, however, factors in addition to those discussed above appear to require consideration.

PERIODIC VORTEX SHEDDING

Both the Model I and II solutions were successful in demonstrating a Strouhal number of 0.2. Approximately one-hour computer runs with each version produced basically similar time variations in lift and drag coefficient. The main difference between the two solutions appears to be the significantly higher magnitude of lift and drag resulting from the Model II solution. To a certain extent, this may be explained by the fact that according to the Helmholtz vortex theorems, particles of fluid, once entrained in a vortex, remain with the vortex. As a result, fluid inertia forces created by the side motion of the vortices result in dynamic effects not unlike the motion of a spring mass system. The short movie that was made with the Model II solution clearly illustrates this type of side-to-side oscillatory motion of the vortices in the formation of the near wake. In the Model I solution, this type of motion would be restrained by the stationary feeding point.

Perhaps the most encouraging result from this study of periodic vortex shedding is the demonstration of the strength of the basic phenomenon of periodicity of the shedding with a Strouhal number of 0.2. In the Model I program, an asymmetry of feeding point location of 20 degrees together with constant vorticity transport rate at the feeding points did not appear to significantly affect the solution. The most noticeable discrepancy was the fact that mixing of the vortices from both sides occurred on the lower side but only beyond five diameters downstream.

In studying the effect of numerical integration time interval on the flow development, it was noted that the coarser time interval appears to produce a lead in phase over the flow development obtained by using a finer

integration interval. Presumably, this should lead to some small increase in Strouhal number for the solution with coarser integration interval. However, the difference appears to be slight in view of the good correlation with experimental data.

One other technique, not thoroughly explored in this study, exists for achieving extended real-time solutions, while minimizing the consumption of computer machine time. That is the process of lumping the incremental vortices in a Kármán vortex into a few vortices of much greater strength. This process should be satisfactory if its application is limited to Kármán vortices located some distance downstream. Experimentation would be necessary to develop a systematic method of accomplishing a reduction in the number of vortices by this method. Vortices close to the cylinder should be lumped in this manner with caution, since some type of local transient in the velocity potential is unavoidable. Close to the cylinder this could result in appreciable alteration of lift and drag forces.

In contrast with symmetrical flow solutions, a stability condition does not govern the vorticity transport rate for periodic vortex shedding flow. Therefore, the vorticity transport reduction factor, ϵ, has much more significance for unsymmetrical flow. Vorticity reduction by the creation of counter vorticity from reverse flow over the rearward portion of the cylinder followed by a significant amount of vorticity cancellation is believed to be the primary mechanism for reducing the net vorticity from the boundary layers that is transported downstream. Three-dimensional characteristics of this type of mixing are generally of first order importance and contribute to further reduction of experimentally observed forces. The elemetary approach taken in this study of simply reducing the vorticity transport rate by applying the factor ϵ at the feeding point appears to result in a satisfactory reduction of lift and drag coefficients.

An ϵ of around 0.7 results in force coefficients that seem to agree with those for subcritical Reynolds numbers. A lower value of ϵ would result in drag coefficient in agreement with $C_D = 0.7$ measured by Roshko, Reference 2, for transcritical Reynolds number. By this technique, the peak lift coefficient would also be expected to decrease to around 0.7 as shown in Figure 29.

This technique of accounting for vorticity cancellation does not properly account for local effect on pressure distributions as shown by the significant reversed tangential velocities which still occur as shown by Figure 32. Use of additional feeding points in these areas of high velocity is believed to be the most desirable approach to account for vorticity cancellation. While this represents some additional complication in computer programs, the technique is believed to be practicable. Further investigation along this line could not be accomplished within the limitations of this study.

It is considered fortunate that results from the Model I and II programs are basically similar, since in the chronological sequence of events, the Model I approach reached operational status first.

Correlation studies made with results of the Model I solution in the areas of cylinder pressure distribution and wake fluctuations are believed to be applicable, for the most part, to results that would be obtained from the Model II approach. Depending upon the magnitude of ϵ that would be used with the Model II program, the cylinder pressure and wake characteristics would be expected to become correspondingly smoother and more in agreement with experimental data.

Certain discrepancies occurred in computed cylinder forces based on the generalized Blasius theorem as compared with those obtained by numerical integration of unsteady cylinder pressures. Basically this discrepancy stemmed from the fact that it was not realized at the outset that a simple vortex cannot by itself grow in strength without being attached to a feeding vortex sheet. In this respect, the development of forces on a cylinder in a field of moving and growing vortices presented by Sarpkaya in Reference 9 is believed to be incomplete. The development involving impulse from a pair of vortices of opposite sign and connected by a vortex sheet in a manner similar to that taken by Bryson in Reference 10 produces forces which check with those obtained by numerical integration of unsteady cylinder pressures.

The pressure distributions exhibit a discontinuous behavior near the region of vortex sheet attachment, due not only to the vortex sheet but also to proximity of discrete vortices at and near the feeding points. However, this is a local effect as attested to by the good agreement between pressure integrated forces and those obtained by the Blasius theorem. Except for these local effects, the distributions are relatively smooth. Even the pressure and velocity profiles of wake sections taken directly through a Kármán type vortex such as Figures 16 and 17 show a remarkably smooth behavior.

Good correlation of wake velocities is evident above an x/d ratio of 6; where x is the distance downstream and d is the cylinder diameter. Disagreement of wake velocity curves for the region closer than six diameters behind the cylinder is considered largely the result of insufficient vorticity cancellation for the reverse flow involved. This reversal of flow imparted by the shed vortices is felt to be the basic mechanism for creating vorticity. The condition is further aggravated by the tendency toward excessive vortex growth which increases the effects of flow reversal.

The agreement of average wake centerline pressure in Figure 18, shown in comparison with that of Roshko, Reference 17, (Reynolds no. = 14,500), is fair for $\frac{x}{d} \rightarrow 5$. The distinct departure from experimental data

in the near wake is another indication that vorticity cancellation effects are important. Near wake velocity characteristics shown in Figure 19 compared with those of Kovásznay (Reference 18) for a Reynolds no. of 56 are only vaguely similar. The wake fluctuation data are sketchy at best, since they are based upon only nine discrete time samplings. However, the general similarity with Spitzer's data, Reynolds no. = 2.5×10^5, is evident. The wider wake shown by these data is considered to be another consequence of the fact that vorticity cancellation has not been accounted for. Also, viscous diffusion effects would become more pronounced as the vortices continued to develop.

The Strouhal number of 0.2, computed from these results, agrees with that for subcritical Reynolds number range. According to Roshko, Reference 2, the Strouhal number for transcritical Reynolds numbers is 0.27. This reduction is explained by the fact that the wake is narrower. The underlying difference in the two types of flow, however, is in the fact that at subcritical Reynolds numbers, the boundary layer remains laminar beyond the separation point, and at transcritical Reynolds numbers the boundary layer undergoes transition to turbulence distinctly ahead of the separation point.

Strangely enough, perhaps, a phenomenon similar to the transition of a laminar shear layer to turbulence was observed in the investigation of shear layer motion past a half plane. It was also observed in some of the earlier studies with the cylinder, Figure 9(A), for example.

Now, if it is true that the near wake is essentially nonviscous, and results of the study provide evidence that it is, the mechanism for shear layer transition to turbulence should also be of a nonviscous nature, since it is a near wake phenomenon. It is therefore hypothesized that the simulation of transcritical Reynolds number flow utilizing potential theory requires proper control of the shear layer instability encountered in this study. A considerably finer discrete vortex representation would be required in areas near the cylinder surface. The general objective in using a more detailed vortex representation would be to induce shear layer instability while it is still essentially following the cylinder contour.

In all of these comparisons with experimental data on two-dimensional tests, it should be remembered that three-dimensional effects could have been, and very often were, of first-order importance. It would be expected that these three-dimensional effects would reduce force magnitudes associated with periodic vortex shedding, and smooth out cylinder pressure distributions.

REFERENCES

1. Reed, Wilmer H. Models for Obtaining Effects of Ground Winds on Space Vehicles Erected on the Launch Pad, presented at the Conference on The Role of Simulation in Space Technology, Virginia Polytechnic Institute, Blacksburg, Virginia (August 1965).

2. Roshko, Anatol. "Experiments on the Flow Past a Circular Cylinder at Very High Reynolds Number," Journal of Fluid Mechanics, Vol. 10 (May 1961), pp. 345-356.

3. Fung, Y. C. "Fluctuating Lift and Drag Acting on a Cylinder in a Flow at Supercritical Reynolds Number," Journal of the Aerospace Sciences, Vol. 27, No. 11 (November 1960), pp. 801-814.

4. Spitzer, Robert E. Measurements of Unsteady Pressures and Wake Fluctuations for Flow Over a Cylinder at Supercritical Reynolds Number. California Institute of Technology, Pasadena, California (1965).

5. Küchemann, D. "Report on the I. U. T. A. M. Symposium on Concentrated Vortex Motions in Fluids," Journal of Fluid Mechanics, Vol. 21, Part 1 (1965), pp. 1-20.

6. Abernathy, Frederick H. and Richard E. Kronauer. "The Formation of Vortex Streets," Journal of Fluid Mechanics, Vol. 13 (1961), pp. 1-20.

7. Schlichting, Hermann. Boundary Layer Theory. McGraw-Hill (1960).

8. Milne, T. Theoretical Hydrodynamics, The MacMillan Company, (1955).

9. Sarpkaya, Turgut. "Lift, Drag, and Added-Mass Coefficients for a Circular Cylinder Immersed in a Time Dependent Flow," Journal of Applied Mechanics (March 1963), pp. 13-15.

10. Bryson, A. E. "Symmetric Vortex Separation on Circular Cylinders and Cones," Journal of Applied Mechanics (December 1959), pp. 643-648.

11. Kuethe, A. M. and J. D. Schetzer. Foundations of Aerodynamics. John Wiley and Sons (1950).

12. Lin, C. C., On the Motion of Vortices in Two Dimensions, University of Toronto Studies, Applied Mathematics, Series No. 5, University of Toronto Press (1943).

13. Takami, H. A Numerical Experiment with Discrete-Vortex Approximation, with Reference to the Rolling up of a Vortex Sheet. Air Force Office of Scientific Research, SUDAER No. 202 (September 1964).

14. van de Vooren, A. I. A Numerical Investigation of the Rolling-up of Vortex Sheets, presented at the I. U. T. A. M. Converence, Ann Arbor, Michigan (July 1964).

15. Roshko, Anatol. A New Hodograph for Free-Streamline Theory. National Advisory Committee for Aeronautics, Technical Note 3168 (July 1954).

16. Acrivos, Andreas, et al. The Steady Separated Flow Past a Circular Cylinder at Large Reynolds Numbers, Journal of Fluid Mechanics, Vol. 21, Part 4 (1965), pp. 737-760.

17. Roshko, Anatol. On the Drag and Shedding Frequency of Two-Dimensional Bluff Bodies. National Advisory Committee for Aeronautics, Technical Note 3169 (July 1954).

18. Kovásznay, L. S. G. Hot-wire Investigation of the Wake Behind Cylinders at Low Reynolds Numbers, Journal of Fluid Mechanics, Vol. 198 (1949), pp. 174-190.

19. Schwabe, M. Pressure Distribution in Nonuniform Two-Dimensional Flow. National Advisory Committee for Aeronautics, Technical Memorandum 1039 (January 1943).

20. Gerrard, J. H. The Calculation of the Fluctuating Lift on a Circular Cylinder and Its Application to the Determination of Aeolian Tone Intensity. North Atlantic Treaty Organization, Advisory Group for Aeronautical Research and Development, Report No. 463, presented at AGARD Specialists' Meeting in Belgium (April 1963).

21. Buell, Donald A., George B. McCullough, and William J. Steinmetz. A Wind-Tunnel Investigation of Ground-Wind Loads on Axisymmetric Launch Vehicles. NASA TN D-1893 (October 1963).

BIBLIOGRAPHY

The following bibliography was accumulated and reviewed in the course of this study. Although not specifically referred to in the text, this literature has been important to overall accomplishments of the study.

Acrivos, A., F.H. Shair, A.S. Grove, and E.E. Petersen. "The Effect of Confining Walls on the Stability of the Steady Wake Behind a Circular Cylinder," Journal of Fluid Mechanics, Vol. 17 (1963), pp. 546-550.

Allen, H. J. Pressure Distribution and Some Effects of Viscosity on Slender Inclined Bodies of Revolution, NACA TN 2044 (March 1950).

Arita, Yukio, Kenji Nakagawa, Tsutomu Fujino, Yoji Ogata and Kazumi Masaki. An Experimental Investigation of Aerodynamic Instability of Circular Cylinders at Supercritical Reynolds Numbers, Proceedings of the 9th Japan National Congress for Appl. Mech. (1959), pp. 235-240.

Arita, Yukio, Kenji Nakagawa, Tsutomu Fujino, and Tetsuo Takahei. The Dynamic Behavior of Tall Stacks Under the Action of Wind, Proc. of the 7th Japan National Congress for Applied Mechanics (1957), pp. 387-392.

Batchelor, G.K. "Axial Flow in Trailing Line Vortices," Journal of Fluid Mechanics Vol. 20, part 4 (1964), pp. 645-658.

Benjamin, T.B. "Theory of the Vortex Breakdown Phenomenon," Journal of Fluid Mechanics 14 (1962), pp. 593-629.

Birkhoff, Garrett. "Formation of Vortex Streets," Journal of Applied Physics, Vol. 24, No. 1 (January 1953), pp. 98-103.

Birnbaum, S. and A.A. Ezra. Design Criteria for Space Vehicles to Resist Wind Induced Oscillations, presented at Structural Design of Space Vehicles Conference, Santa Barbara, California (April 6-8, 1960).

Campbell, I.J. "The Transverse Potential Flow Past a Body of Revolution," Journal of Mechanics and Applied Mathematics, Vol. IX, part 2 (1956), pp. 140-142.

Carpenter, L.H., and Garbis H. Keulegan. "Forces on Cylinders and Plates in an Oscillating Fluid," Journal of Research of the National Bureau of Standards, Vol. 60, No. 5 (May 1958), Research Paper 2857, pp. 423-439.

Domm, Ulrich. "The Stability of Vortex Streets with Consideration of the Spread of Vorticity of the Individual Vortices," Journal of the Aeronautical Sciences, Vol. 22, No. 11 (November 1955).

Dosanjh, D.S., S. Eskinazi and E.P. Gasparek. "Decay of a Viscous Trailing Vortex," The Aeronautical Quarterly (May 1962), pp. 167-188.

Drasky, J. On Some Particular Cases of the Solution of LaPlace's Equation Describing the Principal Properties of Vortex Formations in Fluids. National Research Inst. of Heat Engineering, Prague.

Eskinazi, Salamon, and John W. Schaefer. "An Analysis of the Vortex Street Generated in a Viscous Fluid," Journal of Fluid Mechanics 6 (1958), pp. 241-260.

Garrison, C.J. and Turgut Sarpkaya. "Vortex Formation and Resistance in Unsteady Flow," Journal of Applied Mechanics (March 1963), pp. 16-24.

Grove, A.S., F.H. Shair, E.E. Petersen, and Andreas Acrivos. "An Experimental Investigation of the Steady Separated Flow Past a Circular Cylinder," Journal of Fluid Mechanics, Vol. 19, part 1 (1963), pp. 60-80.

Harvey, J.K. "Some Observations of the Vortex Breakdown Phenomenon," Journal of Fluid Mechanics, Volume 14, part 4 (1962), pp. 585-592.

Humphreys, John S. "On a Circular Cylinder in a Steady Wind at Transition Reynolds Numbers," Journal of Fluid Mechanics (1960), Vol. 9, part 4, pp. 603-612.

Jones, J.P. The Breakdown of Vortices in Separated Flow. Univ. of Southampton, Dept. of Aeronautics & Astronautics, U.S.A.A. Report No. 140 (July 1960).

Jones, R.T. Effects of Sweep-Back on Boundary Layer and Separation. NACA Report No. 884 (1947).

Jones, R.T. Properties of Low-Aspect-Ratio Pointed Wings at Speeds Below and Above the Speed of Sound. NACA Report No. 835.

Kaplun, Saul. "Low Reynolds Number Flow Past a Circular Cylinder," Journal of Mathematics and Mechanics, Vol. 6, No. 5 (1957), pp. 595-606.

Kawaguti, Mitutosi. "Numerical Solution of the Navier-Stokes Equations for the Flow Around a Circular Cylinder at Reynolds Number 40," Journal of the Physical Society of Japan, Vol. 8, No. 6 (Nov.-Dec. 1953), pp. 747-757.

Kronauer, R.E. Predicting Eddy Frequency in Separated Wakes. Presented at the IUTAM Symposium at Ann Arbor, Michigan (July 1964).

Kulin, Gershon. Solitary Wave Forces on Submerged Cylinders and Plates. National Bureau of Standards Report 5876 (April 22, 1958).

Landweber, L. The Axially Symmetric Potential Flow About Elongated Bodies of Revolution. Navy Department, Report 761, NS 715-084 (August 1951).

Landweber, L. and C.S. Yih. "Forces, Moments, and Added Masses for Rankine Bodies," Journal of Fluid Mechanics, Vol. 1, Part 3 (1956), pp. 319-336.

Lotz, I. Calculation of Potential Flow Past Airship Bodies in Yaw. NACA TM No. 675.

Mangler, K.W. Improper Integrals in Theoretical Aerodynamics. Royal Aircraft Establishment, Report AERO 2424. (June 1951).

Marris, A.W. "A Review on Vortex Streets, Periodic Wakes, and Induced Vibration Phenomena," Journal of Basic Engineering (June 1964), pp. 185-196.

Michalke, A. "Vortex Formation in a Free Boundary Layer According to Stability Theory," Journal of Fluid Mechanics, Vol. 22, part 2 (1965), pp. 371-383.

Morison, J.R., J.W. Johnson and M.P. O'Brien. Experimental Studies of Forces on Piles, Chapter 25, Proceedings, First Conference on Coastal Engineering, pp. 340-370.

Morkovin, M.V. Flow Around Circular Cylinder—A Kaleidoscope of Challenging Fluid Phenomena.

Munk, Max M. The Aerodynamic Forces on Airship Hulls. NACA Report No. 184.

Newman, B.G. "Flow in a Viscous Trailing Vortex," The Aeronautical Quarterly (May 1959), pp. 149-162.

Ozker, M.S. and J.O. Smith. "Factors Influencing the Dynamic Behavior of Tall Stacks Under the Action of Wind," Transactions of the ASME (August 1956), pp. 1381-1391.

Pagon, W. Watters. "What Aerodynamics Can Teach the Civil Engineer," Engineering News-Record (March 15, 1934), pp. 348-353.

Pierce, D. "Photographic Evidence of the Formation and Growth of Vorticity Behind Plates Accelerated from Rest in Still Air," Journal of Fluid Mechanics, Vol. 11, part 3 (1961), pp. 460-464.

Pierce, Jesse and A.M.O. Smith. Exact Solution of the Neumann Problem. Calculation of Non-Circulatory Plane and Axially Symmetric Flows About or Within Arbitrary Boundaries. Douglas Aircraft Co. Report No. ES 26988 (1958).

Powell, A. "Theory of Vortex Sound," The Journal of the Acoustical Society of America, Vol. 36, No. 1 (January 1964), pp. 177-195.

Prandtl, L. General Considerations on the Flow of Compressible Fluids. NACA TM No. 805 (October 1936), paper presented at Volta meeting in Italy Sept. 30 - Oct. 6, 1935.

Prandtl, L. On Boundary Layers in Three Dimensional Flow. Joint Intelligence Objectives Agency, Washington, D.C. File No. B.I.G.S. -84 (6 August 1946).

Reed, Wilmer H., III. Ground Wind Loads Analysis for Saturn I Block II Vehicles, presented at MSFC (June 20, 1963).

Rosenhead, L. "The Formation of Vortices from a Surface of Discontinuity," Proc. Royal Society, No. 134 (1931), pp. 170-192.

Rosenhead, L. "Vortex Systems in Wakes," Advances in Applied Mechanics, Vol. 3, Academic Press, N.Y. (1953), pp. 185-195.

Roshko, Anatol. "On the Wake and Drag of Bluff Bodies," Journal of the Aeronautical Sciences (February 1955), pp. 124-132.

Sacks, A.H. and John R. Spreiter. "The Rolling Up of the Trailing Vortex Sheet and Its Effect on the Downwash Behind Wings," Journal of the Aeronautical Sciences, (January 1951), pp. 21-32.

Sacks, Alvin H. "Vortex Interference Effects on the Aerodynamics of Slender Airplanes and Missiles," Journal of the Aeronautical Sciences, Vol. 24, No. 6 (June 1957).

Schaffer, Allan. "A Study of Vortex Cancellation," Journal of the Aerospace Sciences, Vol. 27, No. 3 (March 1960).

Schindel, L. H. Investigation of the Formation of Vortices in the Flow About Bodies at Angle of Attack. MIT DSR 5139 (1964).

Schindel, L. H. Separated Flow About Lifting Bodies. MIT DSR 9221, Technical Report 80 (September 1963).

Scruton, C. On the Wind-Excited Oscillations of Stacks, Towers and Masts, presented at International Conference on the Wind Effects on Buildings and Structures, held at the National Physical Laboratory, Teddington, Middlesex, (June 26-28, 1963). Paper No. 16.

Sevik, M. "Lift on an Oscillating Body of Revolution," AIAA Journal, Vol. 2, No. 2 (1963), pp. 302-305.

Squire, H. B. Analysis of the 'Vortex Breakdown' Phenomenon. Part I. Department of Aeronautics, Imperial College, London, Report No. 102.

Taneda, S. "Experimental Investigation of the Wakes Behind Cylinders and Plates at Low Reynolds Numbers," Journal of the Physical Society of Japan, 11, 302 (1956).

Taneda, S. "Oscillation of the Wake Behind a Flat Plate Parallel to the Flow," Journal of the Physical Society of Japan, Vol. 13, No. 4 (April 1958), pp. 418-424.

Taneda, S. "Downstream Development of the Wakes Behind Cylinders," Journal of the Physical Society of Japan, Vol. 14, No. 6 (June 1959), pp. 843-848.

Taneda, S. "The Stability of Two-Dimensional Laminar Wakes at Low Reynolds Numbers," Journal of the Physical Society of Japan, Vol. 18, No. 2 (February 1963), pp. 288-296.

Thom, A. The Forces on a Cylinder in Shear Flow. A. R. C. 23,930, F.M. 3209, (July 12, 1962).

Ting, L. and Tung, C. "Motion and Decay of a Vortex in a Nonuniform Stream," The Physics of Fluids, Vol. 8, No. 6 (June 1965), pp. 1039-1051.

Tritton, D. J. "Experiments on the Flow Past a Circular Cylinder at Low Reynolds Numbers," Journal of Fluid Mechanics, Vol. 6, part 4, (1959), pp. 547-567.

Tsien, Hsue-Shen. "Supersonic Flow Over an Inclined Body of Revolution," Journal of the Aeronautical Sciences (1938), pp. 480-483.

von Berger, E. "Supression of Initial Turbulence of Karman Vortex Streets in the Wake of Circular Cylinders, by Means of Controlled Transverse Oscillations of the Generating Cylinder in the Transition Region Above Re = 160." WGLR Yearbook (1964).

von Ka'rma'n, Theodore. A Special Issue Containing a Selection of Original Papers by his Former Students Commemorating the Seventy-Fifth Birthday of Dr. Theodore von Ka'rma'n. Journal of the Aeronautical Sciences, Vol. 23, No. 5 (May 1956).

Wagner, Von Herbert. Generation of Dynamic Lift on Wings. (February 1925).

TECHNICAL REPORT INDEX/ABSTRACT

ACCESSION NUMBER						DOCUMENT SECURITY CLASSIFICATION	
						UNCLASSIFIED	

TITLE OF DOCUMENT

AN ANALYTICAL STUDY OF SEPARATED FLOW ABOUT A CIRCULAR CYLINDER

LIBRARY USE ONLY

AUTHOR(S)

B. H. Ujihara

CODE	ORIGINATING AGENCY AND OTHER SOURCES	DOCUMENT NUMBER
	S&ID, NAA	SID 65-1730

PUBLICATION DATE	CONTRACT NUMBER
25 January 1966	NAS8-20140

DESCRIPTIVE TERMS

vortex shedding, separated flow, potential flow, fluid dynamics

ABSTRACT

Incompressible separated flow about a two-dimensional circular cylinder has been investigated on the basis of potential flow theory. It has been shown that the primary non-steady force characteristics can be adequately predicted in agreement with experimental data for subcritical Reynolds numbers, both for symmetrical flow and periodic vortex shedding. A detailed account is given of the fundamental investigations, including development of shear layer in flow past a half-plane, symmetrical flow past a 10:1 ellipse normal to the stream, and symmetrical and unsymmetrical flow past a circular cylinder.